TEL-Atomic
Incorporated

TEL-Atomic
Incorporated

PS 15 NMR spectrometer

NMR lock Programmer   Power
On   DC offset
  − +

TEL-Atomic
Incorporated

PS 15 NMR electromagnet

Ser.

NMR Pulse Spectrometer   PS 15

experimental manual

NMR Pulse Spectrometer PS 15

Experimental Manual
for MS Windows

TEL-Atomic
Incorporated

CONTENTS

1   INTRODUCTION

The PS15 pulse spectrometer is a teaching tool as well as an excellent unit for conducting research in the field of proton NMR spectroscopy.

This **Experimental Manual** is a laboratory companion to the **Operating Manual** of the PS15 NMR pulse spectrometer distributed by TEL-Atomic, Inc.

Each section of this manual provides introductory information about the subject, specifies the problem and gives detailed instructions on conducting the experiment. All of these experiments have been performed using an off-the-shelf PS15 NMR spectrometer and only originally acquired data are presented.

The purpose of this manual is to show the potential of the use of the PS15 spectrometer. Teachers and students have freedom in selecting their own samples, using the described sequences as well as other pulse sequences which are not described. Acquired data can be manipulated with the tools on the data acquisition page or if binary data is exported in ASCII format users, can use their own software to perform Fast Fourier Transform or calculate relaxation times.

A complete treatment of NMR phenomenon is far beyond the scope of this manual. For more details refer to textbooks and papers related to specific experiments (see list of books and papers in **References** on page 141).

2   FREE INDUCTION DECAY AND SPIN ECHO

2.1 Theory

2.1.1 Introduction

The response of a nuclear magnetic spin system polarized by a constant magnetic field B_0 to a radio-frequency (RF) pulse, whose spectrum covers the resonance frequency of spins, is known as "Free Induction Decay" (FID). "Free" refers to the fact that nuclear spins precess freely in the presence of a polarizing, constant magnetic field B_0 - but without the presence of an RF field. The FID signal is of fundamental importance for pulse NMR spectroscopy as this time-domain signal Fourier transformation leads directly to the frequency-domain NMR spectrum.

2.1.2 Rotating frame

To describe the phenomenon of FID we will focus our attention on the net macroscopic magnetization that obeys the laws of classical mechanics instead of on individual spins obeying the laws of quantum mechanics. In this approach we will analyze the interactions between the macroscopic magnetization **M** and static B_0 and RF B_1 magnetic fields in a rotating reference frame and note the relaxation effects that follow. In this concept the rotating frame moves synchronously with the RF field dramatically simplifying the solution of Bloch equations and allows the visualization of effects even after relatively complex pulse sequences.

The spectrometer's quadrature detector (which consists of two phase sensitive detectors) detects both components of the nuclear net magnetization (M_{xy}) that are perpendicular to the constant field B_0. The in-phase signal corresponds to the **y** component and the 90°-out-of-phase signal corresponds to the **x** component of the M_{xy} magnetization. Using complex numbers analogy the **y** component is called **real** and **x** is called **imaginary** part of M_{xy} vector.

2.1.3 $\Pi/2$ ($90^{o)}$), Π (180°), … pulses

For a spin system that has been allowed to reach Boltzmann equilibrium, a net magnetization is aligned along the B_0 or z' axis of the rotating frame. Suppose an RF pulse is applied along the x' axis. In the rotating frame it will cause precession of M_z magnetization about B_1 with a corresponding Larmor frequency: $\omega = \gamma \cdot B_1$. As $\omega = \dfrac{\Theta}{t_p}$, in time t_p, the angle Θ through which M_z rotates is given by:

$$\Theta = \gamma \cdot B_1 \cdot t_p \qquad\qquad \text{Eq. 1}$$

The time t_p determines the length of the RF pulse that produces a **B$_1$** field along the *x'* axis. Frequently we refer to pulses that tip the net nuclear magnetization through a certain angle as **Π/2** or **Π** pulses in radians (90 or 180 in degrees).

Eq. 1 defines the magnetization tip angle that can be achieved by applying the pulse of duration t_p and of the induction **B$_1$**. The upper limit for t_p is determined by relaxation processes that should be negligible during excitation of the nuclei.

The induction **B$_1$** depends on the power incident in the sample's coil and on the coil's electrical and geometrical properties. B$_1$ in the sample coil can be estimated from Eq. 2:

$$B_1 \approx \sqrt{\frac{P \cdot Q}{f_r \cdot V}} \qquad\qquad \text{Eq. 2}$$

P- power of RF pulse
Q- coil quality factor
V- coil volume
f_r- probehead circuit resonance frequency

If Q, V, and f_r are fixed the only other way to change **B$_1$** and as a consequence the flipping angle is by changing the pulse power P. In practice this is done by attenuation of the maximum value of the pulse power. Due to fast relaxation, solid-state samples usually require short and powerful bursts of RF lasting only a few microseconds. Liquid like samples, with their relatively long relaxation times, have less critical demands. The upper limit for the power of RF pulses is determined mostly, not by physical properties of the sample, but rather by the electronic components specifications like maximum working voltage (damage of tuning and matching capacitors in the sample probe resonant circuit due to arcing) or maximum current (limitations of transmitter's end stage transistors).

Figure 1a shows an effect of a $\Pi/2$ (90°) pulse. Assuming perfect homogeneity of the **B$_1$** field across the sample, and that no relaxation occurs during the time t_p following this pulse, **M** lies entirely along the y' axis. Its fast precession along **B$_o$** induces the voltage in the solenoid that is a part of the RLC resonance circuit tuned precisely to the precession frequency. As transverse relaxation occurs, the signal gradually decays. In a perfectly homogeneous **B$_0$** field the time constant of that decay would be T$_2$. Since the **B$_0$** field is not perfectly homogeneous across the sample, nuclei in different parts of the sample experience slightly different magnitudes of **B$_0$**, and hence precess at slightly different frequencies. As a result, the FID signal decays faster with a characteristic time T_2^*. This so-called "tee-two-star" time includes contributions from a natural process that causes nuclei to exchange energy with each other and from the inhomogeneity of the magnetic field. The effective speed of spin-spin relaxation is thus described by Eq. 3.

$$\frac{1}{T_2^*} = \frac{1}{T_2} + \frac{\gamma \cdot \Delta B_1}{2} \qquad\qquad \text{Eq. 3}$$

In Eq. 3 ΔB_1 is the magnetic field inhomogeneity. The whole term $\gamma \cdot \Delta B_1 / 2$ is called $1/T_2^{'}$ or inhomogeneous broadening as it broadens the natural line width of the spectra which is determined only by molecular processes.

In the language of the "rotating frame", during spin-spin relaxation some nuclear spins rotate faster (move clockwise in the rotating frame) and some rotate slower (move counter clockwise in the rotating frame) with regard to the **B₁** field as shown in Figure 1b. Therefore in the "rotating plane" the macroscopic **M_y** component exponentially decreases as individual magnetic moments dephase.

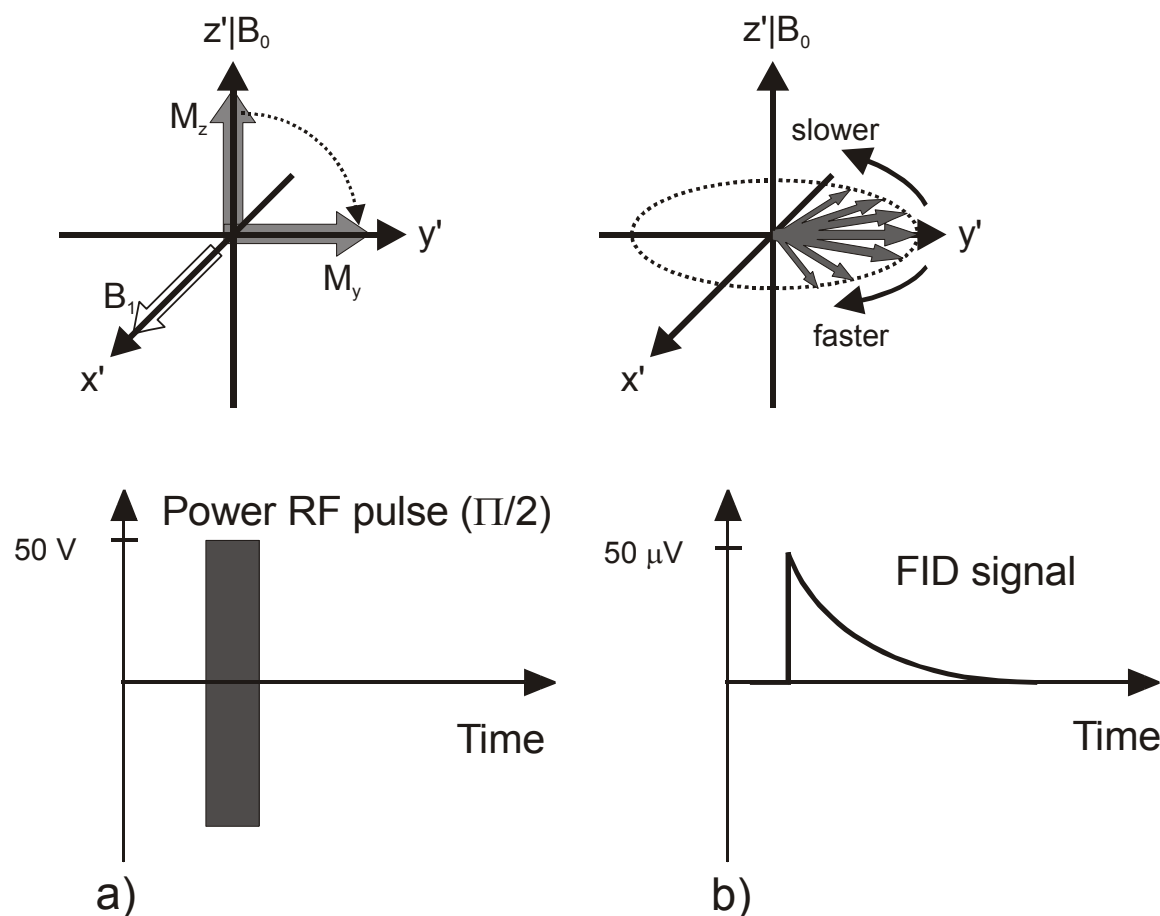Figure 1a). A Π/2 RF pulse and its effect on equilibrium magnetization M_z. b) Gradual decay of M_y magnetization as an effect of the dephasing of individual moments

Spin-lattice relaxation also occurs as nuclear moments loose energy to their

surroundings and the macroscopic magnetization **M** unavoidably tips back towards the **B$_0$** field or z' axis.

2.1.4 On-resonance and off-resonance

The RF pulse of frequency ω_{RF} excites only these nuclei that precess with frequency ω_0 within its spectral bandwidth $\Delta\omega_{RF}$. Generally square pulses cover a range of frequencies wide enough to excite all nuclei in the sample, except some solid-like samples. If the frequency of the RF pulse is exactly the precession frequency of a single type of nucleus ($\omega_{RF}=\omega_0$) the phase sensitive detector produces a signal with pure exponential decay as shown in Figure 2a. This decay directly corresponds to the decrease of nuclear magnetization in the xy plane.
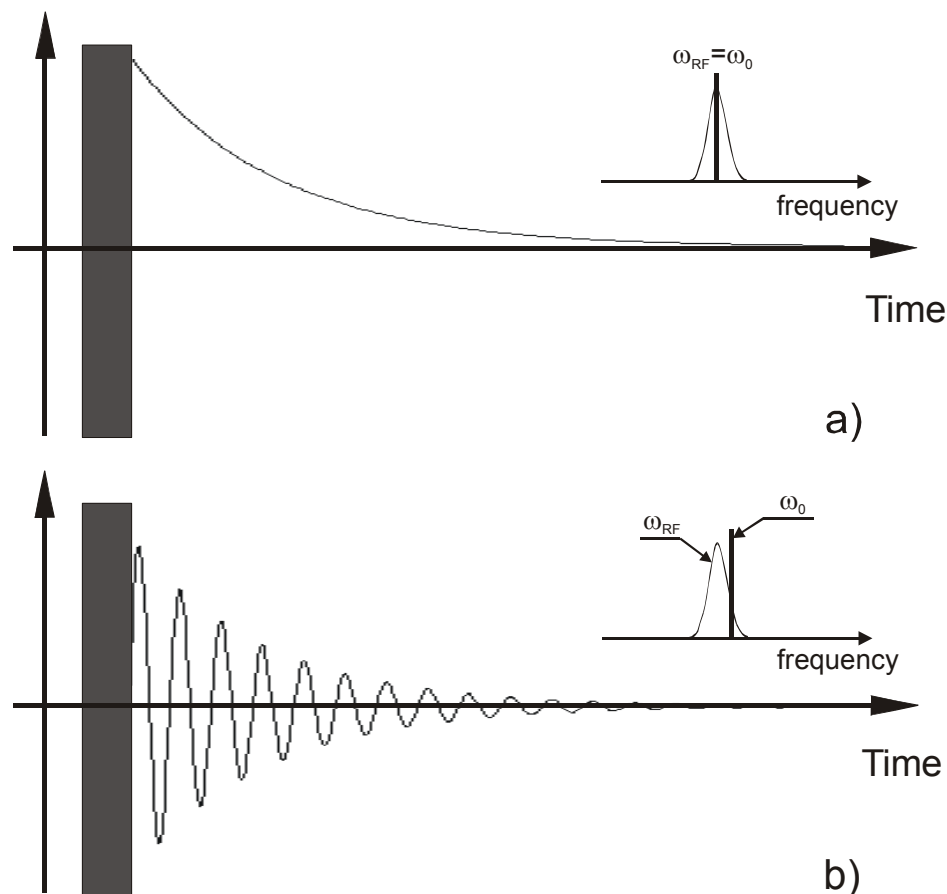
Figure 2. a) On- resonance FID ($\omega_{RF}=\omega_0$). b) Off-resonance FID ($\omega_{RF}\neq\omega_0$).

Suppose now that the RF signal is slightly different from the resonance frequency of the precessing nuclei ($\omega_{RF}\neq\omega_0$). Immediately after the $\Pi/2$ pulse **M$_z$** lies along y' axis. However, due to the difference in frequencies the magnetization moves relative to the rotating frame. The phase sensitive detector senses this movement. It produces an exponentially decaying FID modulated by the signal whose frequency is the difference

$\Delta\omega = \omega_{RF} - \omega_0$ between the Larmor frequency of the observed nuclei and the frequency of the detector reference (see Figure 2b). A Single-phase sensitive detector does not sense the sign of $\Delta\omega$.

2.1.5 Spin-Echoes

Pulse excitation of polarized nuclear spins was first proposed by *Hahn* in 1950 in a serious of ingenious experiments published four years after the major discovery of the NMR effect by groups of *Purcell* and *Bloch*. *Hahn* also introduced the term "spin-echo". Slightly euphemistic, this term combines categories from two extreme fields, quantum mechanics and acoustics.

Hahn realized that the part of the free induction decay signal that vanishes faster due to magnetic field imperfections (called inhomogeneity) could be retrieved in a two-pulse experiment. Originally he used two consecutive $\Pi/2$ pulses separated by a certain time delay. It is much clearer, however if one analyzes the appearance of spin echo when a $\Pi/2$ pulse, followed by a pulse of Π, is applied as suggested by *Carr* and *Purcell* two years later. The natural FID decay caused by spin-spin relaxation can not be retrieved.
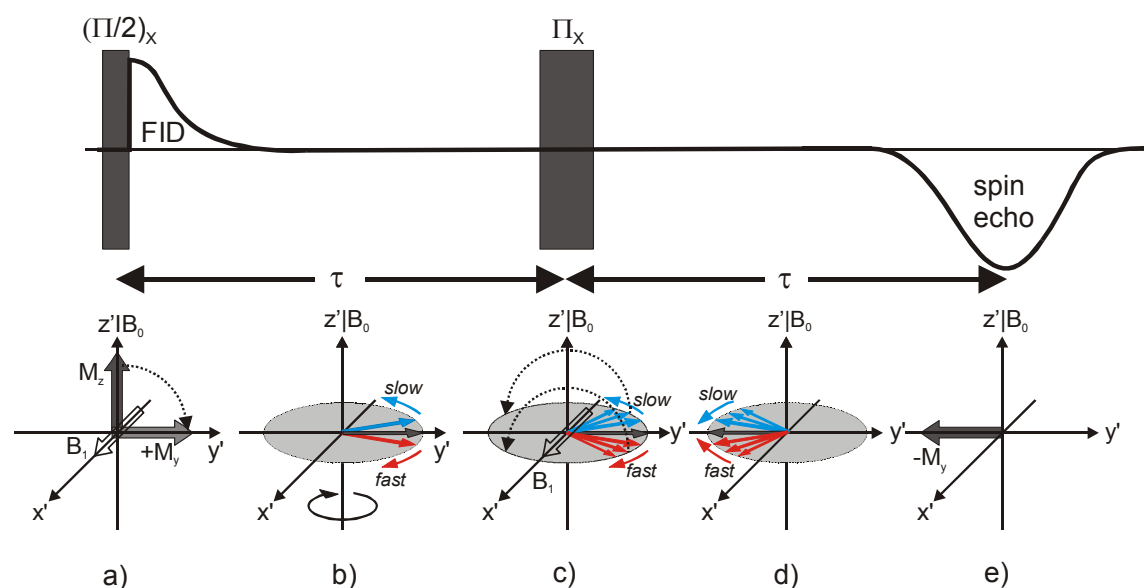
Figure 3. Spin-echo creation after a $(\Pi/2)_X$-τ-Π_X sequence. **a)** Pulse of $(\Pi/2)_X$ tips the net magnetization from the z-axis on the xy plane. **b)** Due to the magnetic field inhomogeneity "pockets" of magnetizations lose the coherence that manifests in a faster decay of My. **c)** A Π_X pulse applied along the x' axis after a time τ rotates a whole set of differently moving magnetizations. **d)** In this spin race, faster moving magnetizations (clockwise) meet slower moving magnetizations (counterclockwise) exactly at the –y axis. **e)** After an additional time period of time τ the spins generate a strong echo signal.

The net magnetization **M** can be considered as a vector sum of elementary magnetizations originating from nuclei located in different parts of the sample $\mathbf{m_i}$. Due to

magnetic field inhomogeneity these magnetizations experience slightly different fields. As a result magnetizations in **higher fields precess faster**, whereas those in a **lower fields precess slower**. Magnetization M_z tipped by a $(\Pi/2)_X$ pulse to the xy plane starts to decompose (see Figure 3b) because of two contributions: spin-spin relaxation and magnetic field inhomogeneity. The first process leads to an inevitable decay of free induction with the time constant T_2. Fortunately the second contribution can be compensated by an additional Π_X RF pulse (Figure 3c). If $T_2^* < \tau < T_2$ we will see the signal from the net magnetization again weakened only by the spin-spin relaxation process (Figure 3e). This signal that is made of refocusing almost simultaneously magnetizations m_i we call **spin-echo** (SE). Once focused along the –y axis the net magnetization loses coherence again unless another RF pulse is applied.

The Carr-Purcell sequence was originally designed for measuring T_2 spin-spin relaxation times not affected by magnetic field homogeneity. After $(\Pi/2)_X$ and Π_X pulses, separated by a time τ, there will follow a train of Π_X pulses in 2τ intervals with consecutive echoes refocused between Π_X pulses. This method suffers, however, from accumulative error of inaccuracy of Π_X setting when many Π_X pulses are applied. Even a slight inaccuracy of the echo refocusing pulses of **CP** sequence results in spins focusing above or under the x'y' plane which is the plane of detection causing rapid decay of later echoes.

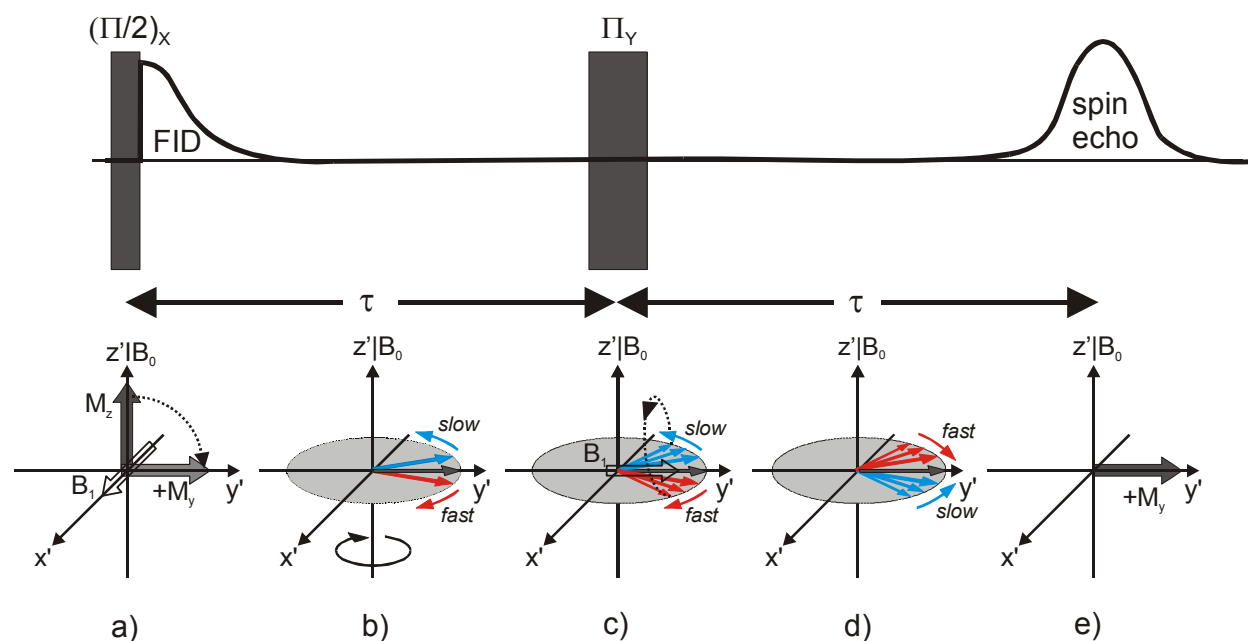Figure 4. Spin echo formation under the *Carr-Purcell-Meiboom-Gill* sequence.

By shifting the phase of Π pulses by 90° and the use of a Π_y pulse instead of Π_X *Meiboom* and *Gill* modification of **CP** sequence reduces the effect of the angle rotating inaccuracy significantly (Figure 4).

The Π_y pulse rotates the dephasing nuclear spins around the y' axis. Let's assume that it is slightly shorter than a perfect Π_y pulse and is $(\Pi-\varepsilon)_y$. How the self-correction of the Π_y pulse works is illustrated in Figure 5. To simplify the picture, only the movement of the magnetization corresponding to faster spins is shown in an x'y' plane. Y' axis points toward the reader.

a) First pulse, a $(\Pi/2)_X$ pulse, rotates the magnetization on y' axis; the red spot in the center represents its $M_{Y'}$ component.

b) As spins loose coherence due to spin-spin relaxation process, faster spins start to move clockwise; from the reader's perspective, toward left.

c) $(\Pi-\varepsilon)_Y$ pulse rotates the cluster of fast spins along y' axis. As the rotation angle is smaller than 180° the cluster of spins does not reach x'y', but the plane above.

d) Spins continue to move clockwise (toward left).

e) Spins form first echo when they reach y'. Echo is formed above x'y' plane and its xy component is smaller than when an exact Π pulse is applied.

f) Spins start to dephase again.

g) The second $(\Pi-\varepsilon)_Y$ pulse moves the fast cluster of spins exactly on x'y' plane correcting the error of the first pulse.

h) Spins dephase and move toward Y' axis.

i) Spins meet again at y' axis and form perfect echo in xy plane. Process repeats for next $(\Pi-\varepsilon)_Y$ pulses. Every time odd echoes are slightly displaced, whereas even echoes focus along Y'.

Figure 5. "Self-correcting" properties of Π_Y pulses in CPMG sequence. Only cluster of faster spins are shown.
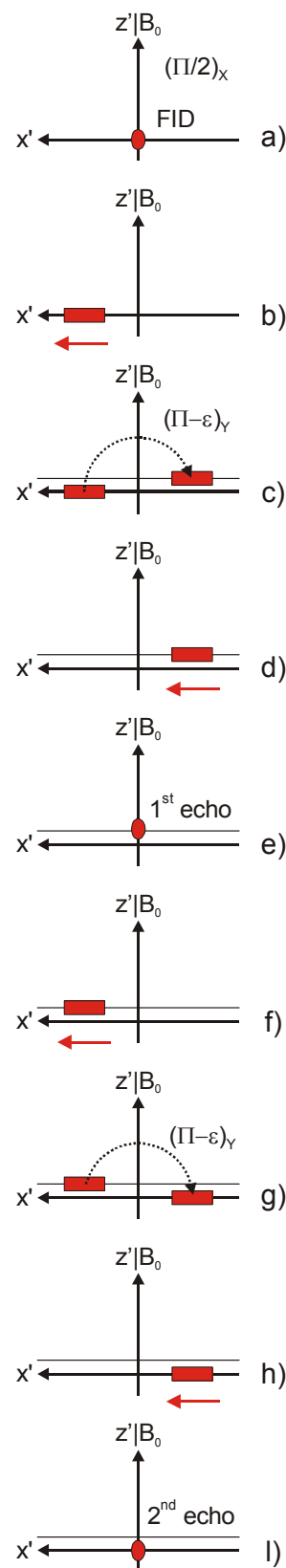
2.2 Experimental

2.2.1 Obtaining on-resonance FID

Introduction

Obtaining an on resonance free induction decay signal is essential for understanding physical and instrumental details of NMR pulse spectroscopy. The experiment requires using any one-pulse sequence. You can apply either the **1P_X**, **1P_-X**, **1P_Y** or **1P_-Y** sequence to prepare the necessary setup as described below. Either sequence will allow you later to acquire and store data in the file.

Directions

We strongly recommend the use of the **glycerin** sample as it displays some physical properties (short relaxation and abundance of protons) convenient for quick setup and fast data acquisition.

For details on how to obtain an on-resonance FID from a glycerin sample, refer to the comprehensive instructions in the **Operating Manual** or modify parameters of the **Setup** page as shown in Figure 6.
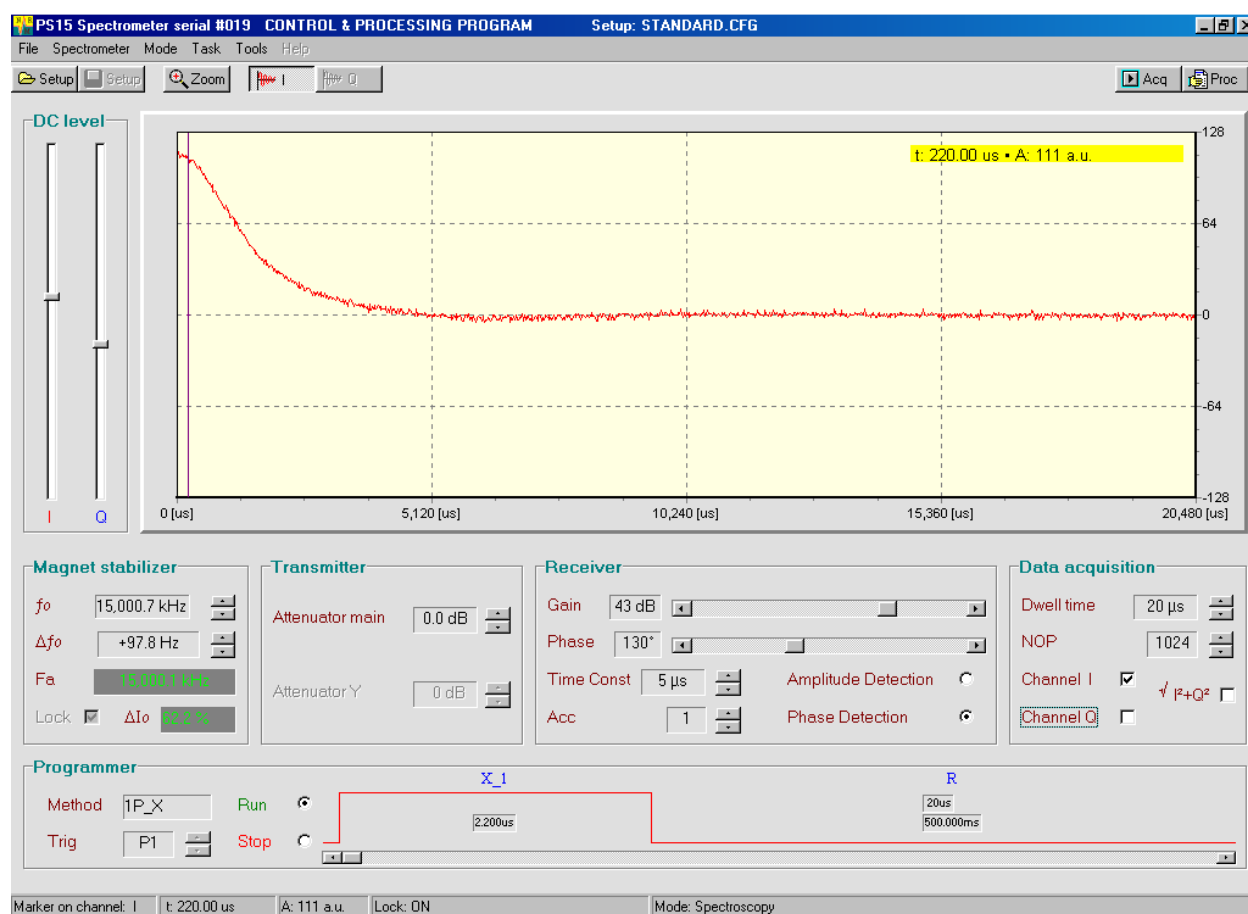

Figure 6. Preparing on-resonance one-pulse experiment.

2.2.2 Determining Π/2, Π, 3/2Π... pulses

Introduction

The RF pulse rotates the magnetization by a certain angle from its equilibrium position along $\mathbf{B_0}$ the static magnetic field. It is of utmost importance to know Π/2 and Π for further spin-echo experiments and relaxation measurements. This experiment helps one to determine the correct length for Π/2, Π, 3/2Π and any other pulse that rotates magnetization.

Object

Determining Π/2, Π, 3/2Π pulses by measuring the FID's signal amplitude dependence on pulse length.

Directions

- Start **1P_X** one-pulse experiment.
- Achieve on-resonance conditions in one channel (**I** or **Q** checked) with no attenuation of the RF power (**Transmitter>Attenuator main**=0).
- Move data marker beyond the "dead time'; usually 25μs is enough.
- Set pulse width to minimum 0.2μs (**Programmer>X_1** =0.2μs).
- Compensate DC offset to zero (**DC leve**l slider).
- Read and record the FID amplitude in the marker position.
- Repeat previous measurements every 0.2μs to about 15μs.
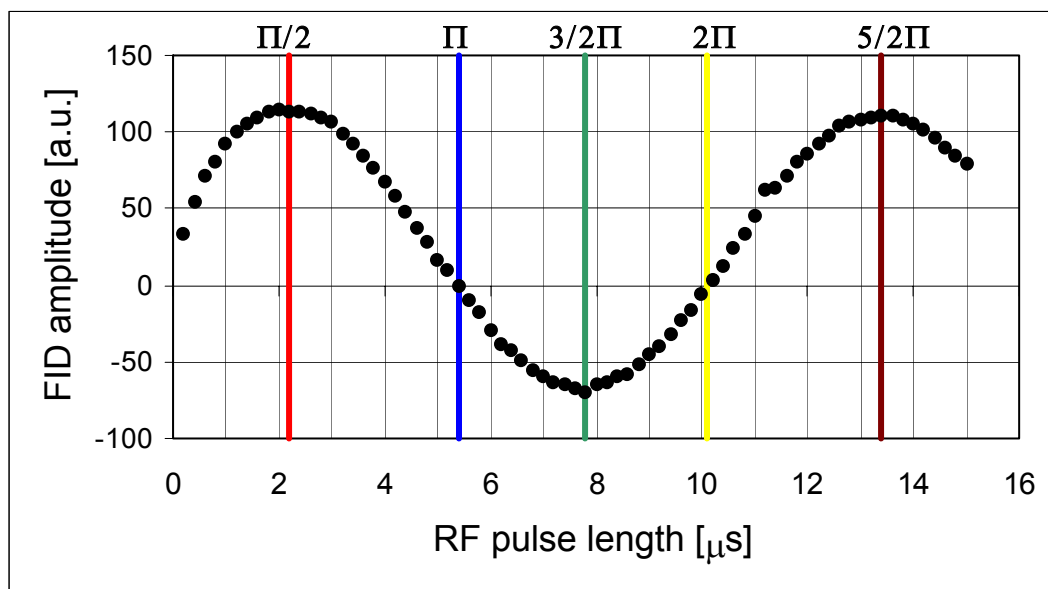- Plot FID amplitude vs. pulse width (see example in Figure 7).

Figure 7. The amplitude of FID signal induced in the RF coil plotted against the RF pulse width.

- From the plot determine the length of Π, $\Pi/2$, **and 3/2Π** pulses:
  - first maximum corresponds to use of $\Pi/2$ pulse (read line at 2.2μs),
  - first transition through zero is caused by Π pulse (blue line at 5.4μs),
  - first minimum is due to **3/2Π** pulse (green line at 7.6μs), etc.

Note that Π pulse is not simply twice as long as $\Pi/2$ pulse. This effect is of purely instrumental nature.

2.2.3 Adjusting phase for the spectrometer phase detector

Introduction

The amplitude of on-resonance FID after phase detection strongly depends on the phase of the reference signal. Researchers can not afford to loose or have an error in the signal that latter will affect the precision of measurements.

The analysis of the phase detector operation (see page 76) shows that a maximum of the detected on-resonance signal can be achieved when the phase of the RF modulated FID (remember that FID you see is simply an alternate electric current induced in the resonant circuit coil by processing nuclear magnetic moment) differs from the reference signal by 0°. A digitally controlled electronic circuit, called phase shifter, introduced into the reference signal path of the PS15 enables the change of the phase by 2°.

Object

Finding the right phase shift of the phase detector reference signal.

Directions

- Start **1P_X** one-pulse experiment.
- Achieve on-resonance conditions in one channel with $\Pi/2$ pulse.
- Move data marker beyond the "dead time".
- Set phase of reference signal in the phase sensitive detector to zero degree (**Receiver>Phase** = 0)
- Compensate carefully any DC offset to zero (**DC leve**l slider).
- Read and record the FID amplitude in the marker position.
- Repeat previous measurements every 2° from 0° to 258°.
- Plot FID amplitude against the phase.
- Find the maximum on the plot that corresponds to optimum phase shift (140° in Figure 8).
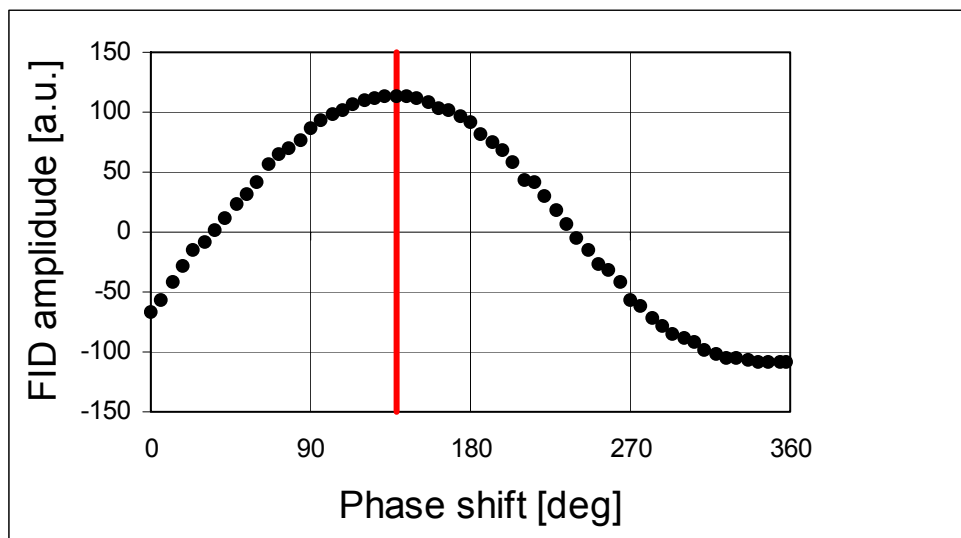

Figure 8. FID amplitude plotted against phase of reference signal.

2.2.4 Fast Fourier Transform of FID signal.

Introduction

Short RF pulses can excite nuclear spins in the frequency region of the spectrum these pulses generate. Square pulses (called "hard pulses") cover a wide range of frequencies around the carrier frequency f_{RF} established by a quartz generator or frequency synthesizer. Other than square shape pulses (called "soft pulses") produce narrower spectrum and are more selective in terms of frequencies that they cover.

In response to the RF pulses, spins generate a time dependent signal that can be also analyzed in terms of spectral contents. Fourier transform is a mathematical operation that transforms function from **time domain** to the **frequency domain**. Fast Fourier transform (**FFT**) is an efficient computer algorithm for performing the **discrete** Fourier transform for a *finite* number of 2^n data points.

$$\text{free induction decay} \quad \xleftrightarrow{\text{FFT}} \quad \text{NMR spectrum}$$

For instance an exponential function in time domain function and a Lorentzian function in frequency domain are Fourier transforms of each other. In nuclear magnetic resonance this exponential function is represented by exponentially decaying free induction decay and Lorentzian function describes the spectrum by using FFT.

Unlike continuous wave spectroscopy that scans slowly through a whole range of frequencies, the pulse FT NMR technique applies a radio frequency pulse containing all of the necessary frequency components in a **preparation** period. In the **detection** period that follows the response from nuclei is recorded and can be quickly converted to the spectrum.

A great advantage of FFT NMR lies in its ability to rapidly acquire a signal as well as to do signal averaging in the process called accumulation. The enhancement of signal to noise due to accumulation is carried over to the spectrum.

FT NMR perfectly fits these digital times as it benefits from the rapid development of fast processors and availability of memory.

Object

The acquisition of the off-resonance FID in two channels of the phase sensitive detector and conducting the Fourier transform of the signal.

Directions

- Start **1P_X** one-pulse experiment with two active channels (**Data acquisition>**check channels **I and Q**)

- Achieve off-resonance conditions by changing **Magnet stabilizer>Δf₀** to see a dozen of oscillations on FID.
- To achieve maximum signal set pulse width as $\Pi/2$.
- Set **Dwell time** to 20μs.
- Carefully cancel any DC offset in both channels by **DC level** function.
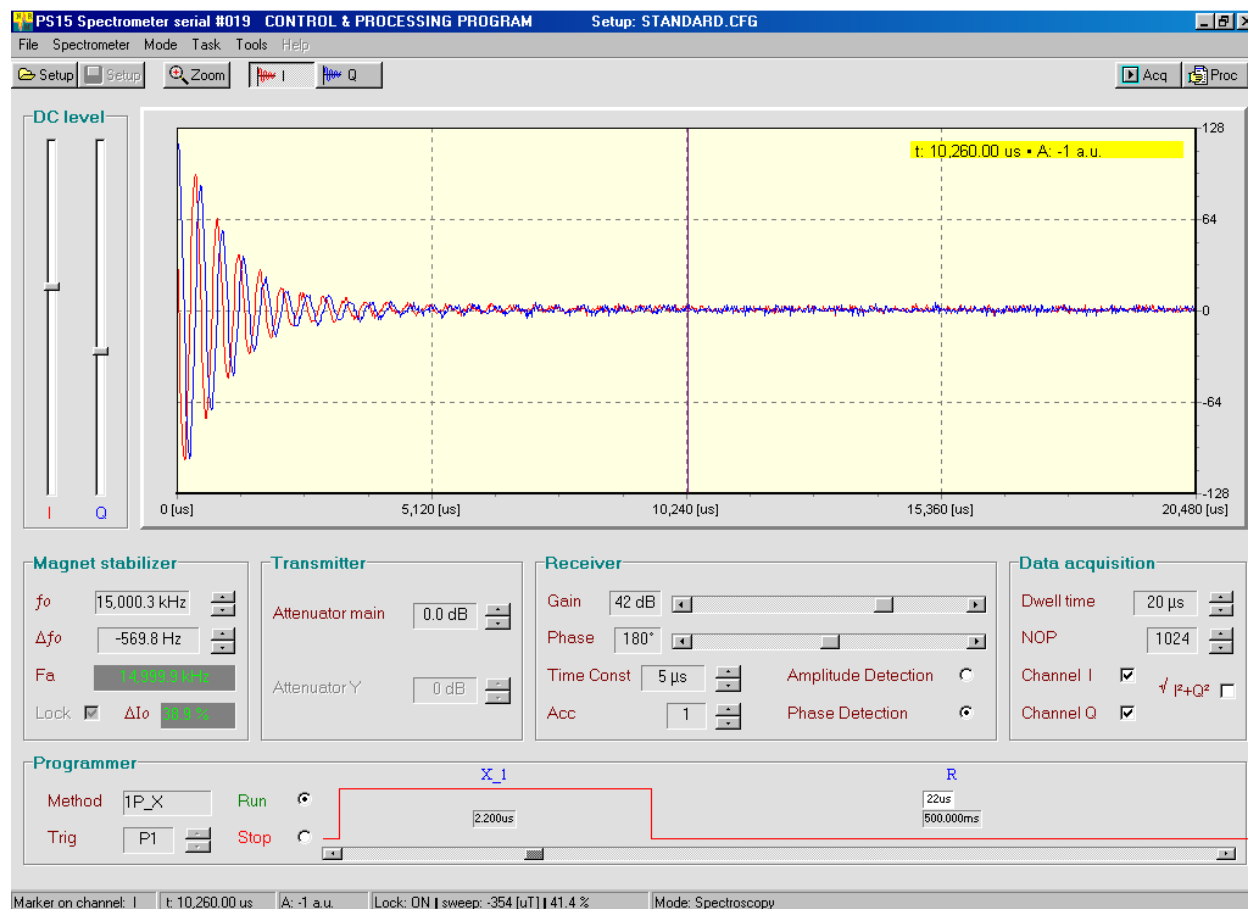

Figure 9. Setup page with off-resonance one-pulse experiment.

- In the **Acquisition** page acquire FID with several accumulations. Save the FID in a file.
- In the **Processing** page load acquired data.
- Click on **FFT** function.
- Correct phase to obtain pure absorption spectrum.
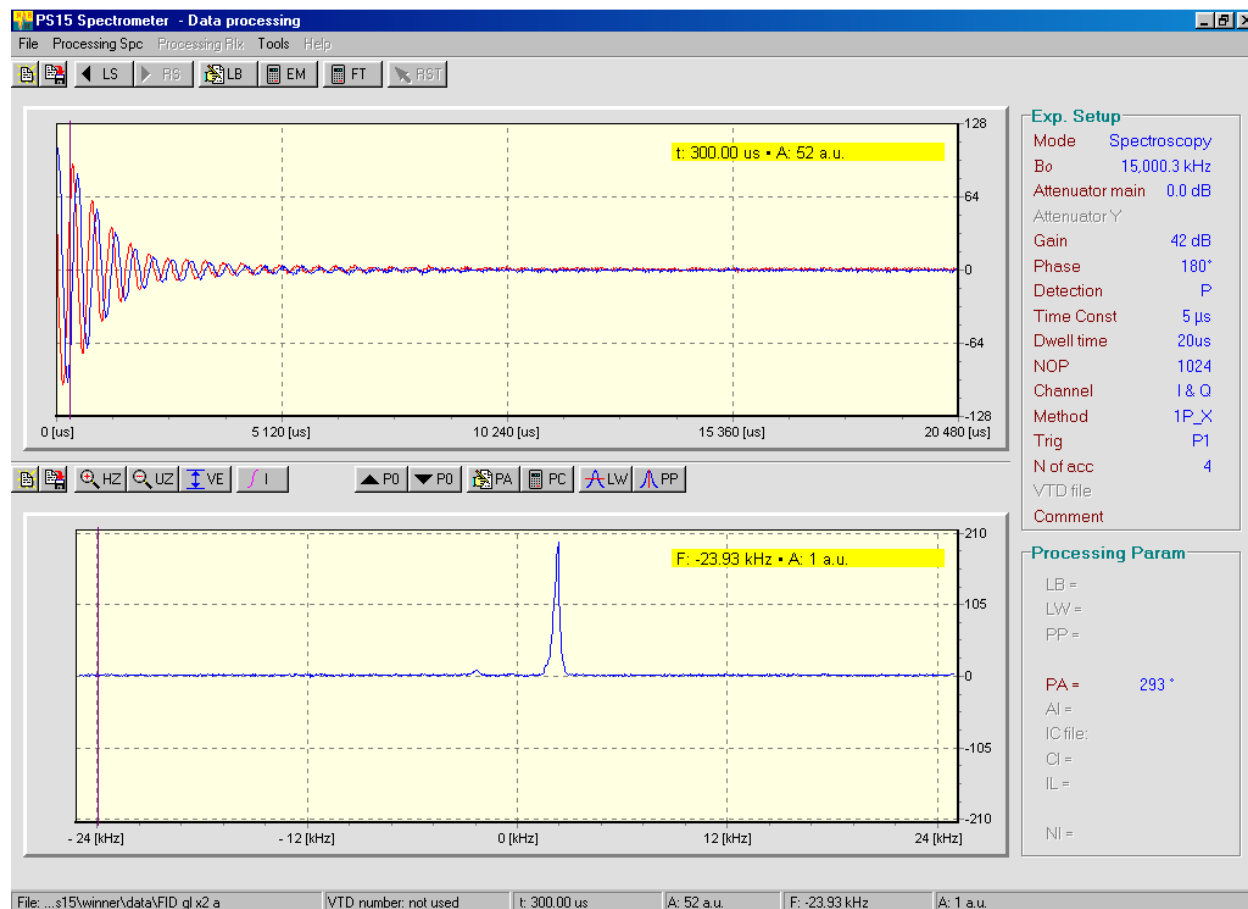
Figure 10. Applying Fast Fourier Transform (FFT) to FID. Signal from glycerin sample obtained after 4 accumulations at room temperature.

- Check the influence of **L**eft **S**hift (**LF**) and **E**xponential **M**ultiplication (**EM**) of FID on the corresponding spectrum.

2.2.5 Liquid-like and solid-like samples. Comparison by NMR.

Introduction

Liquids and solids present two extreme cases for NMR spectroscopy.

Liquids permit the movement of molecules that consequently average internal magnetic dipole-dipole interactions. If not averaged, the dipole-dipole interactions can generate a locally additional magnetic field in the vicinity of the nucleus under investigation which will modify (broaden) the constant magnetic field B_0. Thus NMR lines from liquid-like samples are usually very narrow.

On the other hand the rigid structure of solids limits the freedom of molecular motion preventing time-averaging of local interactions and therefore produces a local magnetic field. This internal field is responsible for the dramatic broadening of the spectrum.

Object

Comparing shapes of FIDs and spectra in distilled water and acrylic sample.

Directions

- On the **Setup** page prepare off-resonance one-pulse experiment with the glycerin reference sample.
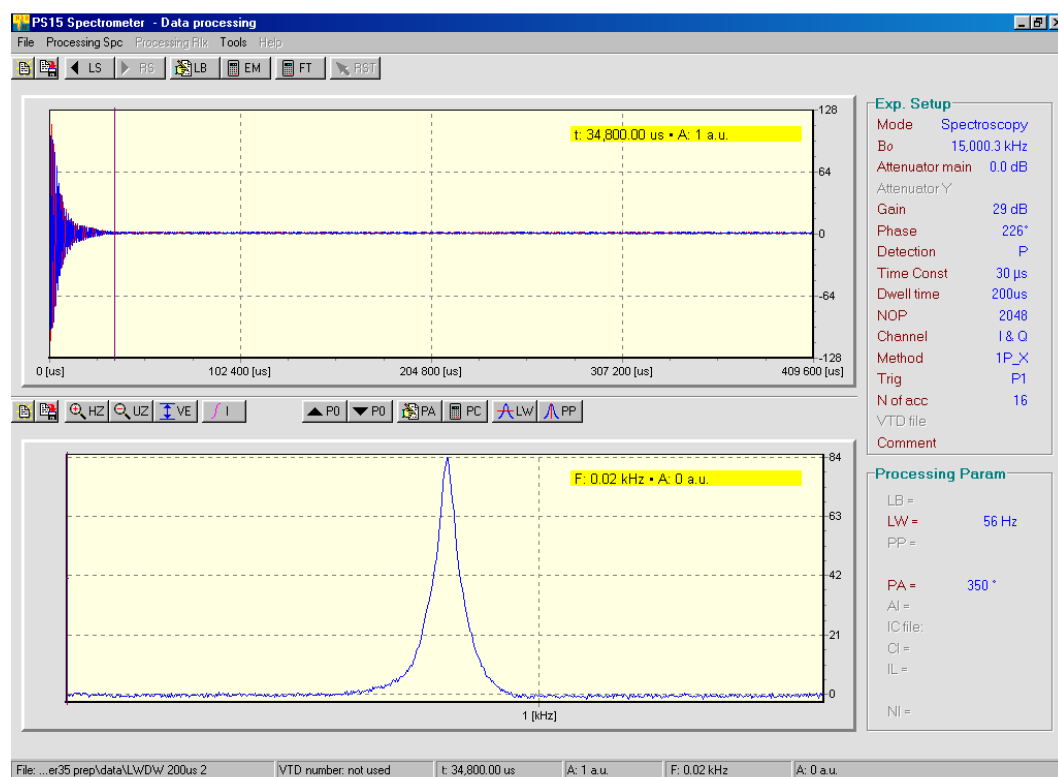
Figure 11. FID and corresponding spectrum in distilled water. Note 56 Hz line width.

- Replace glycerin with distilled water. As water contains more protons per sample volume you will see a stronger signal so decrease **Receiver Gain**. Due to water's long T_1 relaxation time increase repetition time T_R to 20 seconds to avoid saturation effects which reduces S/N ratio. Modify **DW** and **NOP** to see the whole FID and a long base line.

- On the **Acquisition** page acquire FID with 16 accumulations.

- Replace water by acrylic sample.

- Modify **Setup** page: increase **Receiver gain** (less proton than in water), decrease **DW** (broader line much shorter FID) to a minimum of 0.4µs and **NOP** to 512 or 1024, reduce acquisition delay time 2µs below spectrometer's "dead time". Do not be surprised to not see any oscillations on FID. They are invisible due to the enormously broad spectrum of the NMR signal from acrylic.

- On the **Acquisition** page acquire FID with 128 accumulations. The signal from acrylic is much weaker than signal from water and its strongest element (about 25% in time scale) is unfortunately lost due to "dead time".
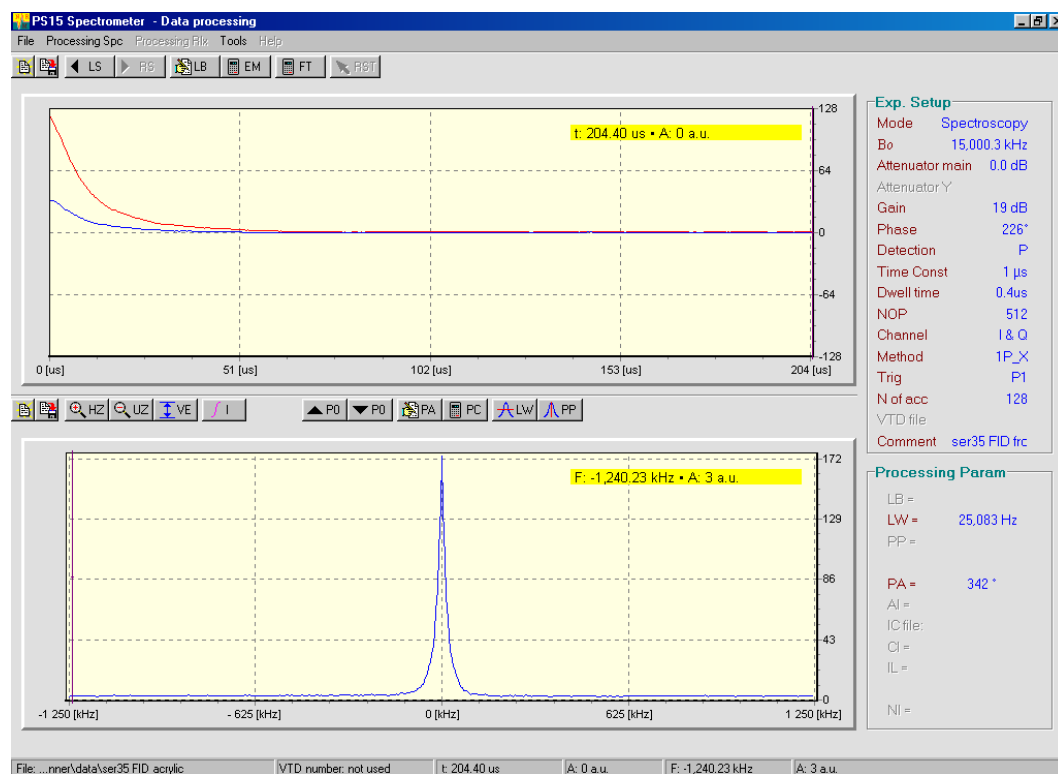
Figure 12. FID and corresponding spectrum in acrylic sample. Note 25,000 Hz line width!

- On **Processing** page estimate FID duration time[1], do FFT, correct spectrum phase and measure spectrum line width for both samples.

Table 1 summarizes results of measurements. Note that FID from water is much longer than FID from acrylic. As a consequence NMR spectrum in water is narrow, whereas in acrylic is extremely broad.

Sample	Phase	FID duration	Spectrum
Distilled water	liquid	35ms	56Hz
Acrylic	solid	80μs	25 kHz

Table 1. Comparison of FID duration time and spectrum width in distilled water and acrylic samples.

---

[1] Remember to add the acquisition delay time, when FID signal was not recorded (usually about 20μs). It significantly contributes to short FIDs.

2.2.6 Two exponential free induction decay in wood

Introduction

Some substances display properties of both liquids and solids. Wood is a good illustration of this case. It contains free, mobile water in capillaries and bound, highly rigid water. The free (liquid-like) water is responsible for the long component in FID signal, whereas bound water (solid-like) for its short component. After Fourier transform, free water is responsible for the narrow peak and bound water for the wide part of the spectrum.

Object

To detect FID signal from protons located in free and bound water in a wood sample.

Directions

- On a **Setup** page prepare an on-resonance one-pulse experiment using the glycerin sample.
- Switch samples and modify **Receiver Gain**, data acquisition time (**Dwell time** and **Number of Points**). Follow screen capture in Figure 13.
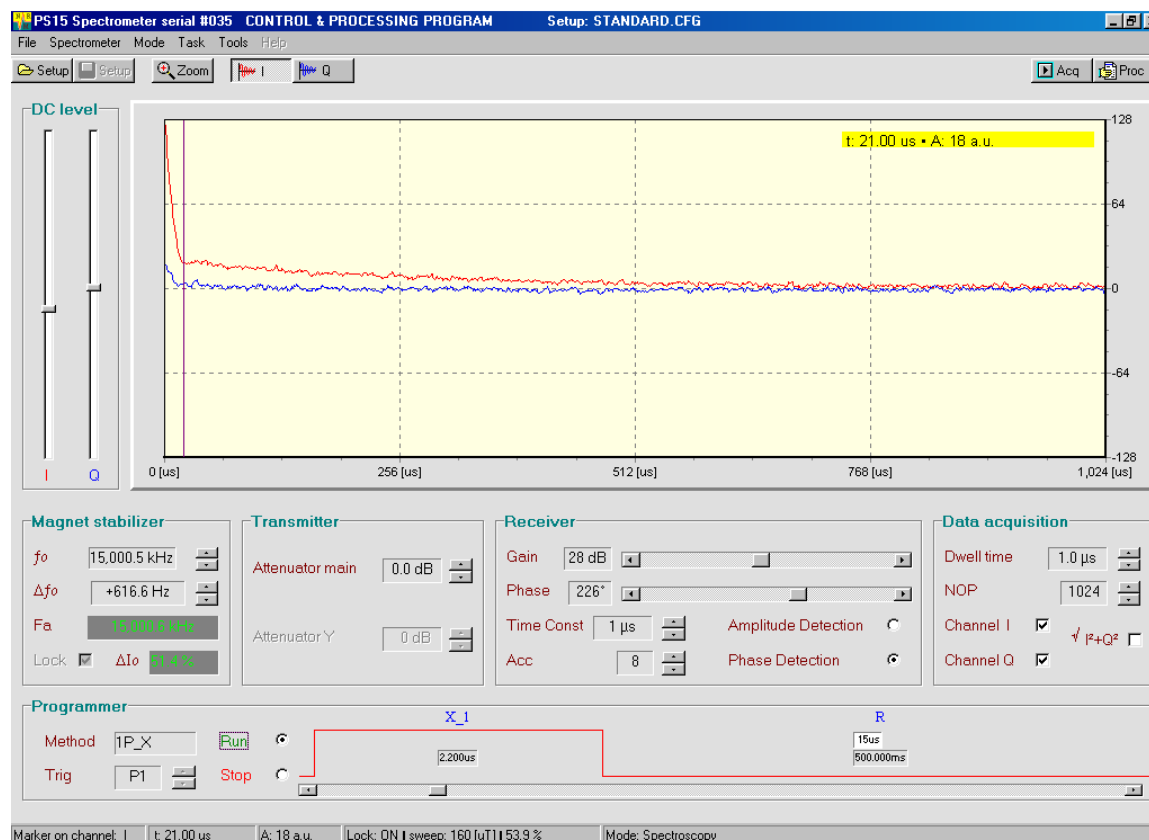
Figure 13. On-resonance FID signal from a dry wood sample.

- Acquire FID on the Acquisition page with 128 or more accumulations.
- On **Processing** page load experimental data and perform Fast Fourier Transform. Estimate manually the line width of the broad and narrow component.
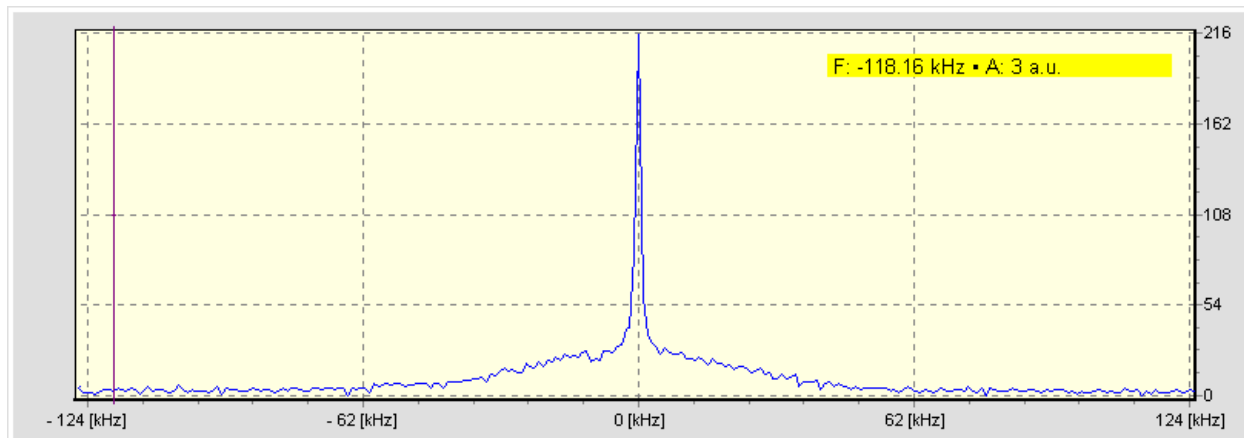
Figure 14. FFT of free induction decay acquired from dry wood. For experimental setup refer to previous figure. Narrow peak is from water in capillaries, broad component originates from bound water.

In the example given in Figure 14 broad component is about 65 KHz and narrow one is about 1kHz. For comparison of FIDs duration times and spectra width see Table 2.

☞   Please keep the wood sample dry to avoid a strong signal from the free water that is responsible for the narrow peak in the center of the spectrum.

Component FID/spectrum	FID duration	Line Width
long/broad	1ms	1kHz
short/narrow	40μs	65kHz

Table 2. FIDs duration time and corresponding line width of two exponential decay in wood sample.

2.2.7 Obtaining off-resonance Spin-Echo

Introduction

Obtaining a spin echo signal requires the application of a two-pulse sequence.

$$\Pi/2 - \text{delay} - \Pi$$

Use 2P_X_D or HAHNECHO sequence. The 2P_X_D sequence consists of two pulses applied along the x' axis, separated by time delay t_D. The length of both pulses as well the time delay is available on the **Setup** page. The HAHNECHO sequence is a simplified version of the 2P_X_D sequence, where the second pulse is automatically set twice as long as first one is. It is very convenient for fast generation of Hahn's spin-echo.

Directions

- With a one-pulse sequence (1P_X preferably) determine the correct conditions necessary to acquire an on-resonance FID after a $\Pi/2$ pulse. Write down the value of the field (**f_0/B_0** and **$\Delta f_0/\Delta B_0$**) and the length of $\Pi/2$ pulse.
- Change the magnetic field using the **Magnet stabilizer>$\Delta f_0/\Delta B_0$** function. Usually adding or subtracting 500Hz is enough to see dozens of FID oscillations i.e. beats between the reference signal and the FID signal from precessing spins in the phase sensitive detector. If a larger offset is required, change **f_0/B_0** by one step. The maximum number of steps available are a maximum of two steps below and ten above the frequency/magnetic field center. Each step coarsely changes the magnetic field by 4.4 kHz/ 0.1 mT. Remember when the value of **f_0/B_0** is changed the program automatically starts to lock at this new field. It takes about three minutes to complete the lock procedure.
- In the **Programmer** select the method: **2P_X_D**. Use the value of the $\Pi/2$ pulse determined in the previously described experiment with FID, as the first pulse value. The second pulse should be made twice as long as the first pulse.
- **Run** the pulse programmer if it is in a **Stop** mode. You should see the picture similar to the Figure 15.
- Select the triggering of the acquisition either after the first or after the second RF pulse. Triggering the acquisition after the first gives you access to both FID and SE signals. Triggering after the second pulse gives access to only the SE signal.
- You may need to change the data **Acquisition time** to cover the duration of FID and the whole spin echo signal, depending of the triggering mode. Proceed to **Data acquisition** and change either **Dwell time** (**DW**) or **Number of Points** (**NOP**) to get the necessary "time window" that will cover FID, spin-echo and some of base line noise (**Acquisition time = DW x NOP)**.
- Go to the **Acquisition** page to acquire data. Type the file name and the

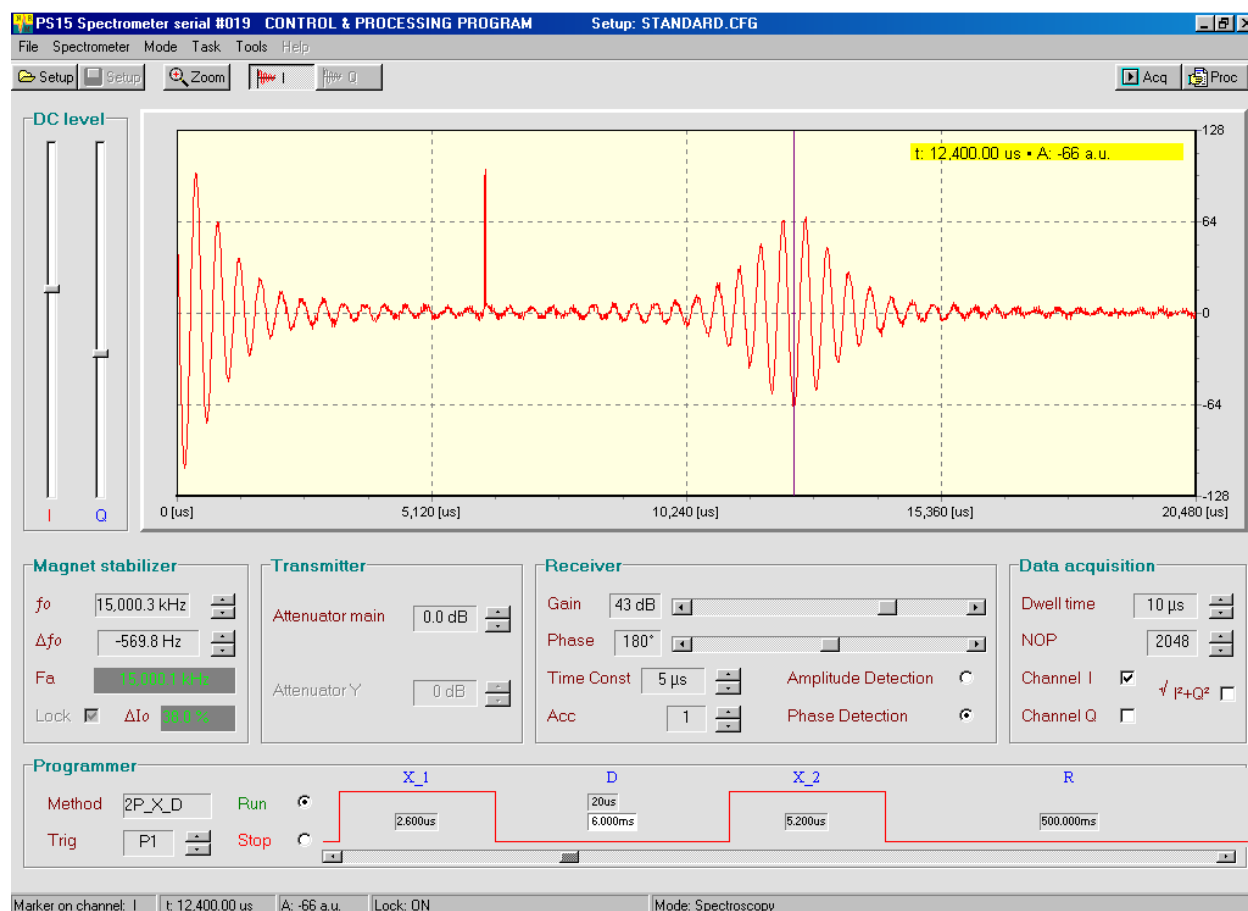number of accumulations to be performed and run the experiment.

Figure 15. Off-resonance Free Induction Decay and Spin Echo signals after two pulse sequence. Spike between FID and SE corresponds to the second pulse.

2.2.8 Obtaining on-resonance Spin-Echo

Introduction

To check the influence of the pulse power and length on the spin echo picture go to on-resonance conditions. On-resonance spin echo is very sensitive to the B_0 field instability, B_1 field inhomogeneity, as well as the pulse and reference phase.

☞   It is rather difficult to acquire on-resonance spin echo in a perfect shape and keep it in long time. PS15 pulse spectrometer provides excellent long-term magnetic field stability by locking field to resonance on ^{19}F nuclei (NMR lock).

Directions

To see nice spin echo you may need to adjust several times following:

- **$\Delta f_0/\Delta B_0$,**
- pulse length,
- phase,
- gain,
- sample position.

Figure 16 shows on-resonance free induction decay and spin echo signals from a glycerin sample taken at room temperature. The spike between FID and spin-echo is a refocusing Π pulse that follows $\Pi/2$ after delay T_D. The center of the spin echo is exactly at $2T_D$. Note the spin-echo signal has inversed polarity with regard to the FID signal as it represents the magnetization component that is produced along the –y' axis.
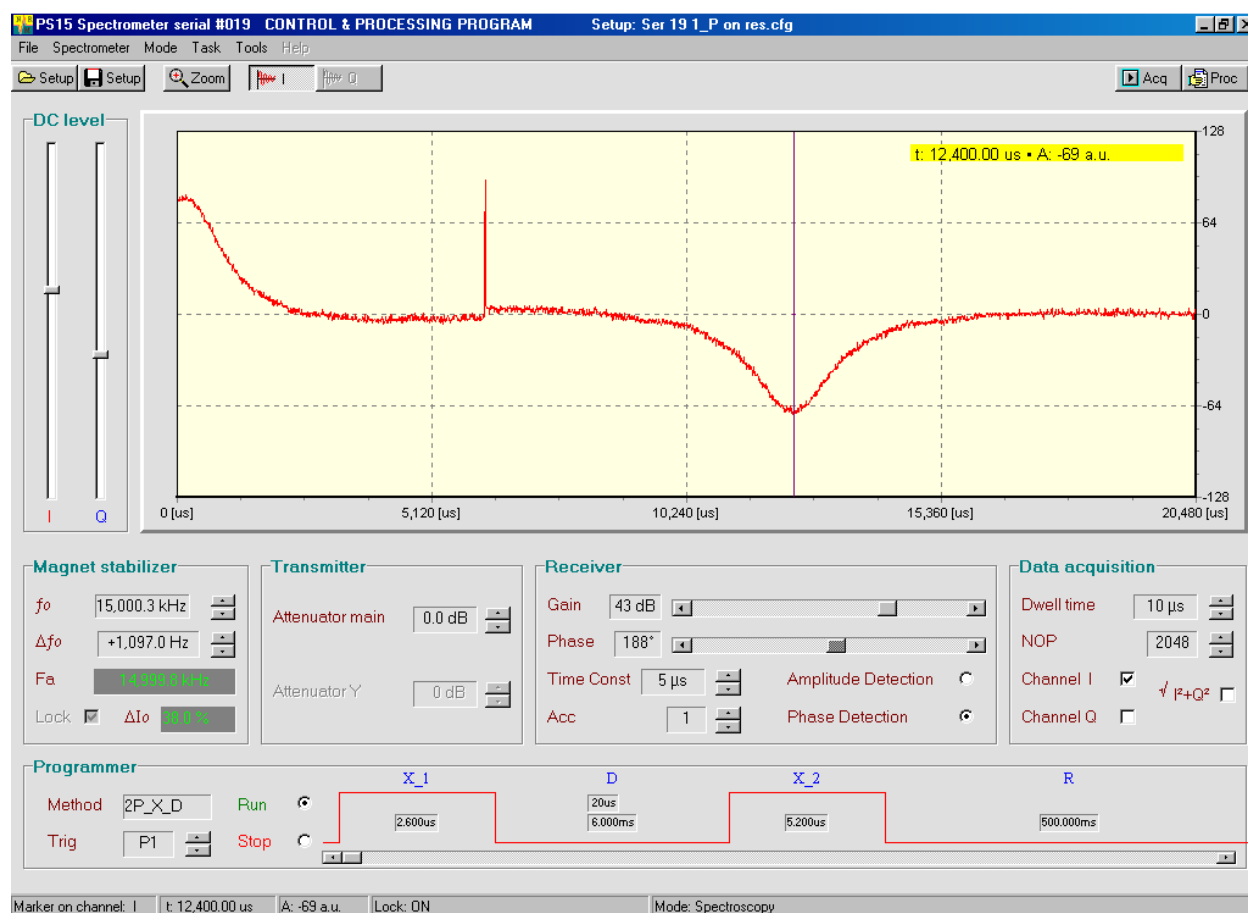
Figure 16. On-resonance FID and spin echo signal in two-pulse sequence

2.2.9 Rotating the magnetization along different axis.

Introduction

The analysis of interaction of the RF pulse with nuclear magnetization **M** in a constant magnetic field **B₀** is simplified in a reference frame that rotates with the Larmor frequency $\vec{\omega}_0 = -\gamma \cdot \vec{B}_0$. At resonance ($\omega_0 = \omega_{RF}$) the component originating from the **B₀** field is cancelled and only the **B₁** component interacts with the magnetization. In a rotating frame, magnetic field **B₁** becomes constant and exerts a torque on a magnetic moment moving it along **B₁** with angular speed $\vec{\omega} = -\gamma \cdot \vec{B}_1$ (in the same way, the **B₀** field causes precession of **M** in a laboratory frame). If after a time t_p, the **B₁** field is turned off the movement of magnetization stops and from angular speed definition $\omega = \dfrac{\Theta}{t_p}$ we can calculate a rotation angle using formula $\Theta = \gamma \cdot B_1 \cdot t_p$. Figure 17 shows magnetization rotation caused by **B₁** field at several steps.
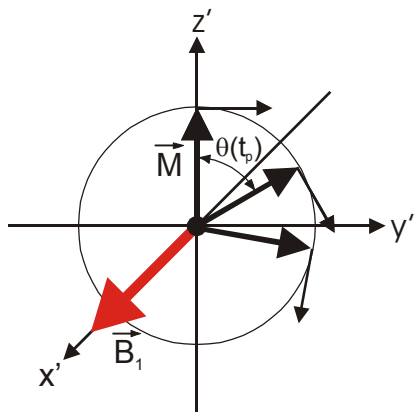
Figure 17. Precession of the nuclear magnetization $\vec{M}$, around $\vec{B}_1$ field in a rotating frame.

For further considerations, we will assign RF pulses along any axis in x'y' plane. The Spectrometer, however, can generate only four types of pulses with their phase shifted by 0°, 90°, 180° and 270° (phase shift is measured with regard to the first pulse so by definition its phase is 0°). We assign arbitrary **B₁** direction of these pulses along +x, -y, -x, +y, respectively. Of course any other assignment of axis is entirely justified.

The phase sensitive detector traces changes of magnetization within the rotating frame due to application of the RF pulse. With a phase shift of the reference signal properly adjusted, the detector produces an electric signal that is proportional **only** to the amplitude of the magnetization component along the y' axis.

Object

- Observation of the effect of the RF pulse phase on nuclear magnetic detection in a rotating frame.

- Acquisition of FID signals after **1P_X**, **1P_-X**, and **1P_Y** pulses.

☞ Note the inversion of the FID after **1P-_X** pulse and disappearance after **1P_Y**.

Directions

- Use a glycerin sample that produces a strong NMR signal.
- Modify **Setup** to obtain on-resonance FID after one-pulse **1P_X** sequence. Screen capture in Figure 6 may help in preparation.
- Adjust the phase of the reference signal (**Receiver>Phase**) to see the strongest positive signal after detection. This signal represents the projection of the macroscopic magnetization on y' axis (see Figure 18).
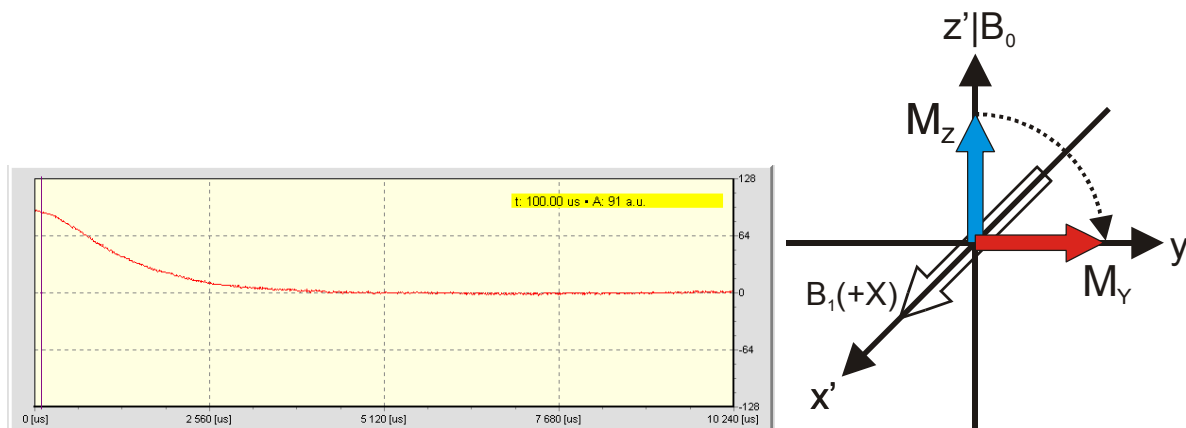
Figure 18. Flipping the magnetization on X'Y' plane by $\Pi/2$ pulse along the X' axis (**1P_X**). Experimentally acquired FID is on the left and vector diagram is on the right.

- Change the phase of the RF pulse by selecting **Programmer>Method>1P_-X**. This pulse rotates the magnetization along the −X axis (180° phase shift). Without manipulating the receiver phase you should see inversion of FID shown in Figure 19.
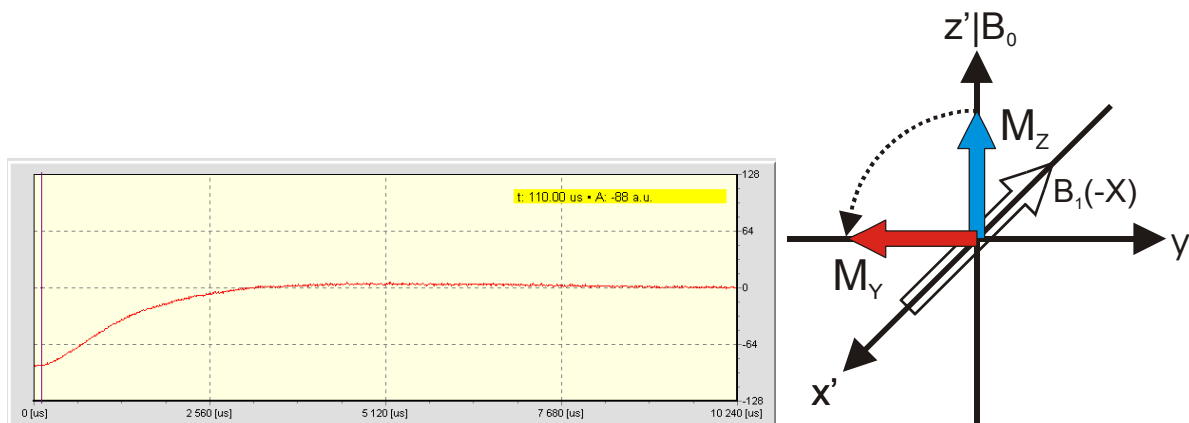
Figure 19. Inversion of the FID polarity after the use of $\Pi/2$ pulse along the –x axis (**1P_-X**).

- Now apply the pulse along the y' axis. This pulse moves the magnetization on the –x' axis. If the phase of the pulse is exactly 270° and the pulse is exactly a $\Pi/2$ pulse, the magnetization component along y' axis should be zero (see Figure 20).
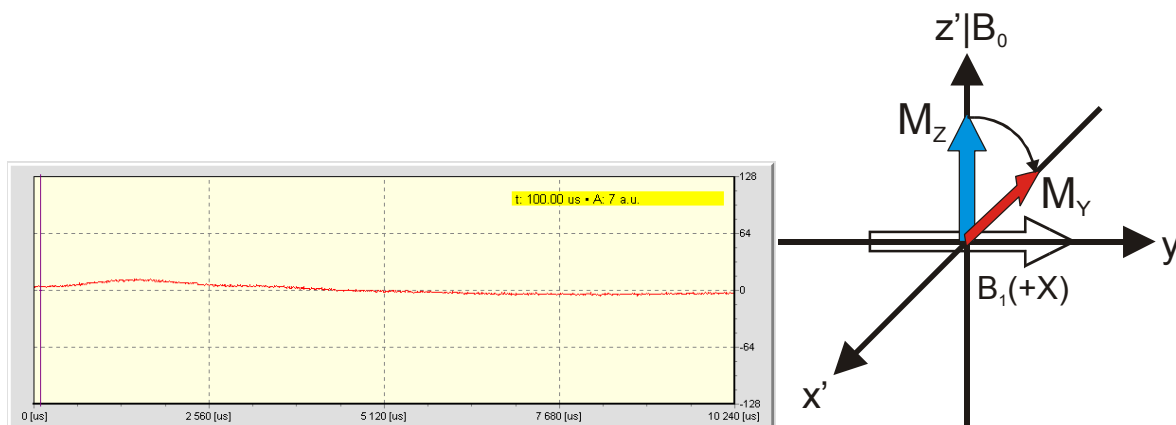
Figure 20. Disappearance of FID signal after applying a $\Pi/2$ pulse along the y' axis (**1P_Y**). The little trace of FID is due to inaccuracy of setting the length and the phase of the exiting pulse.

You can "see" **M$_y$** aligned along –x axis (rather phase detector can detect it) if you will now change phase of reference signal. Of course change by +/-90° delivers the best effect.

2.2.10 Signal-to-Noise measurements

Introduction

Raw data acquired in an NMR experiment (FIDs or spin echoes) usually require further processing to obtain spectra or relaxation time values. Regardless of the method of processing, raw data must be **free** of disturbances that may affect final results.

NMR signals are extremely week and usually disturbed by noise of various origins. The desire of people designing NMR equipment is to **minimize** inherent noise that the spectrometer may introduce. This can be achieved by use of low-noise components, elimination or shielding sources of potential interferences, and signal filtering.

On the other hand researchers can **maximize** signal amplitude by optimizing the experimental parameters like RF pulse width (to achieve a correct flip angle), repetition time (to avoid saturation), selecting correct filters in the detector and adjusting the position of the sample.

The parameter that describes the spectrometer's ability to detect weak signals is Signal-to-Noise ratio (**SNR** or **S/N**). It gives a measure of spectrometer sensitivity and allows the comparison of one spectrometer to another.

The popular definition of SNR is the **ratio of the peak of the observed signal to noise peak-to-peak**.

The **signal peak amplitude** can be easily determined as a tallest peak in the region if it is visible from noise background.

The **noise peak-to-peak** can be approximated as double root mean square of several data point amplitudes taken in the area of pure noise.

$$\text{noise peak} - \text{to} - \text{peak} = 2 \cdot \sqrt{\frac{\sum_{i=1}^{n} A_i^2}{n}} \qquad\qquad \text{Eq. 4}$$

Where:
- A_i is noise data point amplitude,
- n is number of points used for calculations and should be reasonably large to minimize statistical errors.

If the noise background has a random character, then investigators have a powerful tool to increase Signal-to-Noise ratio, namely, **signal averaging.** Averaging depends on the acquisition of consecutive signals and adding them. In this process non-coherent noise reduces gradually to zero whereas coherently appearing NMR signals add and gradually increase the effective amplitude.

Assuming the presence of random noise only (called "white noise") the average improvement of Signal-to Noise ratio is proportional to the **square root** of the number of

accumulations N (see Eq. 5).

$$SNR \approx \sqrt{N}$$

Eq. 5

For example to double Signal-to-Noise ratio approximately four as many signals must be acquired.

Object

Signal-to-Noise ratio measurements of the FID signal. The same measurements can be performed with the spectrum. We strongly recommend to do FFT of acquired FIDs and compare results of S/N in FIDs and spectra.

To illustrate the improvement of SNR we will do different numbers of signal accumulations of a FID from a polymer sample that has a short and weak signal.

Directions

- Achieve on-resonance conditions with **glycerin** sample and one-pulse sequence **1P_X** [$(\Pi/2)_x$ pulse] and repetition T_R=500ms).
- Remove the **glycerin** sample and place the sample labeled as delrin in the sample holder.
- In **Data acquisition** select **Channel I**, set **Dwell time** to 0.4μs, number of points **NOP**= 512.
- In **Receiver** set **Gain** and **Phase** to see good signal but with a lot of noise.
- Carefully compensate any DC offset by **DC level**.
- On the **Acquisition** page acquire FIDs with N=1,2,4,8,16,32,64,128 accumulations and store them in separate files.
- On the data **Processing** page load raw data.
- Measure peak amplitude of the FID and take 15-20 samples of noise from the signal "tail".
- Calculate **noise peak-to-peak** as double rms noise level and **SNR** (see equations).
- Repeat measurements and calculations for all number of accumulations N.
- Make plot of SNR versus N.
- To accelerate calculations you can export raw data as text files and import them to any popular spreadsheet program like Excel.

Figure 21 shows collections of FID signals for different accumulation numbers. A significant decrease of noise due to averaging process is visible.

Calculated values of SNR presented as a function of the number of accumulations are shown in Figure 22. Small insert in the figure illustrates the almost linear dependence of (SNR)^2 versus N for high values of N. For small values of accumulation numbers the SNR improves faster.
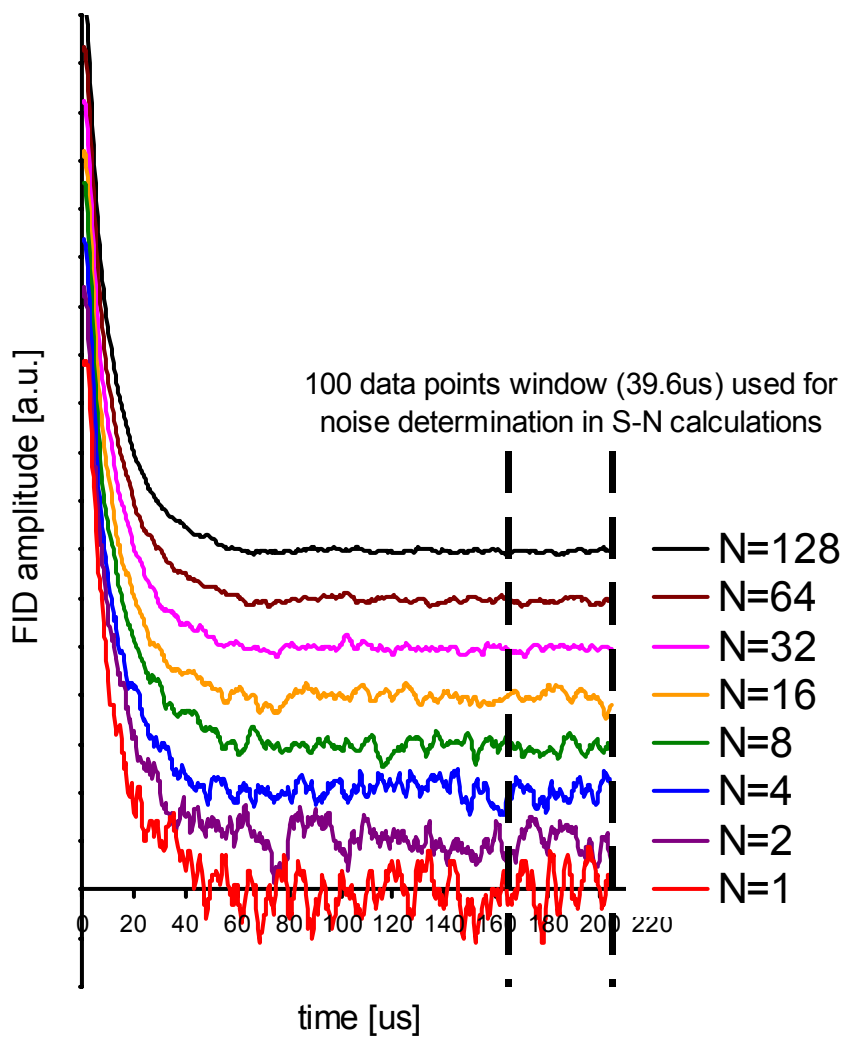
Figure 21. Noise reduction on the FID signal due to averaging process.
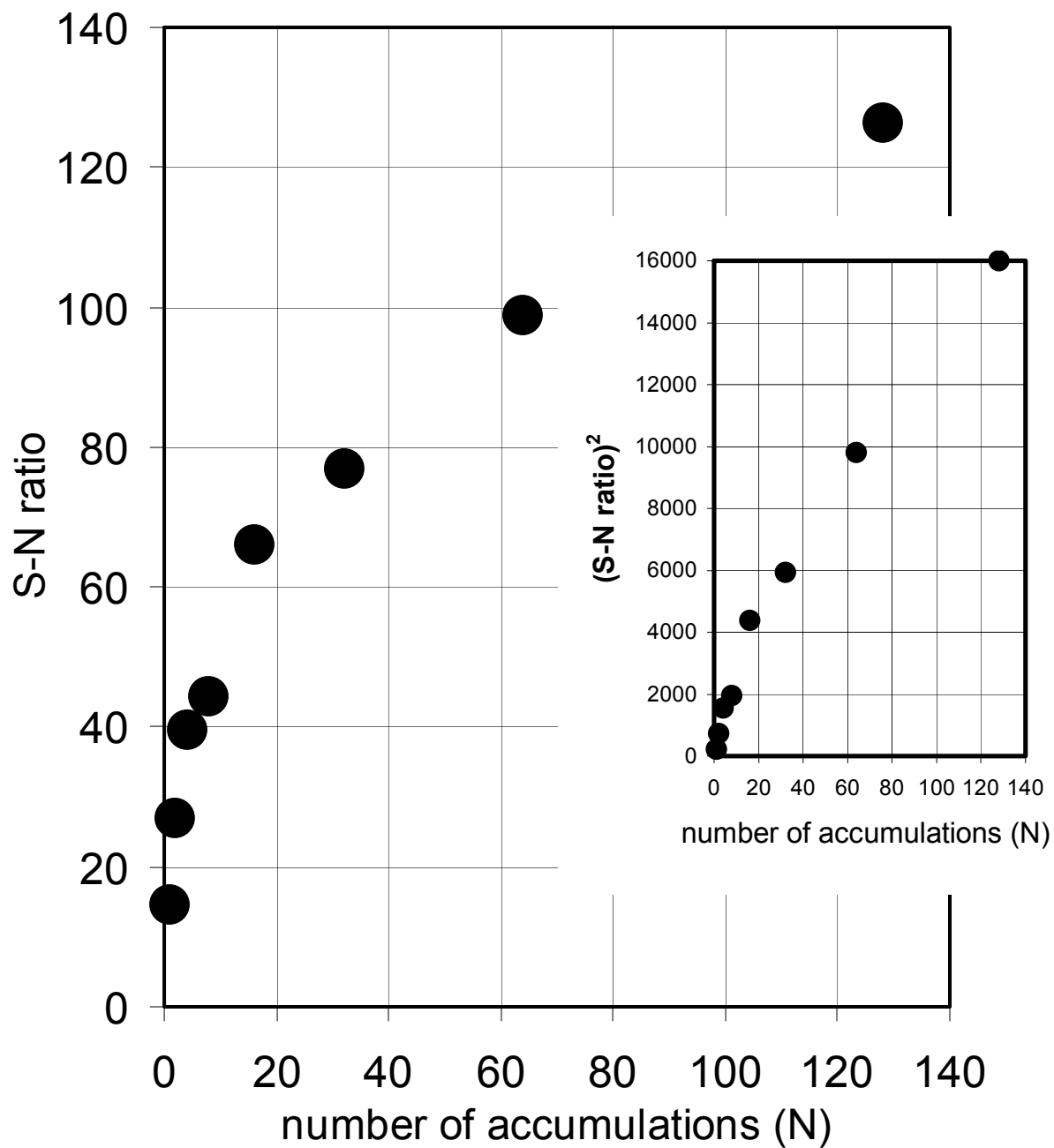
Figure 22. Signal to noise ratio S-N measured for FID in a polymer sample as a function of the number of accumulations N.

2.2.11 Spectrometer "dead time"

Introduction

The nuclear spin evolution due to an RF pulse can not be registered immediately after the end of the RF pulse because some valuable information is irreversibly lost. This happens because of the temporary overloading of the sensitive receiver by a powerful RF pulse. The receiver returns from saturation to function normally after a time called the "dead time". Data acquisition must be postponed for a time longer than the "dead time" as shown in Figure 23.
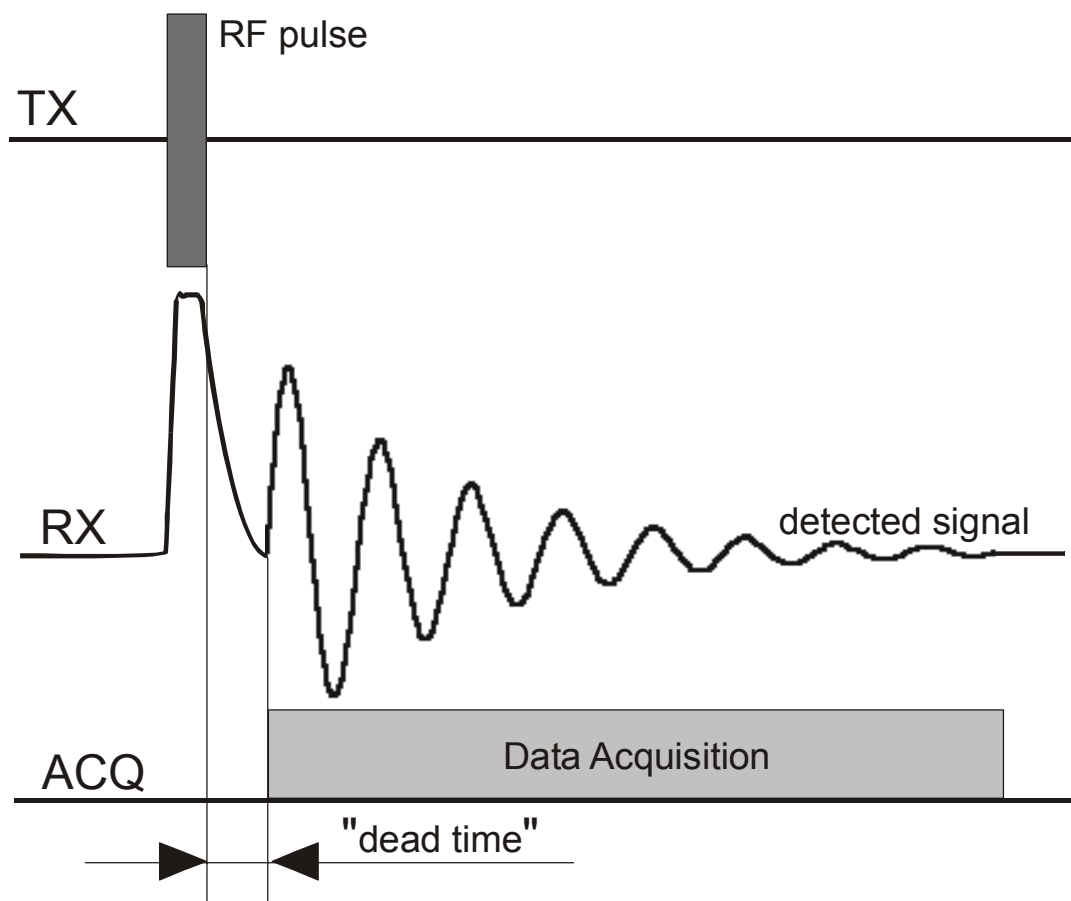
Figure 23. Postponing data acquisition to eliminate spectrometer "dead time" problem.

Quality factor (Q) of the probehead resonance circuit that operates as transmit-receive antenna and pulse power are major contributors to the "dead time". High Q resonant circuits tuned to frequency f_{RF} have tendency to store RF pulse energy longer and as a consequence they ring longer after the pulse stops.

The falling time T_f of the RF pulse in a resonant circuit that is mainly responsible for ringing is related to frequency and quality factor by formula:

$$T_f \cong \frac{Q}{f_{RF}}$$

<div align="right">Eq. 6</div>

The PS15 has a built-in multiplexing system that directs RF pulses from the transmitter to the resonant circuit while blanking the sensitive preamplifier and thus protecting it from high power during the transmit period. During the receive period the transmitter is disconnected and the preamplifier input is open.

The operator can delay the acquisition manually to eliminate all affected data points from registration. For the safety of the preamplifier, this delay can not be shorter than 2µs.

Effective "dead time' varies from model to model and is usually less than 20µs and depends very much on the total amplification of the receiver.

Object

Measurement of spectrometer "dead time".

Directions

- Prepare a one-pulse experiment with the acrylic sample that gives an extremely short and weak FID signal (shorter than 75µs). To avoid integration of the fast transients remember to reduce the RC filter time constant to **1µs** (**Receiver>Time constant>1µs**).
- Set data acquisition for shortest **Dwell time** of 0.4 µs and number of points **NOP**=512. This gives a correct time scale to watch what happens during the beginning of data acquisition. Set acquisition delay time to minimum (2µs, see figure on left) .
- Remove the sample.
- Place the data marker on the end of the transient and read time (Figure 24). Add additional 2µs and this is the **"dead time"** for your particular probehead. "Dead time" in Figure 24 is (2+15.2)µs =17.2µs.
- Insert sample and watch how FID superimposes on "dead time" transients (Figure 25).
- Remove sample again. Increase data acquisition delay from 2µs to 20µs and watch disappearance of unwanted transients (Figure 26).
- Place the sample back in the sample holder and look at "clean" FID. Figure 27 shows undisturbed FID from acrylic. Compare it to results in Figure 25.
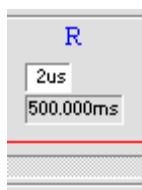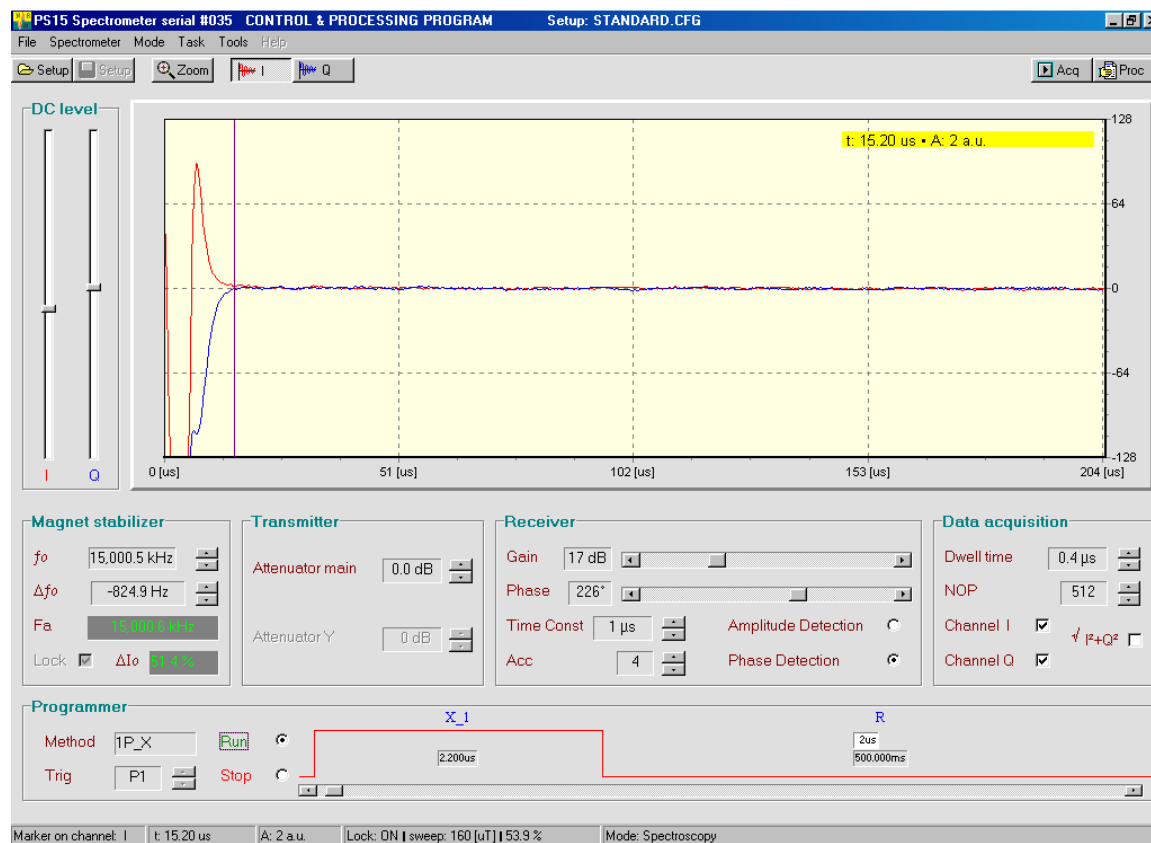
Figure 24. Measuring "dead time" of unloaded resonant circuit in PS15 probehead. Transients disappear after (2+15.2)µs though RF pulse lasts only 2.2µs.
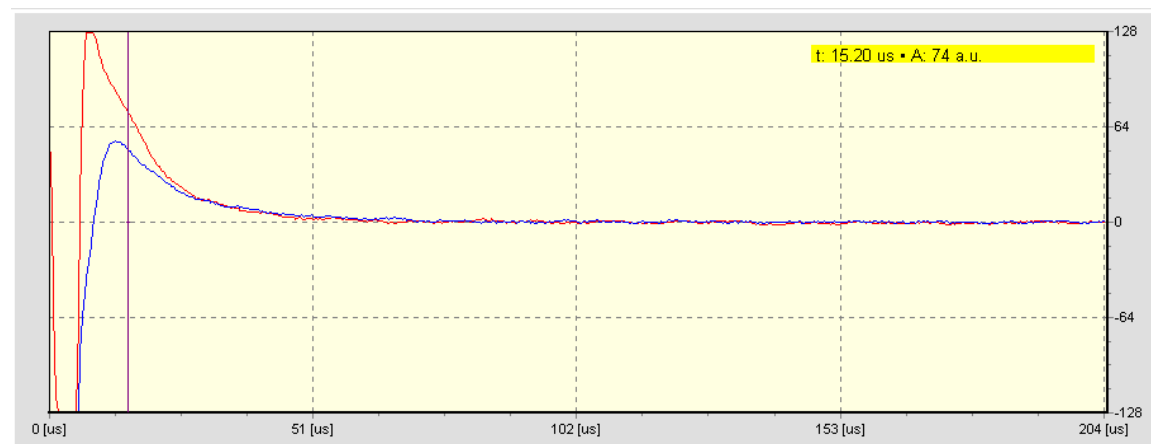
Figure 25. FID signal from acrylic sample disturbed by 17.2µs "dead time".
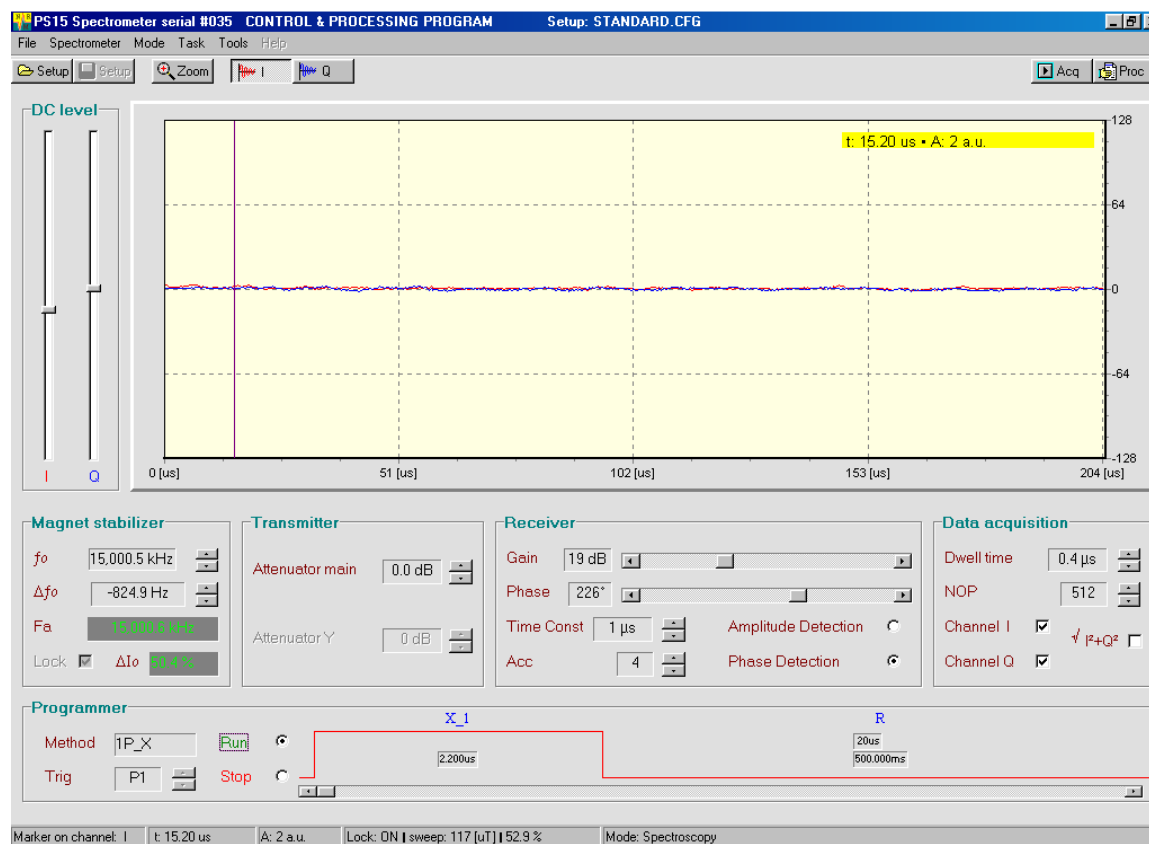
Figure 26. Postponing acquisition by 20μs removes "dead time" transients from the acquisition window. Note that base line is entirely flat.
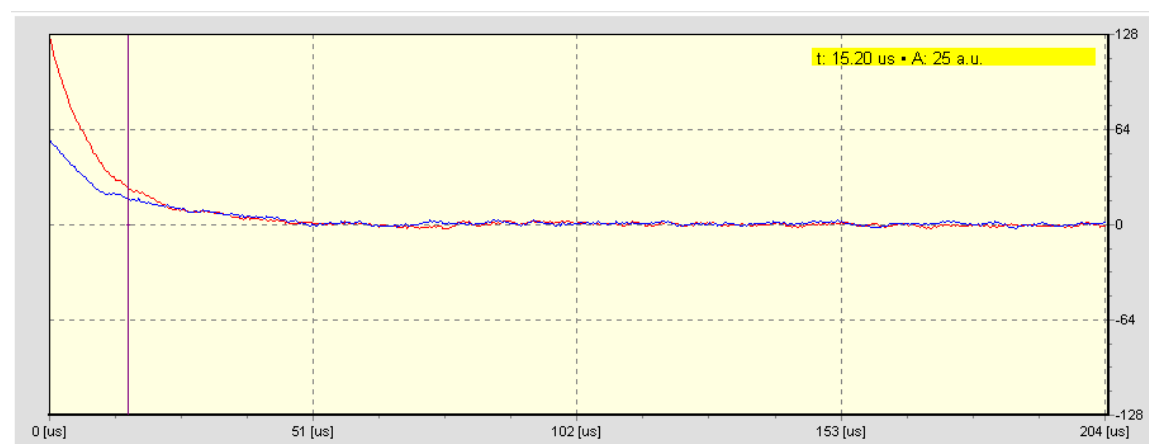
Figure 27. With 20μs acquisition delay data window shows only "clean" part of FID signal. Operator can achieve the same effect by Left Shift (**LS**) operation on the **Processing** page.

3   NUCLEAR SPIN-LATTICE T_1 RELAXATION MEASUREMENTS.

3.1 Theory

Description

At the equilibrium state all nuclear moments in a sample are distributed among the energy levels according to Boltzmann law. The Boltzmann distribution slightly prefers an orientation of nuclear moments towards the polarizing field $\mathbf{B_0}$. This preference builds a minute nuclear macroscopic magnetization $\mathbf{M_0}$ along the $\mathbf{B_0}$ field. Following any process which disrupts this distribution, eg. applying RF pulses, the nuclear spin system returns to equilibrium with the surrounding lattice by a process called spin-lattice relaxation that is characterized by a time T_1.

Pulse NMR provides the most versatile method to measure T_1 relaxation times over a wide range of times. In this manual we will analyze and apply the *Inversion Recovery* and *Saturation Recovery* methods for T_1 measurements.

3.1.1 Inversion Recovery method

Among different sequences used to measure T_1, *Inversion Recovery* is the most popular one. It consists of two pulses: a Π pulse and $\Pi/2$ following pulse separated by variable delay time t_D (see Figure 28).
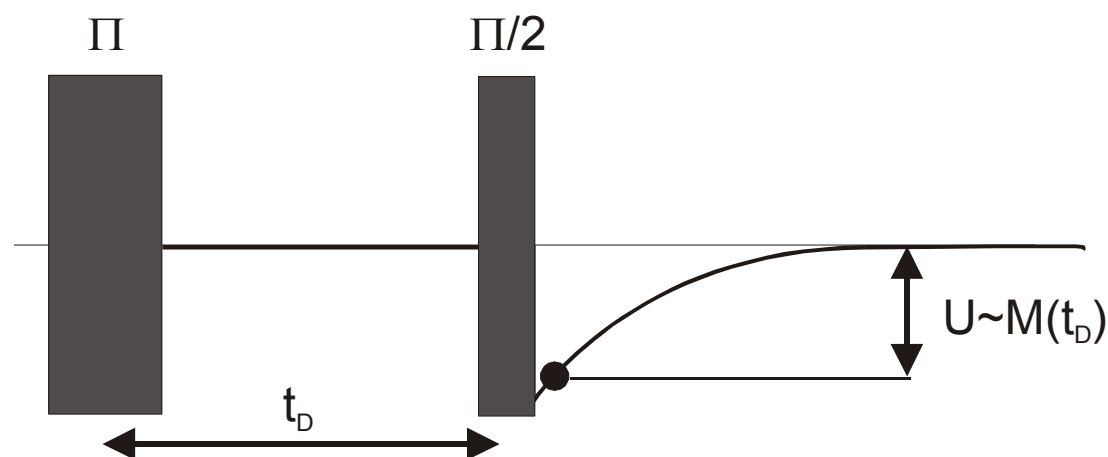
Figure 28 Inversion-recovery sequence. Note that no signal arises after first Π pulse.

The first Π_x pulse flips the nuclear magnetization onto the $\mathbf{-B_0}$ direction. Due to relaxation processes between nuclear spins and the lattice the magnetization returns to its equilibrium from $\mathbf{-M_0}$ through all intermediate values to $\mathbf{+M_0}$ along $\mathbf{+B_0}$. The recovery of the magnetization is monitored after a delay time by a second $(\Pi/2)_x$ pulse. The amplitude of FID is proportional to the nuclear magnetization. To avoid any interference

from the receiver "dead time" generated after a $(\Pi/2)_x$ pulse the FID should be sampled after some additional delay. Figure 29 shows an example of the exponential increase of FID amplitude corresponding to recovery of nuclear magnetization from $-M_z$ to $+M_z$.
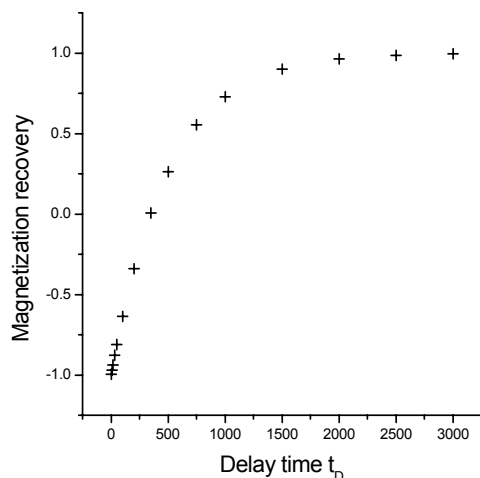
Figure 29. Gradual net magnetization recovery from $-M_0$ to $+M$.

To make calculations simple, each experiment, for a certain delay, must start after magnetization completely returns to equilibrium. This is achieved by waiting a sufficient time T_R (**Repetition Time**) for a complete recovery after the 90° pulse, (after $T_R = 5*T_1$ the nuclear magnetization returns to 99.9% of the initial magnitude).

3.1.2 Solving Bloch equation for the *Inversion Recovery* method

Recovery of the magnetization is given by the Bloch equation:

$$dM_z(t)/dt = - (M_z(t) - M_0)/T_1 \qquad\qquad \text{Eq. 7}$$

Assuming complete inversion after first pulse at t=0 we have $M_z(0)=-M_0$. Integrating the above differential equation gives:

$$M_z(t) = M_0 (1 - 2 * \exp(-t/T_1)) \qquad\qquad \text{Eq. 8}$$

Or in linear form:

$$\ln\left(\frac{M_0 - M_z(t)}{2M_0}\right) = -\frac{1}{T_1} t \qquad\qquad \text{Eq. 9}$$

Thus T_1 can be found from the measurements of $M_z(t)$ as a function of the time delay t_D between Π and $\Pi/2$ and the further fitting of experimental data to the equation Eq. 9.

In experimental practice Eq. 9 can be expressed in terms of spectroscopy measurable parameters:

$$\ln(A_0 - A(t_D)) = \ln 2A_0 - \frac{1}{T_1}t_D \qquad \text{Eq. 10}$$

Where:

A_0 is FID amplitude at the time when magnetization returns to equilibrium state (corresponds to M_0),

$A(t_D)$ is FID amplitude at given time t_D (corresponds to $M_z(t)$

One can calculate T_1 from the slope of a plot of $\ln(A_0 - A(t_D))$ versus t_D.

To have quick but reasonable estimation of T_1 find that when magnetization reaches zero $A(t_D)=0$ from Eq. 10 we have:

$$t_D = \ln 2 \cdot T_1 = 0.69 \cdot T_1 \qquad \text{Eq. 11}$$

Thus one can find T_1 easily from t_D delay that produces zero FID signal after second $(\Pi/2)_x$ pulse ($T_1=T_D/0.69$).

Inversion-recovery sequence and the net magnetization dynamics for several interpulse delays are shown in Figure 30.
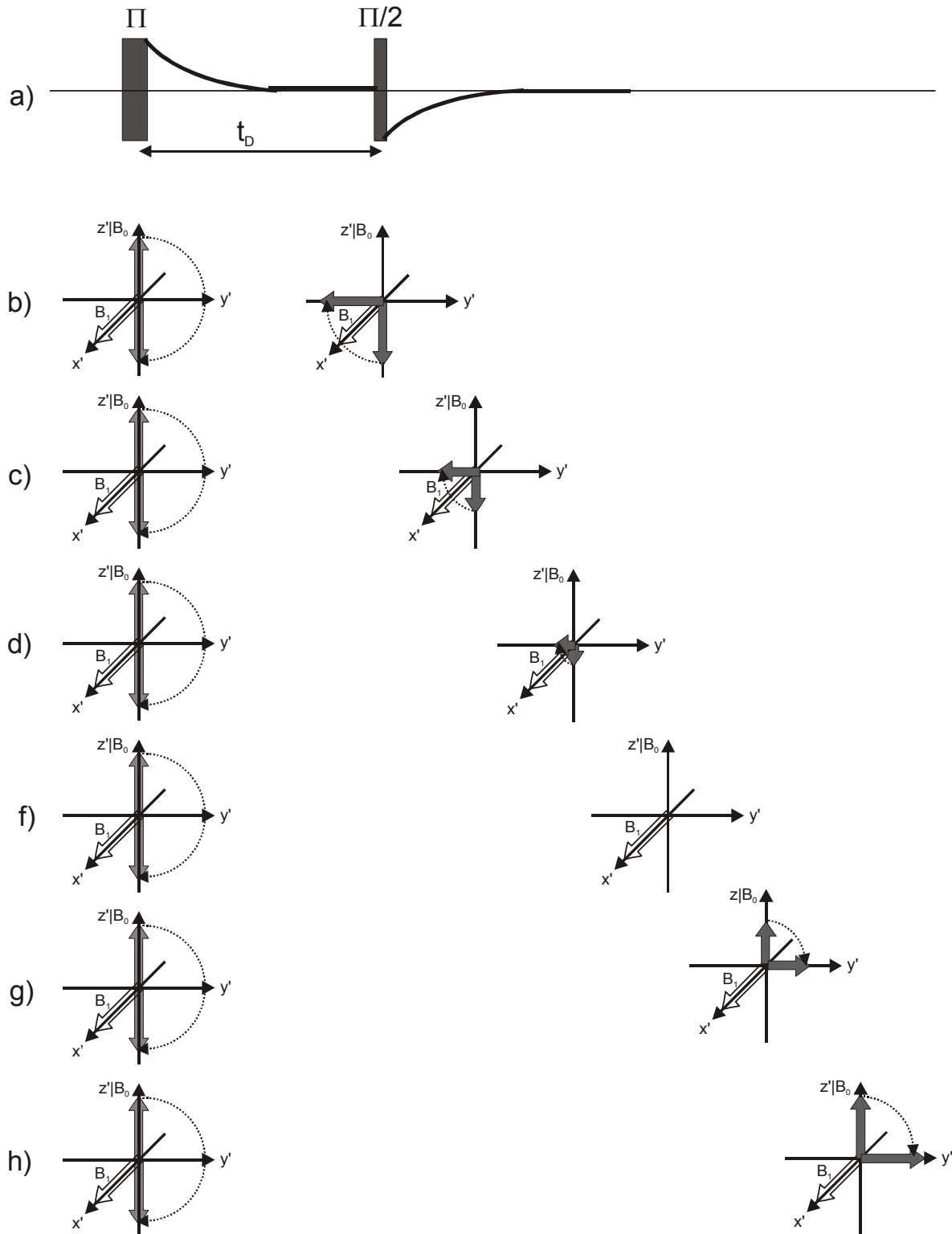
Figure 30. Inversion-recovery sequence and net magnetization dynamics for different interpulse delays t_D.

3.1.3 Saturation Recovery method

The Inversion Recovery method requires a long delay between applying consecutive sequences to allow complete relaxation of spins after the second $\Pi/2$ pulse. This makes the *IR* method more time consuming for samples characterized by long T_1 times. The *Saturation Recovery* (*SR*) method eliminates the need for a long delay by applying a train of $\Pi/2$ pulses separated by time τ at the beginning of the sequence. The train of $\Pi/2$ pulses will quickly destroy any macroscopic magnetization and dynamic equilibrium state will be reached between the spins excitation and relaxation quickly. When pulses stop, spins relax undisturbed and the magnetization along z-axis builds again. The recovery process due to T_1 relaxation from saturation can by monitored by applying the sampling pulse $\Pi/2$ after the t_D delay.
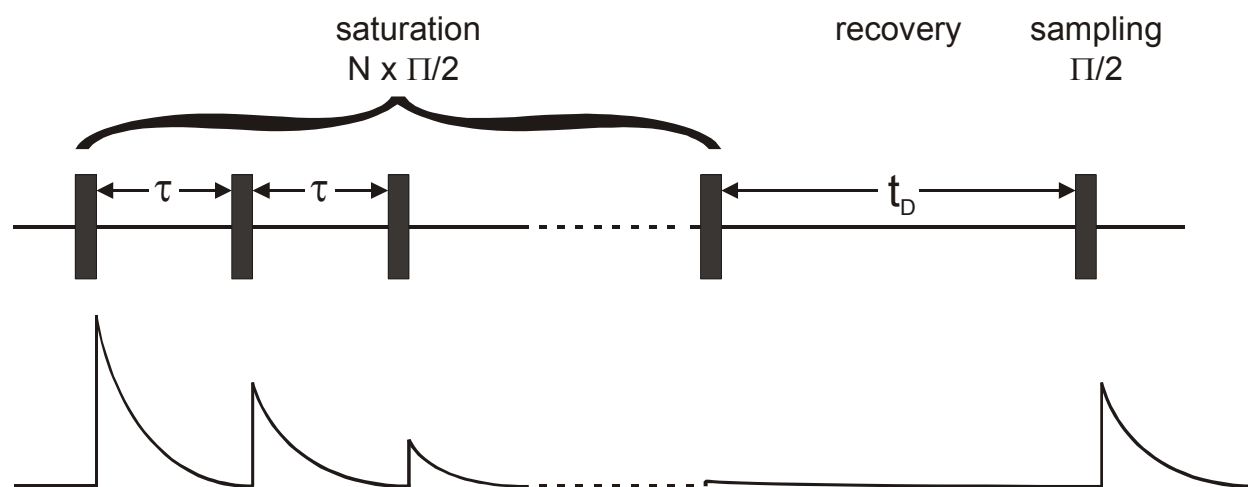
Figure 31. *Saturation Recovery* method.

The Bloch equation for the *Saturation Recovery* can be solved now with new beginning conditions $M_z(0)=0$ (note that for *IR* $M_z(0)=-M_0$):

$$M_z(t) = M_0(1 - \exp(-\frac{t}{T_1}))$$

Eq. 12

Or in more practical version:

$$\ln\left(\frac{M_0 - M_z(t)}{M_0}\right) = -\frac{1}{T_1}t$$

Eq. 13

Plotting semilogarithimic graph of $\ln\left(\frac{M_0 - M_z(t)}{M_0}\right)$ against $t=t_D$ returns $-\frac{1}{T_1}$.

3.2 Experimental

3.2.1 Measuring T_1 by *Inversion Recovery* method in distilled water, ethanol, water doped with $CuSO_4$, glycerin and rubber

Directions on the Setup page

- Start measurements with a glycerin sample. After acquiring satisfactory results continue experiment with rest of samples.
- Activate data acquisition only in one channel (real **I** or imaginary **Q**).
- Use **1P_X** sequence to obtain on-resonance FID (follow directions in chapter 2.2.1).
- Set the data acquisition time to cover entire FID (1024 μs recommended).
- Determine and record the time of $\Pi/2$ and Π pulses,
- Set the proper **Receiver Gain**, **Phase** and **DC level**. With good magnet homogeneity the on-resonance FID signal from glycerin will decay exponentially into noise after about 5 ms. Figure 32 illustrates typical experimental setup.
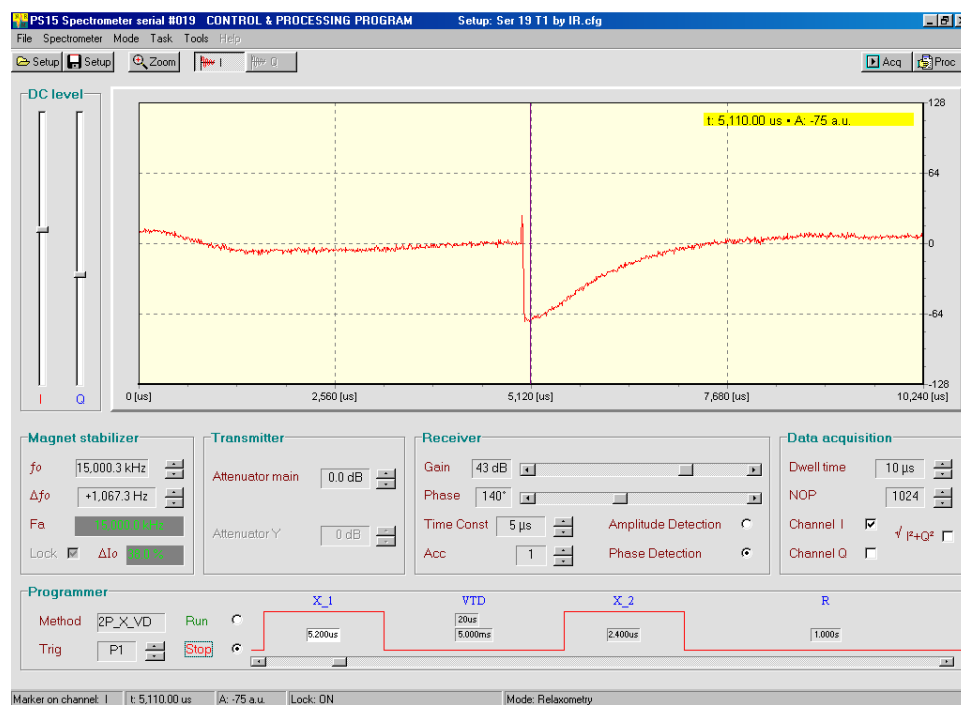
Figure 32. **Setup** page during preparation of T_1 measurements by *Inversion Recovery* method. Before going to **Acquisition** page switch data acquisition triggering **Programmer>Trig** from **P1** (after 1st pulse) to **P2** (after 2nd pulse).

- In **Programmer** click **Method** and select **2P_X_VD**, which is a two-pulse method that uses a list of variable time delays in the pre-prepared file.
- Modify sequence parameters:

- ❑ 1st pulse=Π (If you do not know it start assuming that this pulse is twice as long as the earlier determined $\Pi/2$. Adjust Π precisely later.
- ❑ Delay time 5 ms; not critical as it will be ignored later during data acquisition to file when delay times from prepared list are in use.
- ❑ 2nd pulse=$\Pi/2$.
- ❑ Repetition time **T$_R$=1s**, (generally repetition should be five times longer than expected T$_1$).

☞   **Very important!** To store recovering FID trigger data acquisition (**Trig**) after 2nd pulse (P2).

If properly adjusted there will be no signal after first Π pulse and strong FID after second $\Pi/2$ sampling pulse. In Figure 32, which illustrates the *IR* experiment in glycerin, the residual FID after the first pulse is due to inaccuracy of Π pulse.

Directions on the Acquisition page

- In bottom right dialog window:
  - ❑ Type file name.
  - ❑ Type number of accumulations.
  - ❑ Type comment.
  - ❑ Select variable time delay file. If necessary modify time list.

- **Start** acquiring data ▶ Start . Check on the bottom window if delay times are long enough to reach equilibrium range. You need 3-4 points from this area for **M$_0$** determination used later in T$_1$ calculations. Change timing or add few more points if necessary.
- Before leaving **Acquisition** page check bottom status line to assure that data was stored in a declared file.

Repeat measurements of all samples. After placing a new sample into the holder do again all adjustments on the **Setup** page and complete with data acquisition on the **Acquisition** page. More than likely you will change only the receiver **Gain**, repetition time **T$_R$**, number of accumulations and file with list of pulse delays. Figure 36 through Figure 40 may help you in experimental preparation.

Long spin-lattice relaxation time in distilled water presents an interesting challenge. Complete measurement requires a relatively long time to conduct but illustrates nicely the importance of long time separation to see the complete recovery of spins after the Π pulse. In Figure 35 magnetization still points toward $-B_0$ axis when 100ms after inversion sampling $\Pi/2$ pulse was applied. In Figure 34 magnetization fully recovered when was sampled by $\Pi/2$ pulse after 32 s delay!
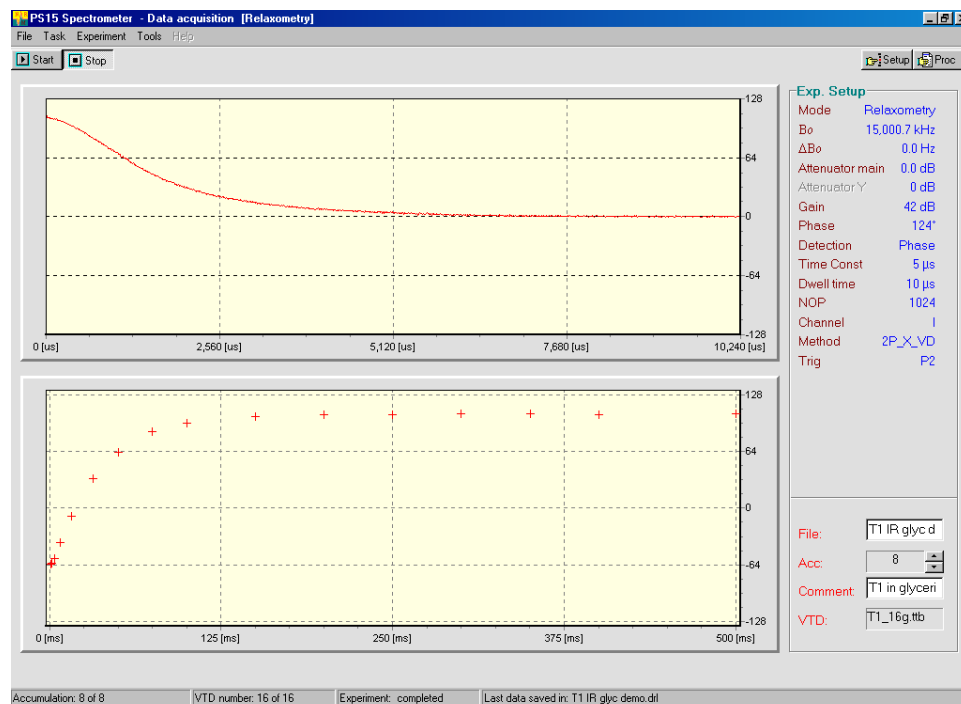
Figure 33. Acquiring data by *Inversion Recovery* method. Note that amplitudes of extracted points increase monotonically from negative to positive values and reach asymptote when nuclear spins completely recover.

Directions on the Data processing page

On the **Processing** page you can process relaxation data using the *Inversion Recovery* calculation routine. You can also extract data points and export as text for further calculations using any software you prefer (Excel, Origin, Mathematica, etc).

- **Load** data.
- **Set Mark** to lock data marker on the beginning of FID.
- **Extract** data points. Extracted data points appear on the bottom window.
- Execute **T_1 by IR** routine, that calculates T_1 by linear regression.
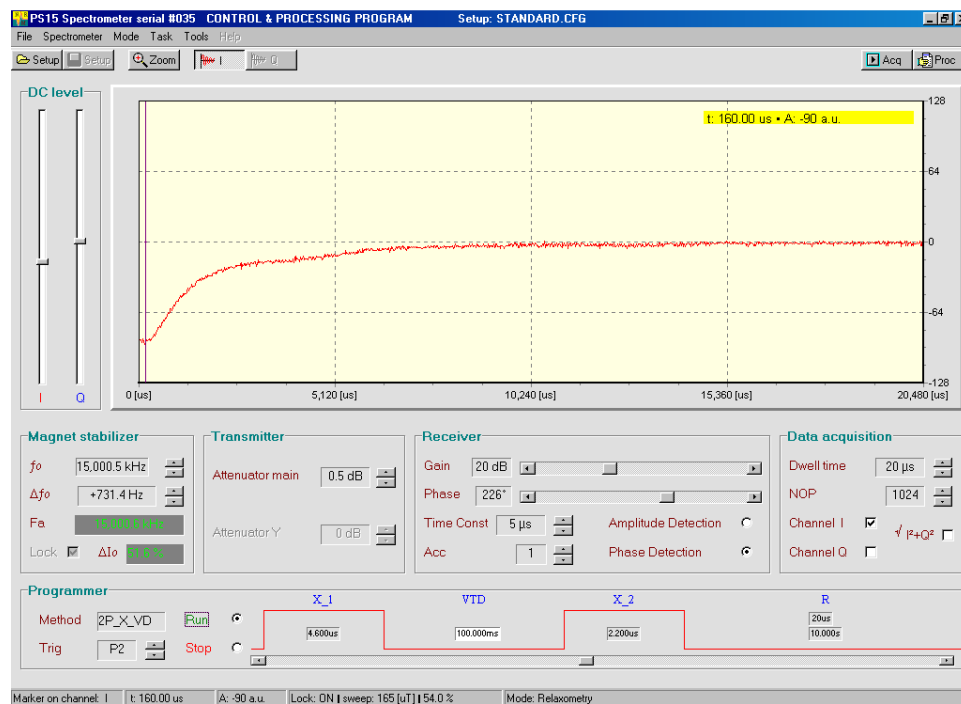
Figure 35. Negative FID from magnetization in water 100 ms after the inversing pulse.
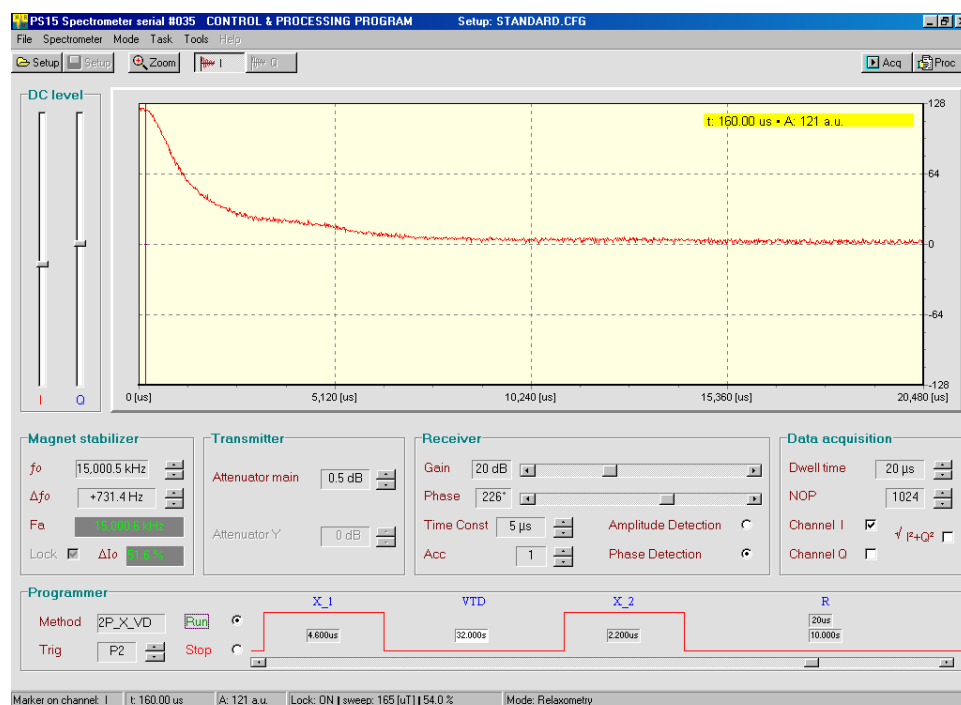
Figure 34. Positive FID from recovering magnetization in water 32s after the inversing pulse.
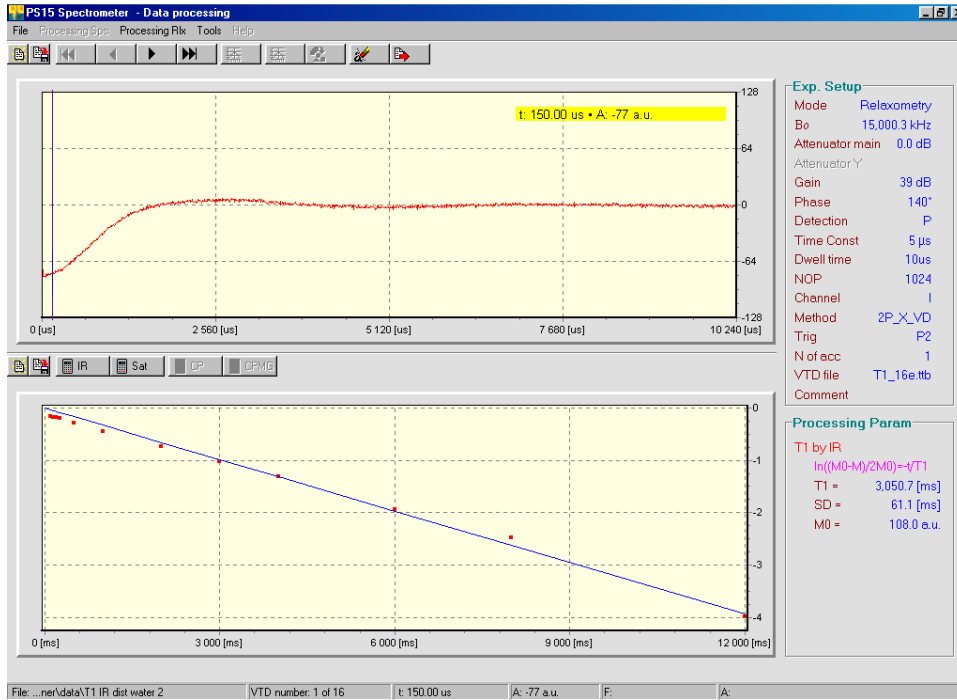
Figure 36. T_1 measurements by *IR* method in distilled water.
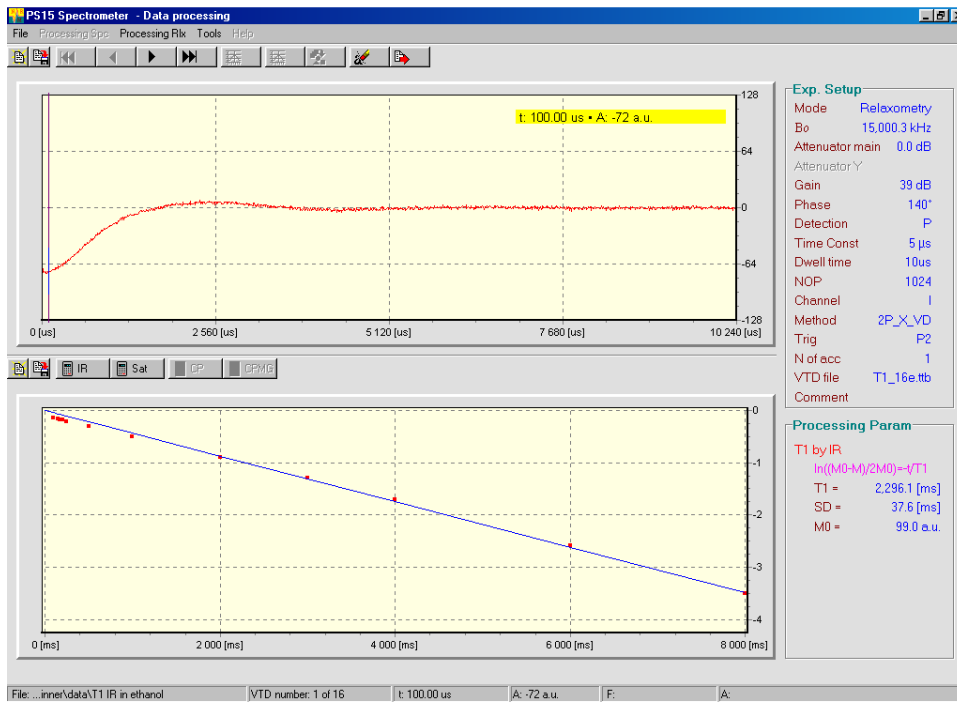
Figure 37. T_1 measurements by *IR* method in ethanol.
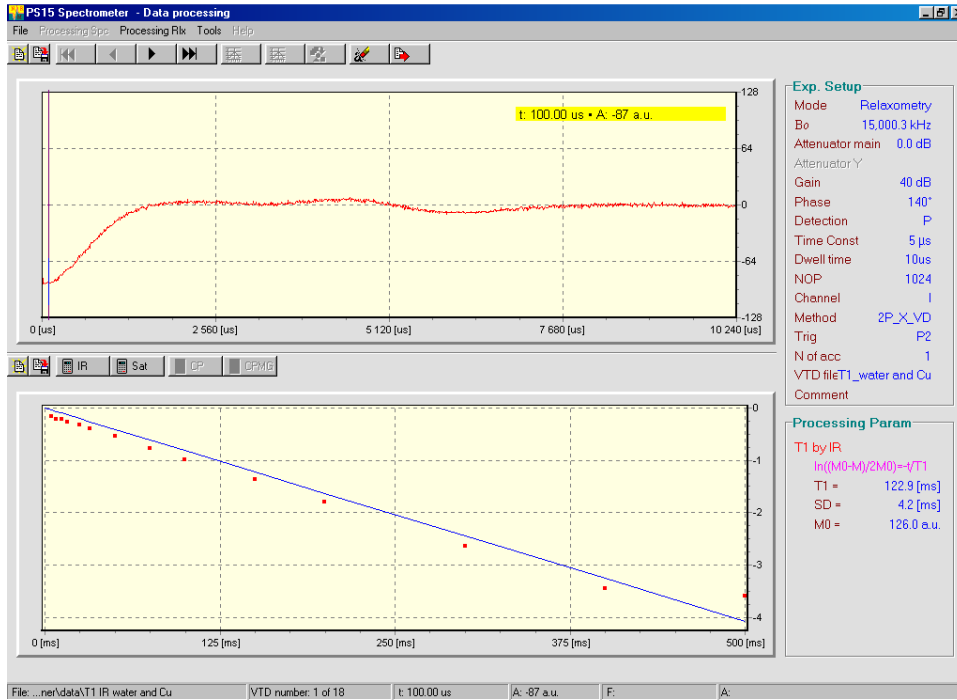
Figure 38. T_1 measurements by *IR* method in distilled water doped with $CuSO_4$.
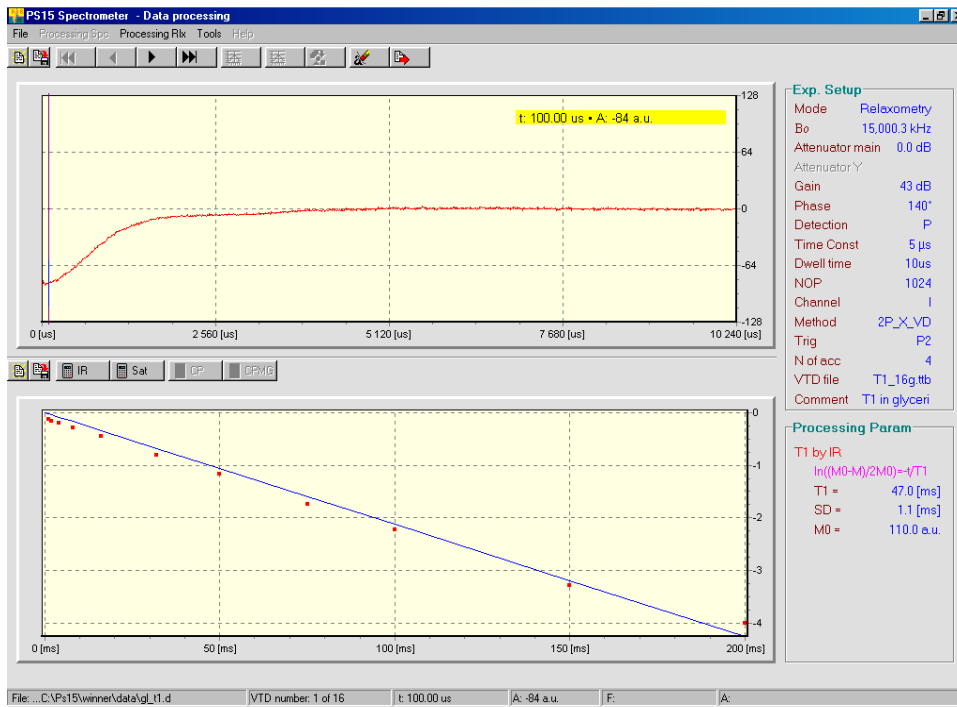
Figure 39. T_1 measurements by *IR* method in glycerin.
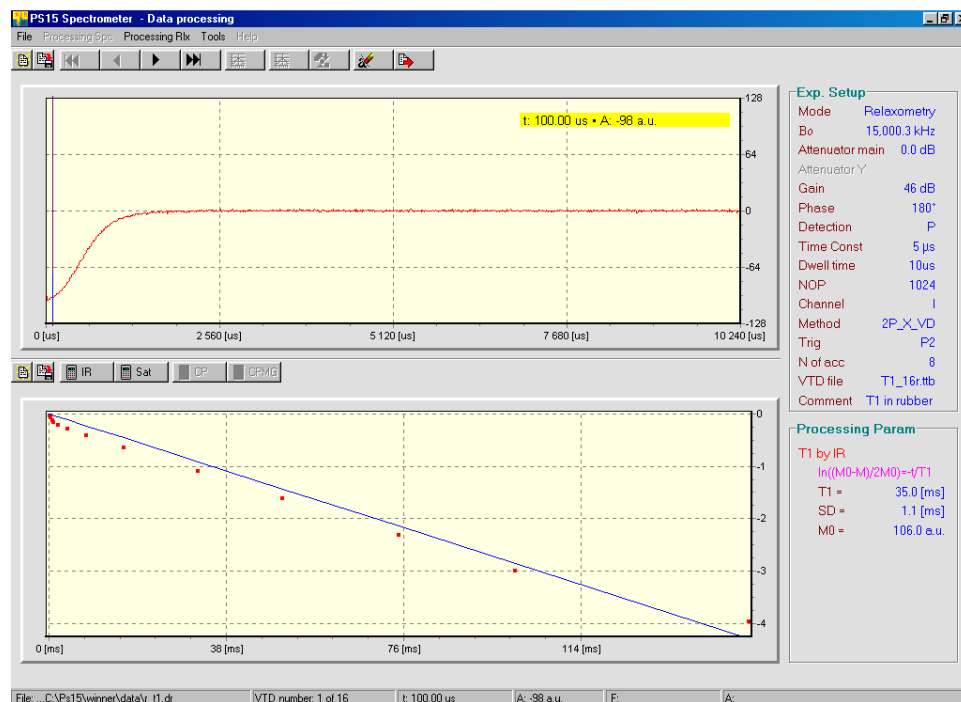
Figure 40. T_1 measurements by *IR* method in rubber.

Summary of T_1 measurements by *Inversion Recovery*.

Spin lattice relaxation times display huge variety of magnitudes. In afore conducted experiments distilled water has the longer T_1. Addition of small amount of paramagnetic ions (for instance cupric sulfate $CuSO_4$) dramatically shortens T_1 in water from 3 s to about 100ms. Rubber (Buna) that by definition contains many impurities leads the pack with shortest T_1.

Substance	T_1 [ms]
distilled water	3,000
ethanol	2,300
distilled water doped with $CuSO_4$	123
glycerin	47
rubber	35

Table 3. Spin lattice relaxation times of different substances measured by **Inversion Recovery** method.

3.2.2 T$_1$ in distilled water by *Saturation Recovery* method

Object

To compare the accuracy and measurement time of *Inversion Recovery* and *Saturation Recovery* methods in determination of very long spin-lattice relaxation times T$_1$.

Directions

- For comparison use distilled water sample. Its T$_1$ relaxation time reaches the range of several seconds. Be advised that T$_1$ strongly depends on the purity of the water and may vary from source to source.
- Prepare experimental **Setup** for on-resonance, one-pulse experiment with glycerin sample.
- Replace glycerin with distilled water sample.
- Call *Saturation Recovery* method (**Sat**) .
- Set long delay time between saturation and sampling: **T$_D$ =32s**.
- Adjust **Receiver Gain** to see unclipped signal as shown in Figure 41. Compare it to FID in Figure 34.
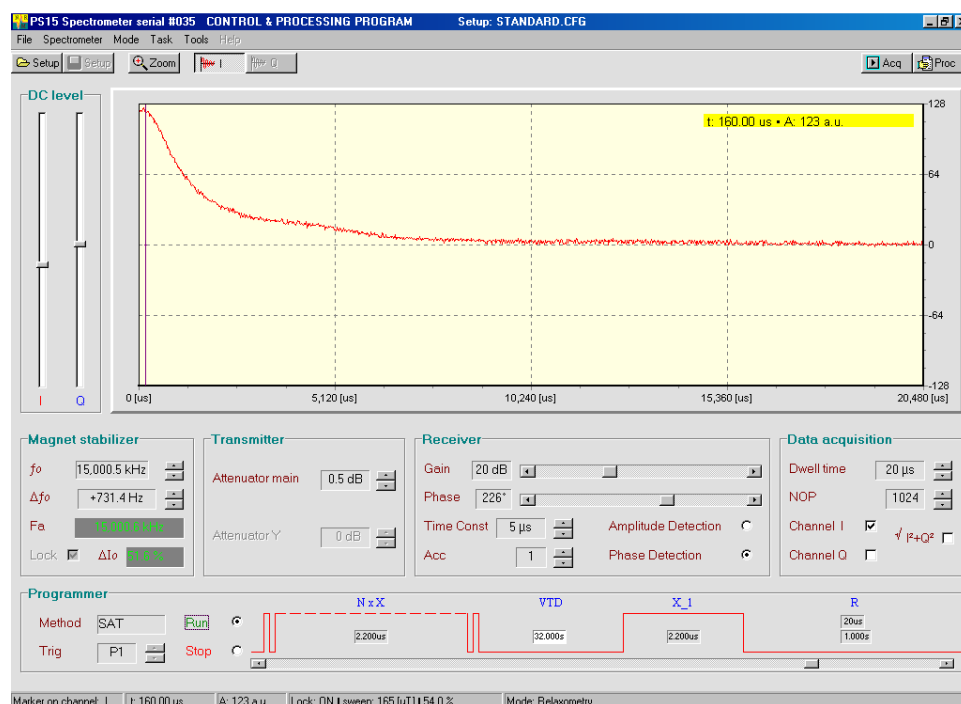
Figure 41. *Saturation Recovery* in distilled water with long delay time T$_D$=32s.

- Adjust **DC level** to compensate DC offset.
- Change delay time to very short T$_D$=100ms.
- If applied pulses are exactly or very close to $\Pi/2$ you should see a straight line along zero after sampling $\Pi/2$ pulse, that now monitors perfect spin

saturation. If positive or negative FID signal appears change pulse length and its power. You can see this case in Figure 42. For longer delay times magnetization recovers and FID reaches its positive image from Figure 41.

- On **Acquisition** page acquire experimental data into the file with proper time delay list (**T1 dist water.ttb**) and at with least 4 accumulations.
- On **Processing** page extract experimental points and calculate T_1 by using **Sat** routine.
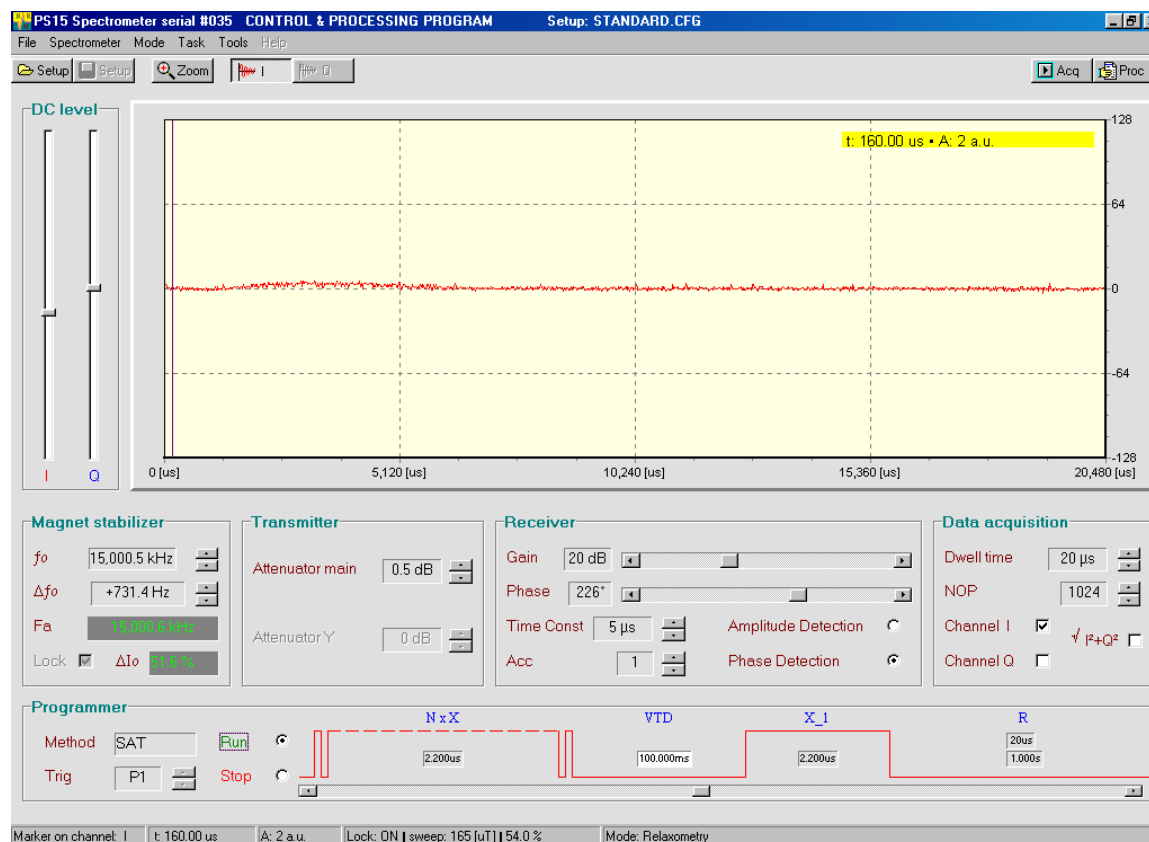
Figure 42. *Saturation Recovery* sequence with short delay time **T_D=100ms**. $\Pi/2$ pulse was slightly adjusted by adding 0.5dB attenuation and almost perfect saturation of resonance signal was achieved.

Results summary

Table 4 shows summary of T_1 measurements *Saturation Recovery* and *Inversion Recovery* methods in distilled water. Both methods deliver close times above 3 seconds. *Saturation Recovery* gives slightly more accurate results and in much shorter time than *Inversion Recovery* does (8'22"s and 17'58", respectively.

Method	T_1	Standard deviation	T_R	Time of 4 accumulations
Inversion Recovery	3.10s	0.07s	10s	1077.5s
Saturation Recovery	3.39s	0.03s	1s	501.5s

Table 4. Comparison of T_1 measurements in distilled water by *Inversion Recovery* and *Saturation Recovery* methods.

4   NUCLEAR SPIN-SPIN T$_2$ RELAXATION MEASUREMENTS.

4.1 Theory

Spin-spin relaxation time describes processes that are responsible for bringing nuclear spins to an equilibrium state with each other after being exciting by an RF pulse. Due to this process spins loose their coherence and as a consequence the dephase of the movement of nuclear spins takes place.

The analysis of the magnetization vector placed in the static field **B$_0$** and the RF field **B$_1$** shows that the absorption component of the solution represents a Lorentzian line centered at f$_0$. The half intensity of this line is given by Eq. 14.

$$f_{1/2} = \frac{1}{\Pi T_2}$$

Eq. 14

Assuming perfect magnetic field homogeneity T$_2$ can be simply determined by measurements of **signal width at half maximum** of the spectrum or shortly **SWHM**.

In a real experiment, however, the sample experiences a variety of magnetic field magnitudes due to imperfections in the magnet called inhomogeneity. Magnet inhomogeneity slightly affects the local resonance frequency of nuclei and as a consequence changes the spectrum width. This new experimental line width $f_{1/2}^{\exp}$ corresponds to the effective spin-spin relaxation time called T_2^* (*tee-two-star*).

$$f_{1/2}^{\exp} = \frac{1}{\Pi T_2^*}$$

Eq. 15

One can separate contributions originating from natural line width and from magnetic field inhomogeneity:

$$\frac{1}{T_2^*} = \frac{1}{T_2} + \frac{1}{T_2^{inh}}$$

Eq. 16

Hahn's two-pulse **[(Π/2)$_x$ - t$_D$ - Π$_x$]** spin-echo method circumvents the magnetic field inhomogeneity problem. As magnetization decreases between pulses because of natural transverse relaxation process, spin-echo signal decays too. Thus one can calculate T$_2$ from the plot of the echo amplitude A(t$_D$) as a function of t$_D$ (Eq. 17).

$$A(t_D) = A_0 \cdot \exp(-\frac{2t_D}{T_2})$$

Eq. 17

There are two other more popular methods that eliminate the instrumental (or

inhomogeneous) contribution, *Carr-Purcell* and *Carr-Purcell-Meiboom-Gill* methods. Both methods are based on the fact that dephasing of nuclear spins due to magnetic field inhomogeneity is reversible under certain conditions allowing the measurement of intrinsic spin-spin T_2 relaxation time.

4.1.1 The Carr Purcell (CP) method

The *Carr-Purcell* sequence used for T_2 measurements consists of a single $(\Pi/2)_X$ pulse followed by a train of Π_X pulses. The $(\Pi/2)_X$ pulse rotates the M_z magnetization toward the +Y' axis. Π_X pulses that appear in the same time intervals flip decaying M_y magnetization between -Y to +Y generating consecutive spin echoes.

If RF pulses are separated by a period of time 2τ as shown in Figure 43 and spin diffusion is absent (this for teaching purposes can be controlled by selecting proper samples) the absolute amplitude of the echoes decay exponentially as:

$$A_N \approx \exp[-(2N\tau/T_2)] \qquad\qquad \text{Eq. 18}$$

-where a A_N is a number of echo under consideration.
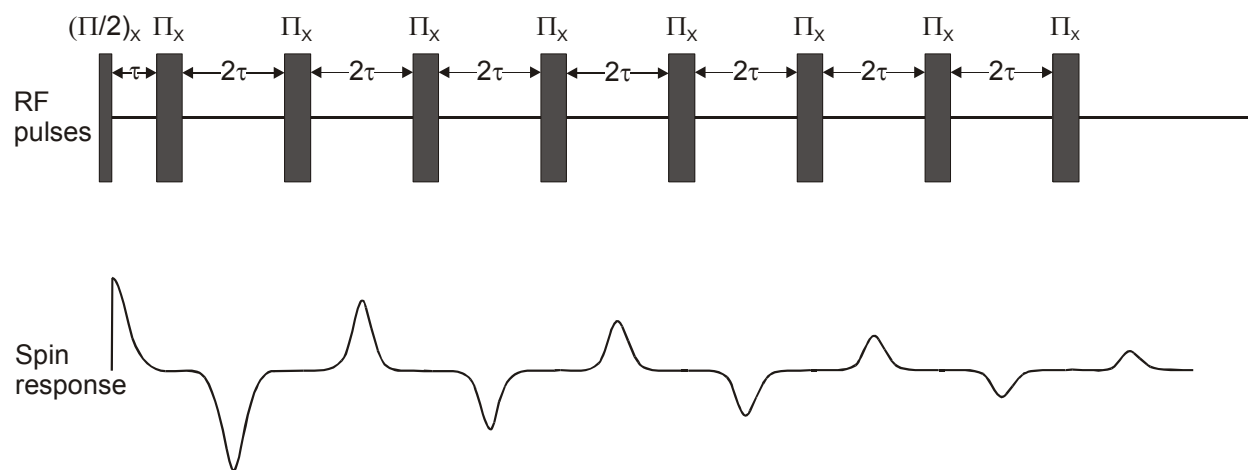
Figure 43. Train of $(\Pi/2)_X$ and Π_X and pulses and corresponding echoes in **CP** method. Note that echoes appear at 2τ, 4τ, 6τ,..., $2N\tau$. Odd-echoes are negative whereas even-echoes are positive.

4.1.2 The Carr-Purcell-Meiboom-Gill (CPMG)

The Carr-Purcell method suffers from possible cumulative errors that originate from the inaccuracy of adjustment of the Π_X pulse length. *Meiboom* and *Gill* modified CP sequence changing the phase of Π pulses by 90°. In the language of the "rotating frame" changing phase of the RF pulse by 90° corresponds to applying it along Y' axis.

Now Π_Y pulses move magnetization around the Y' axis. If the pulse is exactly 180° then echoes are formed in X'Y' along Y' axis. If the pulse is $(\Pi -/+\varepsilon)_Y$ refocusing of **odd-echoes** takes place somewhere in the plane above/below X'Y' plane, whereas refocusing of **even-echoes** appears in exactly X'Y' plane. Thus all odd-echoes are slightly smaller and even-echoes are of correct amplitude (see more detailed analysis in Figure 5). If spin diffusion contributions are neglected, amplitudes of echoes decay exponentially with time constant T_2.
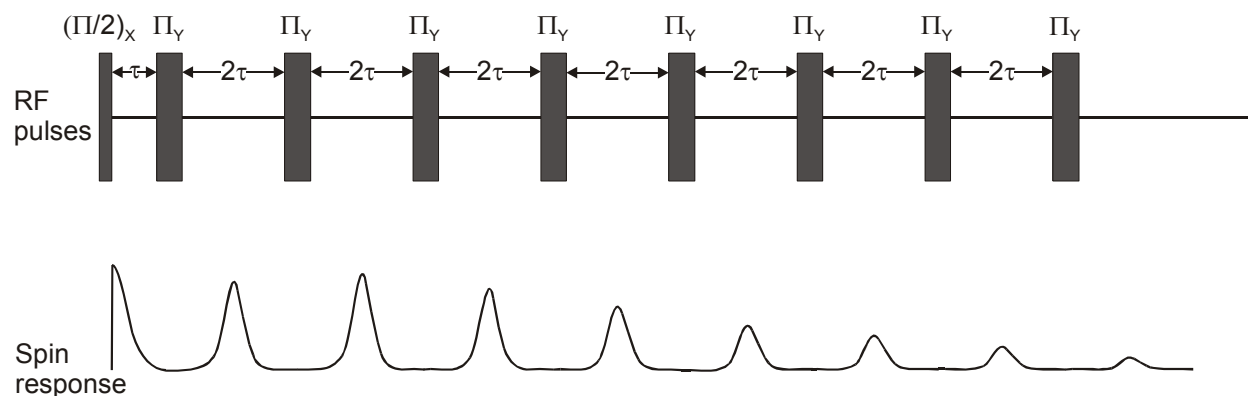
Figure 44. $(\Pi/2)_X$ and Π_Y and corresponding echoes in **CPMG** method. Note that all echoes are positive and that first echo is slightly smaller than 2nd due to slight inaccuracy of Π_Y pulse setting.

4.2 Experimental

Object

To compare T_2 measurements in glycerin using different methods:

- From spectrum line width,
- Manually using Hahn's spin echo.
- Using *Carr Purcell* method.
- Using *Carr Purcell Meiboom Gill* method.

4.2.1 Estimating T_2^* from spectrum line width.

Comment

This is a quick method to estimate spin-spin relaxation time from the NMR spectrum. It requires only acquisition of free induction decay and FFT on this signal.

Directions

- On the **Setup** page prepare off-resonance FID in **I** and **Q** channels as described in 2.2.4 or follow screen capture in Figure 45.
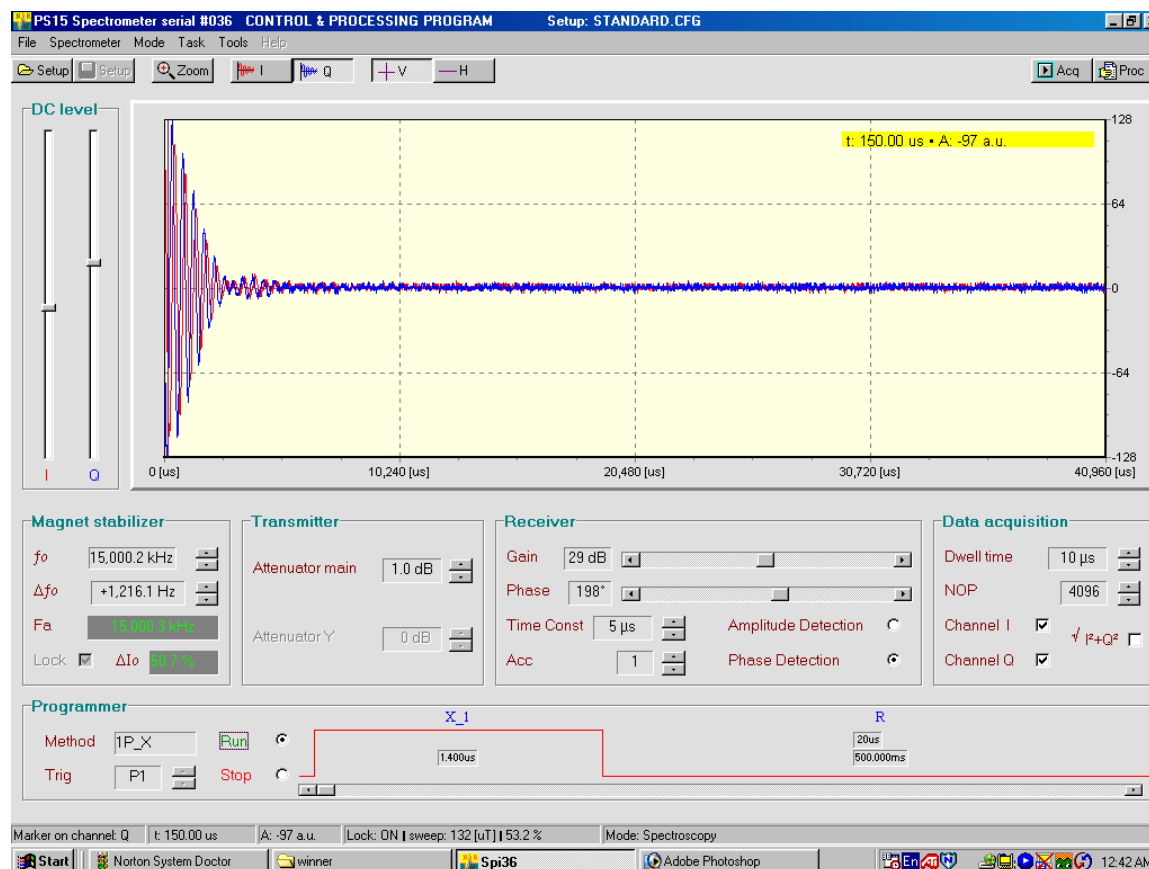
Figure 45. Experimental setup to acquire FID for line width determination.

- On the **Acquisition** page set accumulation number (**Acc**) to 16 to get a good SNR and save the FID to the file.
- On the **Processing** page load experimental data from file and do FFT.
- With data processing tools correct the spectrum phase, expand it horizontally and vertically, and determine line width on half maximum.
- Calculate T_2^* time from $T_2^* = \dfrac{1}{\Pi f_{1/2}^{exp}}$ (or see Eq. 16).
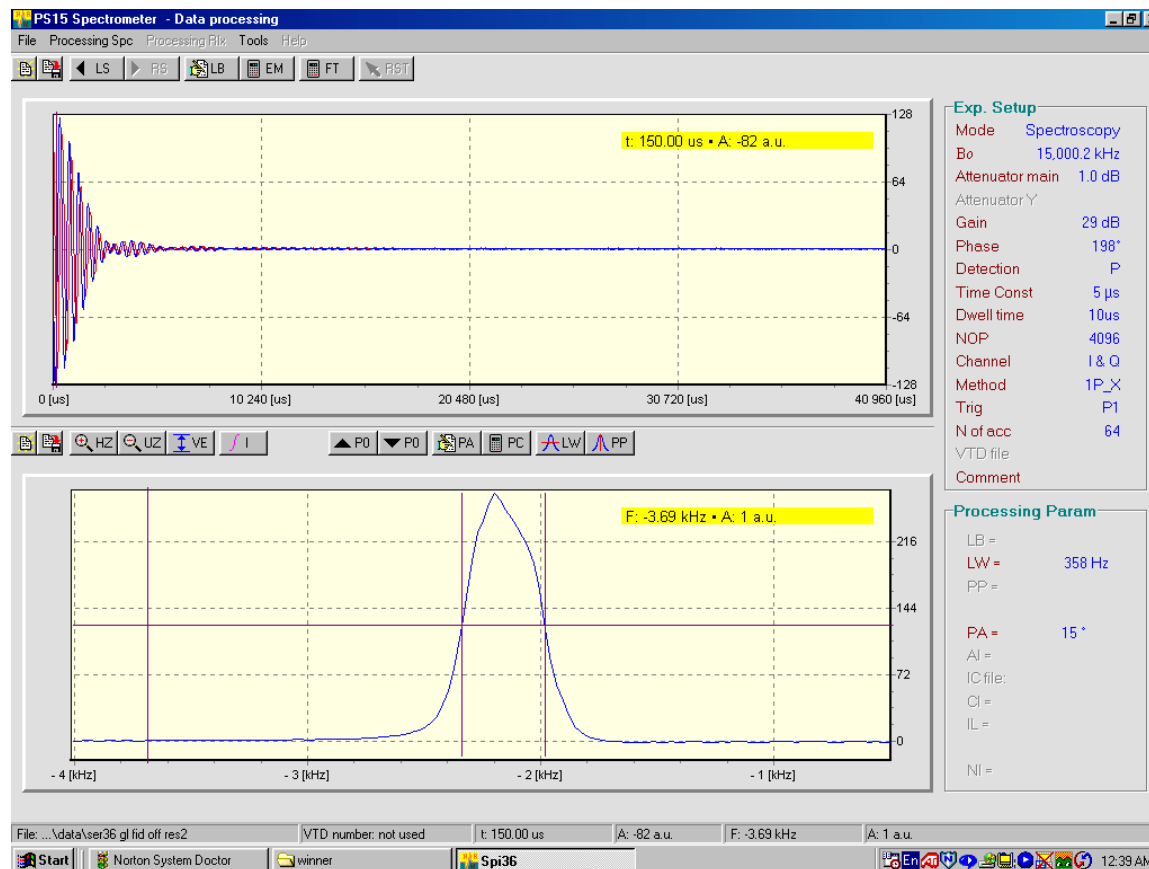
Figure 46. Measuring line width on **Processing** page using line width **LW** tool.

4.2.2 Measuring T_2 time manually using simple spin-echo method

$\{(\Pi/2)_X - \tau - \Pi_X\}$

Comment

T_2 times can be simply calculated from echo amplitudes that decrease exponentially as a time delay between pulses increases. Experiment will be performed on **Setup** page only. Amplitudes of spin-echo signal as function of time delay will be measured and later processed manually or with any independent software (Excel, Origin, etc).

Directions

- Prepare on-resonance spin-echo experiment (use **2P_X_D** sequence) with one channel active.
- Set time delay between pulses to a minimum to see very strong undisturbed echo.
- Set triggering of the acquisition after Π_X pulse: **Programmer>Trig>P2**
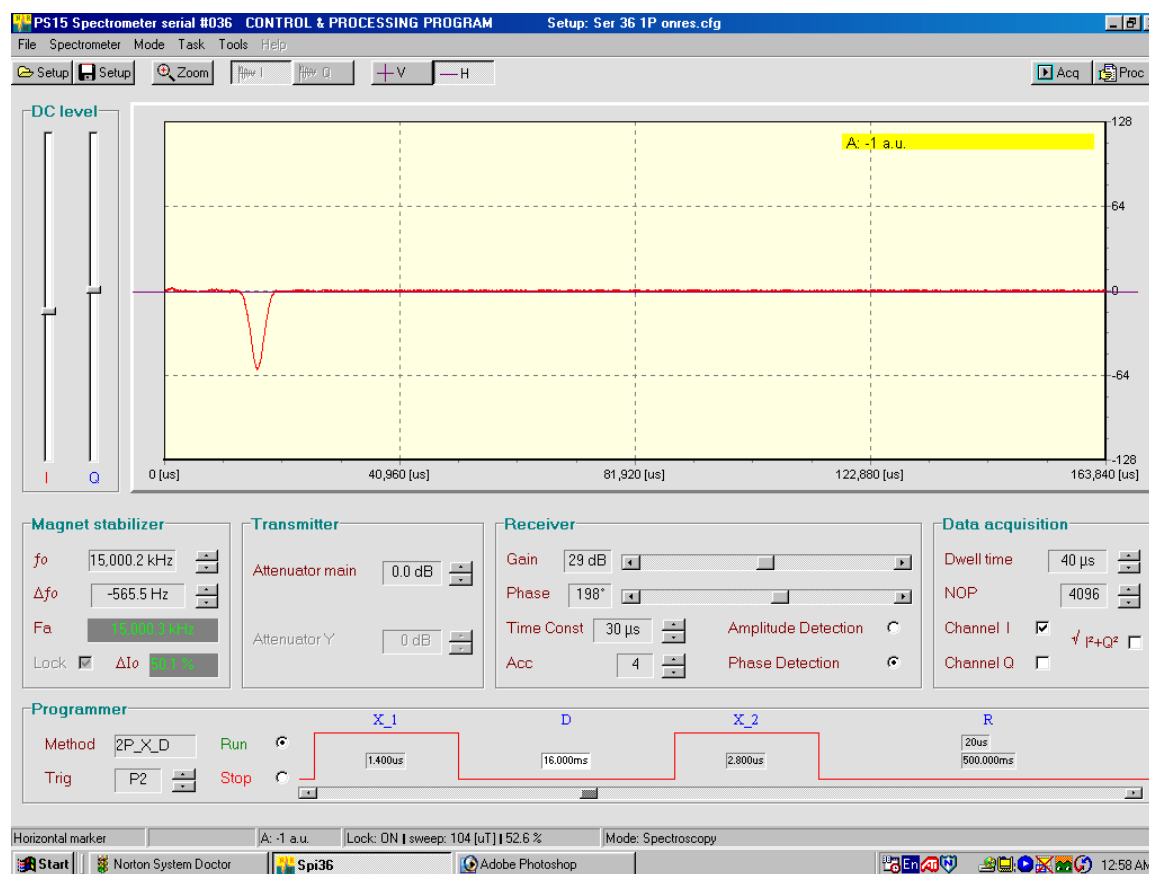
Figure 47. Measuring spin echo amplitude versus different interpulse delays for T_2 calculation.

- Set data marker on the echo center, record time and amplitude.

- Change time delay to see echo decaying in the noise, record time. If echo disappears from acquisition range change **Dwell Time** accordingly.
- Divide time of disappearing echo into 16-25 intervals and make list of time delays.
- Select time delay from a list and measure corresponding echo amplitude. To improve SNR start measurements with several accumulations (16 are usually enough)
- Calculate T_2 from echoes amplitude decay manually using Eq. 17 or fit with any program. Figure 48 shows results of experimental data fit to one-exponential decay function using Origin program.
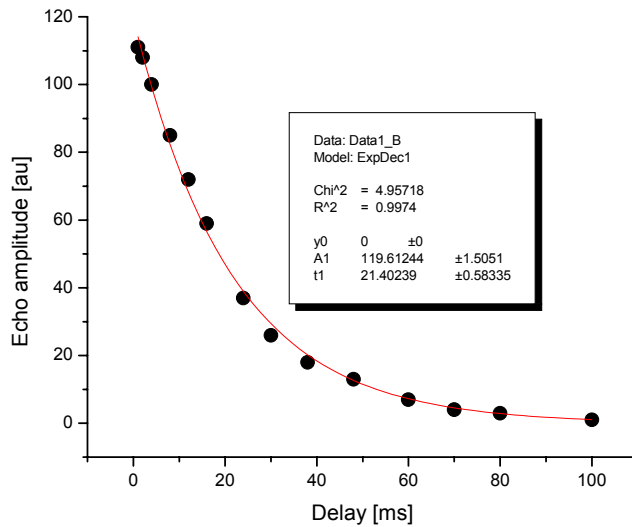
Figure 48. Fit of experimental data to one-exponential decay function $y = y_0 + A_1 exp(\frac{-2t_D}{t_1})$ with Origin program; t_D is interpulse delay, $t_1 = T_2$.

4.2.3   Determining T_2 in glycerin by Carr-Purcell method

$$\{\Pi/2)_X - \tau - [\Pi_X - 2\tau - \Pi_X \ ...]xN\}$$

Comment

By rapidly acquiring a series of echoes at different delay times in a single sequence *the Carr-Purcell* method reduces the spin diffusion effect on the measurement of T_2.

Directions

- Establish on-resonance conditions with one-pulse sequence.
- Determine length of $\Pi/2$ and Π pulses.
- Call **CP25** method. It automatically generates *Carr-Purcell* sequence with 25 echoes.
- At **Setup** page adjust $\Pi/2$ and Π pulses (length and power) to see several echoes.
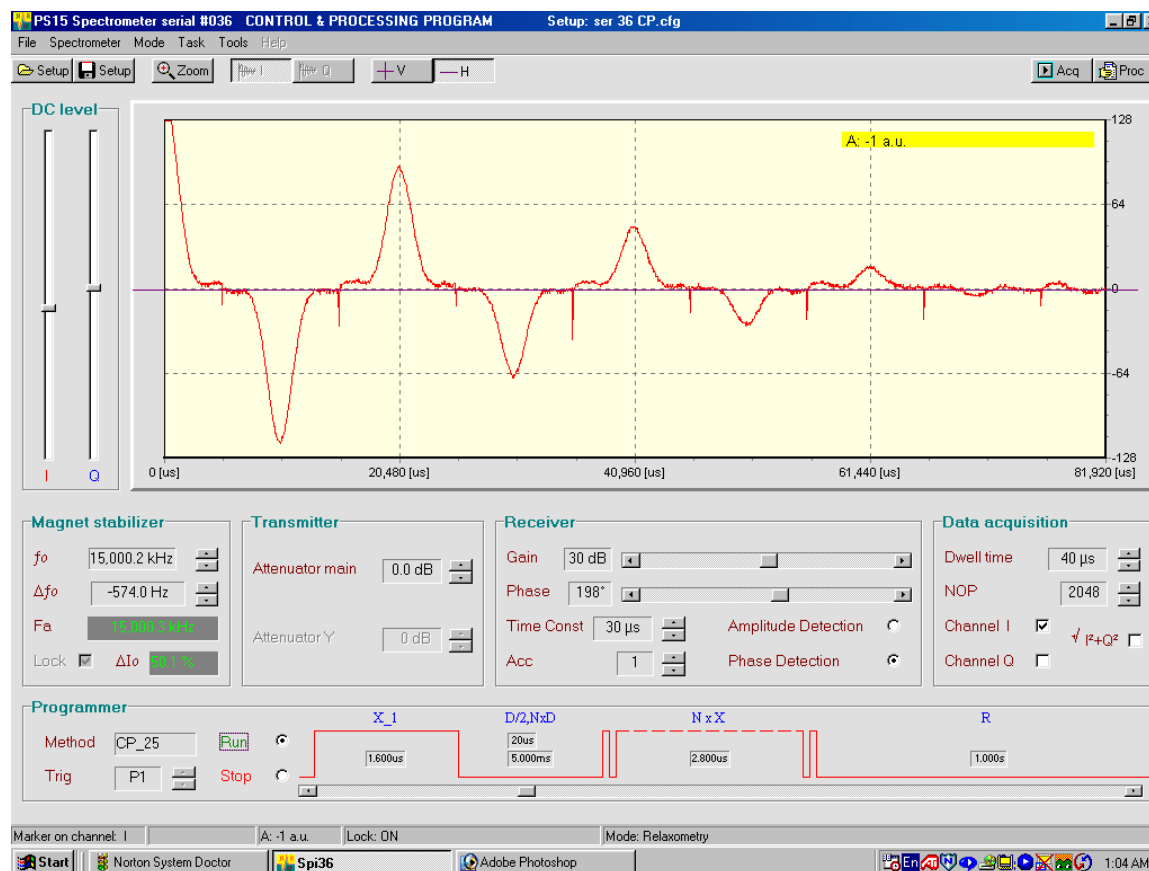
Figure 49. Setup for CP experiment in glycerin.

- On **Acquisition** page save the data to file with at least 16 accumulations.
- On **Processing** page:
  - ❑ Mark a last echo that is visible from noise

❑   Extract echoes coordinates

❑   Perform T_2 calculation by **CP** method.
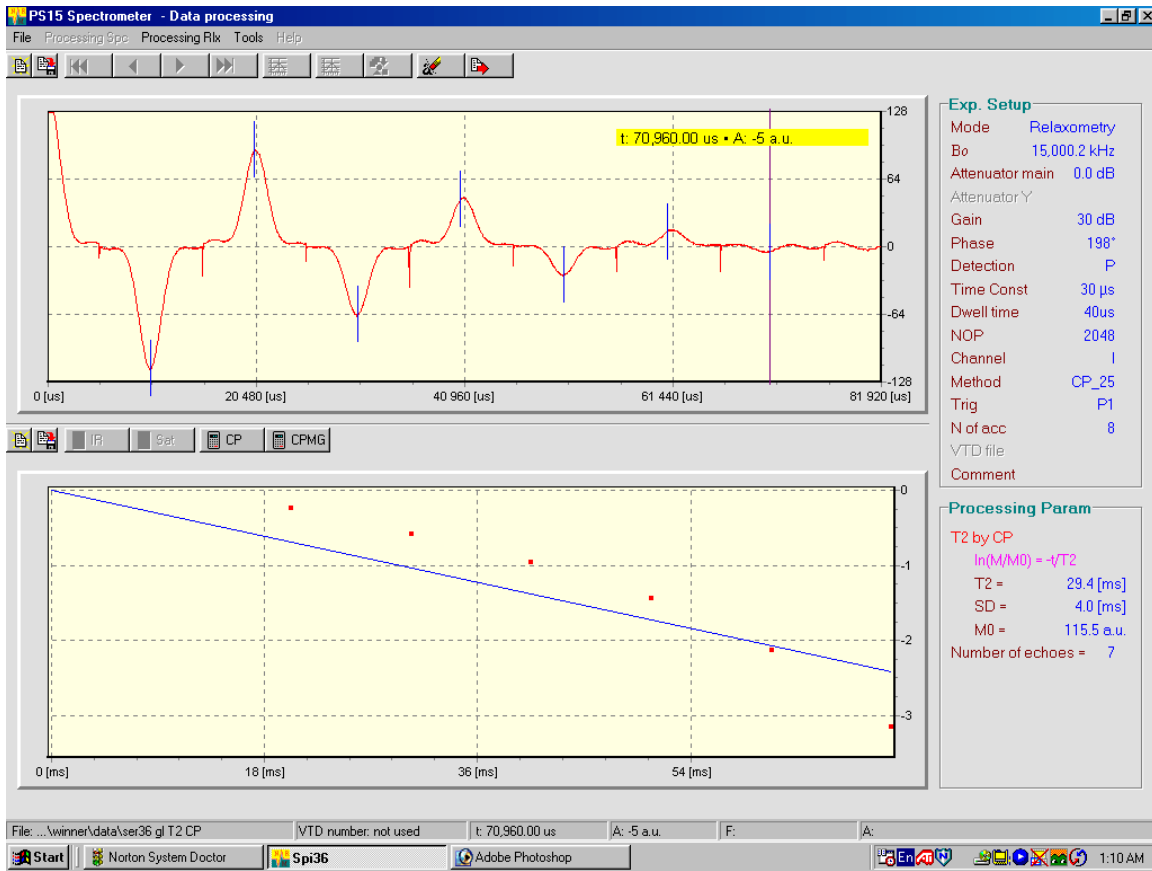
Figure 50. Processing CP data.

4.2.4   Determining T$_2$ in glycerin by Carr-Purcell-Meiboom-Gill method

$\{\Pi/2)_X - \tau - [\Pi_Y - 2\tau - \Pi_Y \text{...}]xN\}$

Comment

CPMG method is a modification of **CP** method that shifts the phase of Π relative to the initial $\Pi/2$ pulse by 90° to compensate for the error of Π pulse setting.

Directions

- Establish on-resonance conditions and determine length of $\Pi/2$ and Π pulses.
- Load **CPMG25** that produces 25 consecutive spin echoes.
- Select proper delay time to see echoes not overlapping on each other.
- Select **Receiver Gain** to obtain strong echoes without signal clipping.
- Select **Dwell Time** to cover time of all 25 echoes.
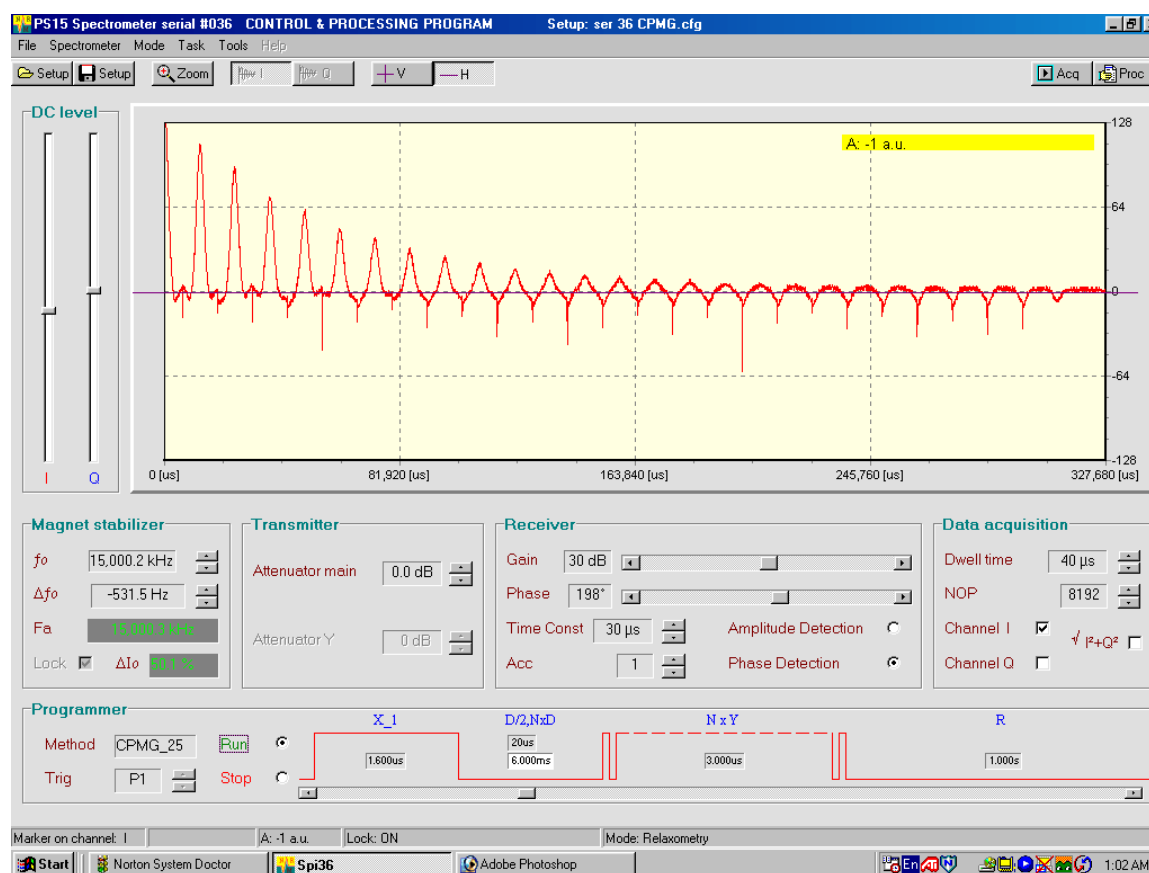
Figure 51. Setup for CPMG experiment in glycerin.

- On **Acquisition** page select at least 16 accumulations and save data to file.
- On **Processing** page:
  - Mark a last echo that is visible from noise

❑ Extract echoes coordinates

❑ Perform T_2 calculations by **CPMG** method.
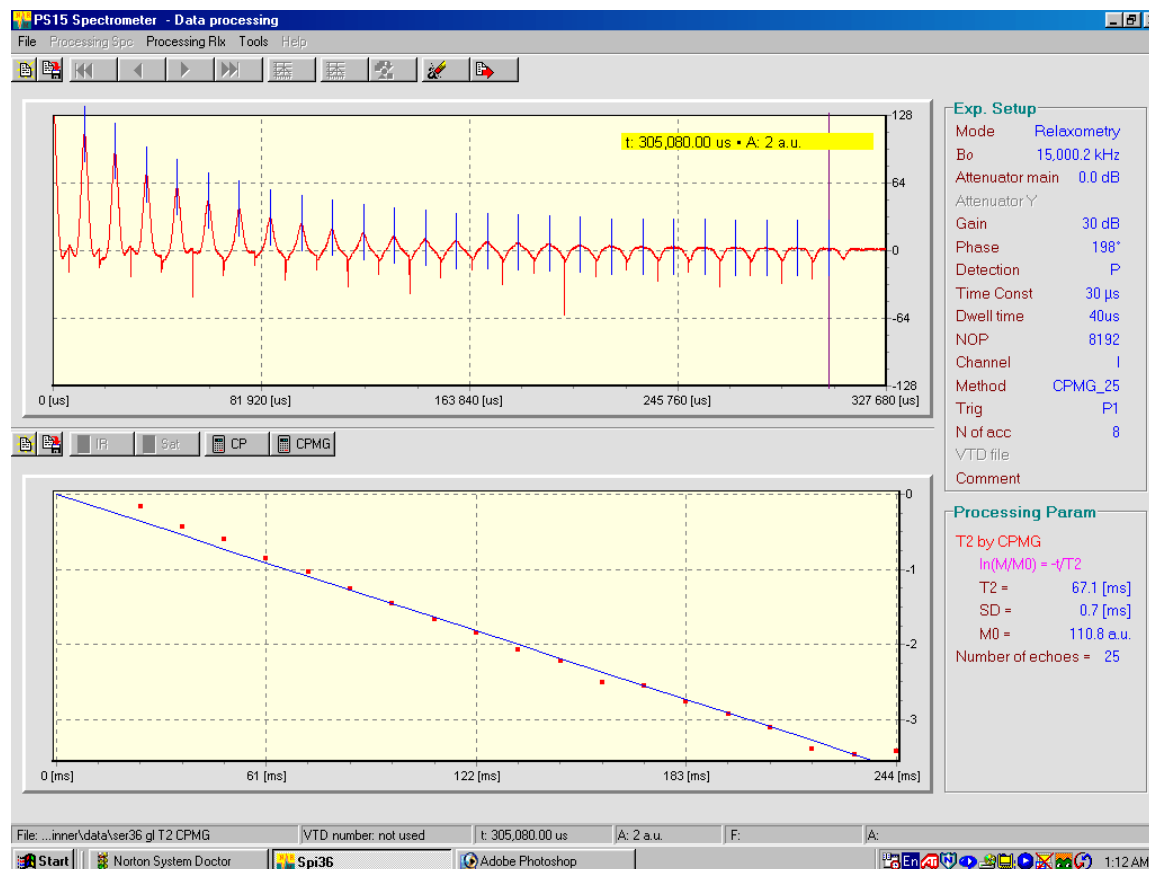
Figure 52. Processing CPMG data.

4.2.5 Summary of T_2 measurements

Method of measurement	T_2 [ms]	Standard deviation [ms]
Line width	0.9	
Hahn spin-echo	21.4	
CP	29.2	4.0
CPMG	67.1	0.7

Table 5. Summary of spin-spin relaxation time measurements in glycerin, using different methods. T_2 from the line width is dramatically short due to strong inhomogeneous line broadening.

5 INSTRUMENTATION

5.1 Mapping the probehead RF coil

Introduction

To observe nuclear magnetic resonance phenomenon, the nuclei precessing around constant magnetic field B_0 must be exposed on the radio frequency field B_1 that rotates in the plane perpendicular to the B_0 field. This rotating field, or circularly polarized field, of magnitude B_1 can be obtained from the decomposition of a linearly oscillating field (linearly polarized) of magnitude $2B_1$ (Figure 53). Only the field component that rotates in coherence with the precessing nuclear magnetization is used. The other one is radiated in space and lost.
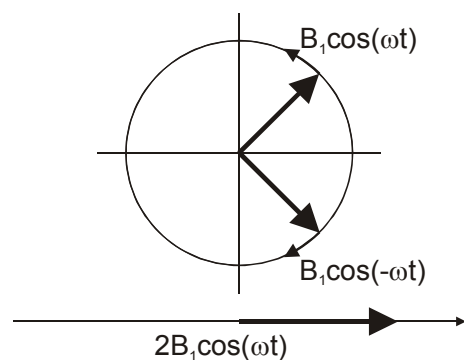
Figure 53. Decomposition of linearly polarized field into two circular fields.

In experimental practice the linearly polarized B_1 field can be easily produced by a single closed loop driven by source of high frequency electromotive force.
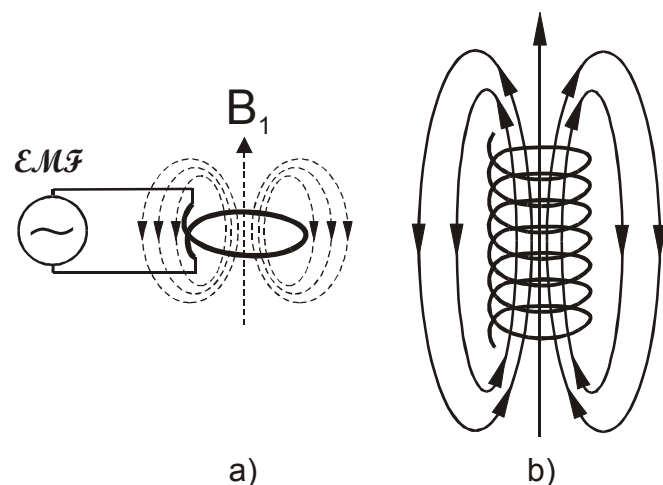
Figure 54. Single loop driven by a source of Electromotive Force (a) and solenoid b) as a source of linearly polarized field B_1.

Homogeneity of a B_1 field generated by a single loop is rather poor. It can by improved by combining a series of single loops into a solenoid (Figure 54). The solenoid incorporated into the probehead resonance circuit is the most popular kind of transmit/receive antenna used in pulsed NMR spectroscopy. Its high homogeneity remains an important issue in experiments that require precisely defined rotating angles (*Carr-Purcell*). One can address B_1 field homogeneity by reducing the sample volume but it has its limit due to degradation of S/N ratio.

Object

To measure B_1 field distribution along the solenoid longitudinal axis (**z**).

Instructions

- Connect experimental setup as shown in Figure 55.
- Place the pick-up coil in the RF coil center.
- Load one-pulse **1P_X** method and set transmitter attenuation for 12dB, pulse width for 50μs and repetition time for 300ms.
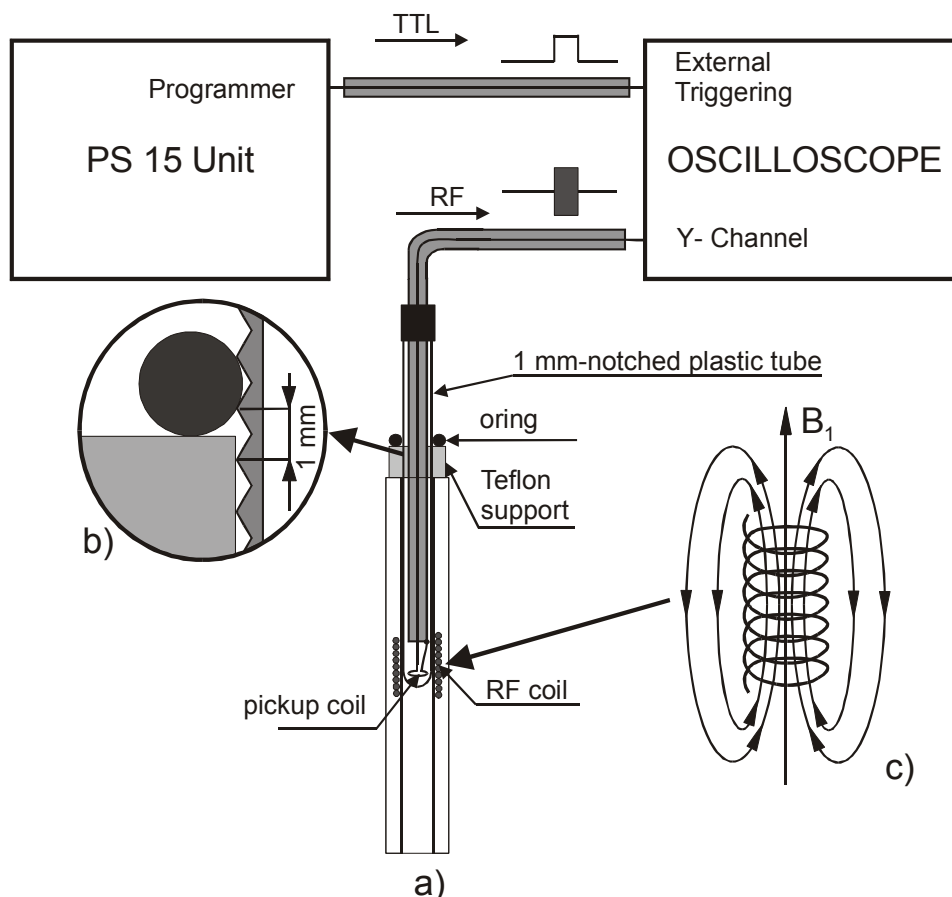
Figure 55. Experimental setup to map the B_1 intensity inside the RF coil and to monitor RF pulses. a) Pick-up coil inside the RF coil, b) pickup coil holder (some holders are glass tubing and same are plastic with 1-mm notched outer wall), c) linearly polarized B_1 field within the solenoid.

RF coil mapping
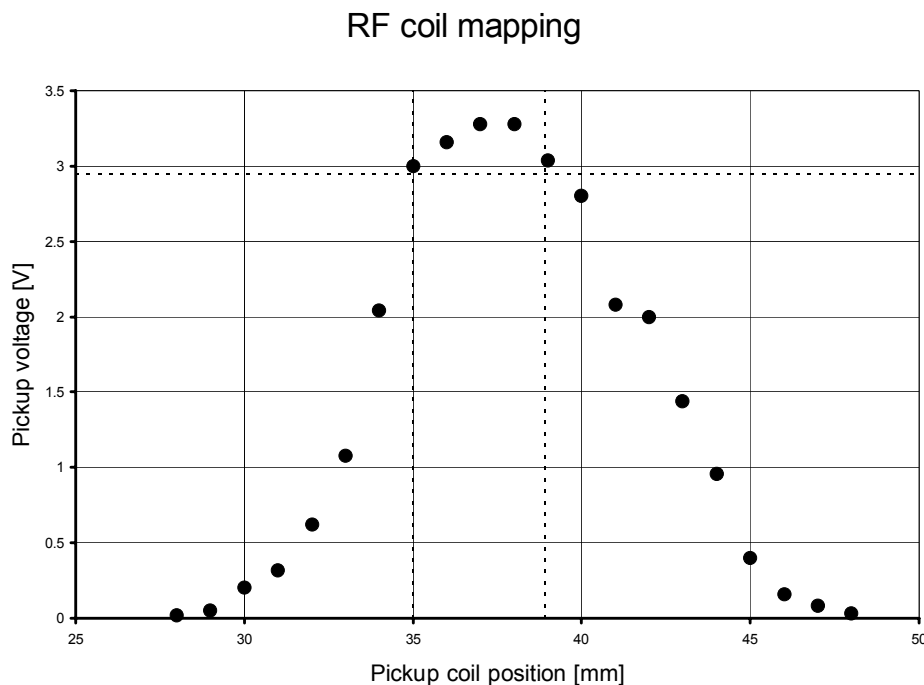
Figure 56. Intensity of signal induced in the pickup coil vs. its position relative to the upper edge of probehead sample holder.

- On the scope panel:
  □ Select Trigger source as External.

  □ Select Trigger mode as Normal

  □ Adjust the Level and Holdoff of the triggering to see stable RF pulse.

  □ Adjust vertical gain to see bottom and top part of the pulse

- Move pickup coil up and down and record the peak-to-peak **amplitude** of the pulse and the corresponding pickup coil **position**.
- Repeat measurements until amplitude of the pulse drops to about of 1% of peak value.
- With spreadsheet program (Excel) make plot intensity of RF pulse versus pickup coil position, Figure 56.
- Find the position of the maximum signal and the area of its 10% drop. Consider this area as most useful in terms of B_1 homogeneity. Mark it on the sample positioner and use as reference in your experiments. For fine experiments like **CP** and **CPMG** try to reduce size of the sample to the value you have gotten (3mm in an example).

5.2 Watching pulse sequences

Object

To see real RF pulses. In particular to check how their shape changes due to different RF attenuation, pulse width and delays.

To watch the automatic change of pulse delay time when executing **2P_X_VD** sequence during T_1 measurements.

Instructions

Watching RF pulse
- Connect experimental setup with pickup coil in the center of RF coil as shown in Figure 55.
- Load any one-pulse method (**1P_X**).
- Set pulse time for 50µs and repetition time for 250ms.
- On the oscilloscope:
  - Select Trigger source as External.
  - Select Trigger mode as Normal.
  - Adjust the Level and Holdoff of the triggering to see stable RF pulse.
  - Adjust vertical gain to see bottom and top part of the pulse.
- On **Setup** page change **Transmitter>Attenuation** from 0dB to 12dB and watch the change of RF pulse amplitude (see Figure 57).
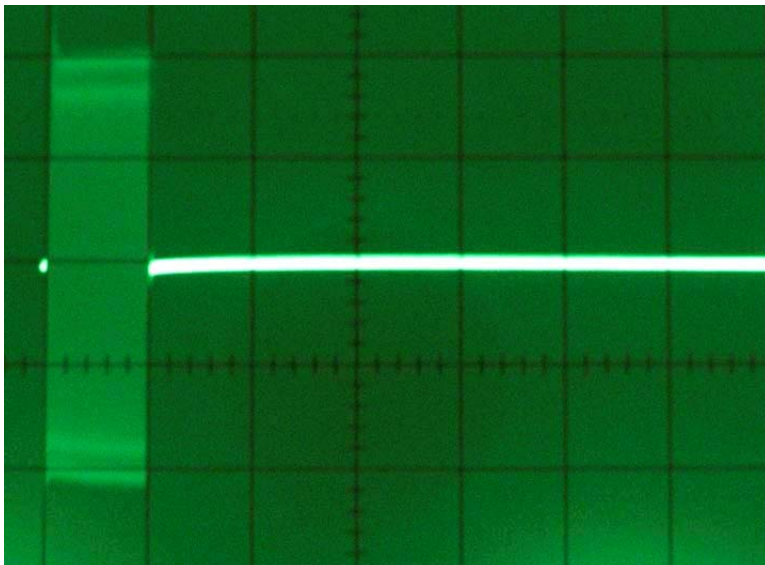
Figure 57. Radiofrequency pulse visible with a pickup coil on an oscilloscope. Horizontal scale is 20µs/div, vertical scale is 0.5V/div.

Observing effect of pulse delay during automatic T1 measurements

- Switch spectrometer **Mode** of operation to **Relaxometry** and load **2P_X_VD** sequence.
- Set both pulses for 50µs[2], keep repetition time 250ms and set triggering after first pulse (**Programmer>Trig 1P**).
- On **Acquisition** page select variable time delay file **t116_r**. This file contains 16 different delay times (*0.3, 0.5, 1, 2,4,8, 16, 32, 50, 75, 100, 150, 175, 200, 250*; all in milliseconds) normally used for T_1 relaxation times measurements with *Inversion Recovery* and *Saturation Recovery* in rubber.
- Start acquiring data on the **Acquisition** page without typing file name.
- Watch second pulse moving automatically as program calls consecutive delay times. This is real thing that happens during automatic T_1 measurements!

Diagrams of each pulse sequences are shown graphically on a Setup and Processing pages. Pickup coil and scope gives flexible means to see what exactly happens inside probehead RF coil.

During the experiment user can monitor RF sequences continuously without using the pickup coil by connecting oscilloscope Y channel to **TX 1:10** output on the PS15 electronic unit rear panel.

If RF pulses do not produce enough contrast on the oscilloscope screen use TTL Programmer output to see pulses envelopes (see Figure 58).
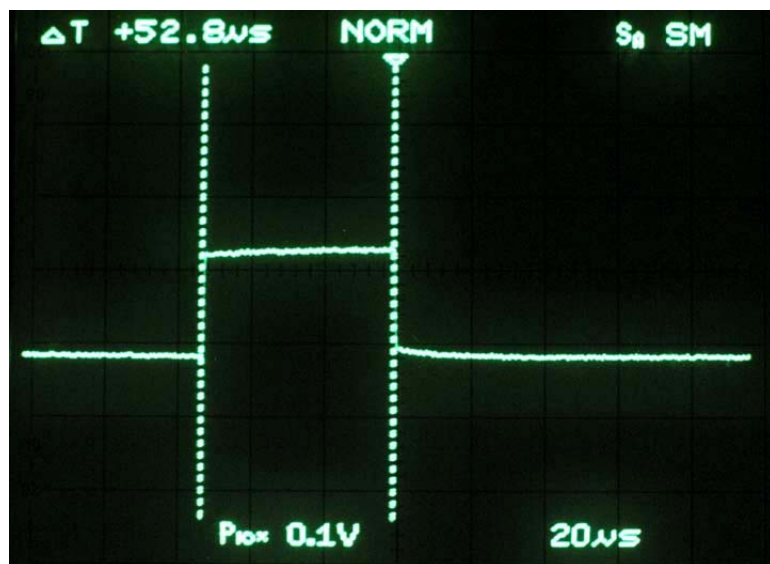
Figure 58. An envelope of the 50µs RF pulse monitored on Programmer output.

---

[2] Keep attenuation at 12dB to reduce transmitter power when long RF pulses are generated.

5.3   Amplitude detector and phase sensitive detector

Introduction

During the receiving period the NMR spectrometer records the movement of weak magnetization component in the plane perpendicular to the **B$_0$** magnetic field. As this component decays due to spin-spin and spin-lattice relaxation the induced signal decays too.

The voltage coming from the RF coil is in the shape of sine wave signal (of precession frequency) modulated by the exponentially decaying function (T_2, T_1). The envelope of this signal carries valuable information about precessing nuclei. If treated by Fourier transformation the envelope converts to an **NMR spectrum**. If acquired with different time delays, signal envelopes deliver information about **relaxation times**.

Extracting the envelope from the radio frequency takes place in the process called **signal detection**.

5.3.1   Amplitude detector

The easiest way to obtain the envelope of FID or spin echo is simply by amplifying and rectifying the signal induced in the RF coil. This kind of detection is called **amplitude detection** as it is primarily sensitive for signal amplitude, or diode detection as the diode is used as detecting device. Diode amplitude detection suffers from the nonlinear response of a semiconductor element.
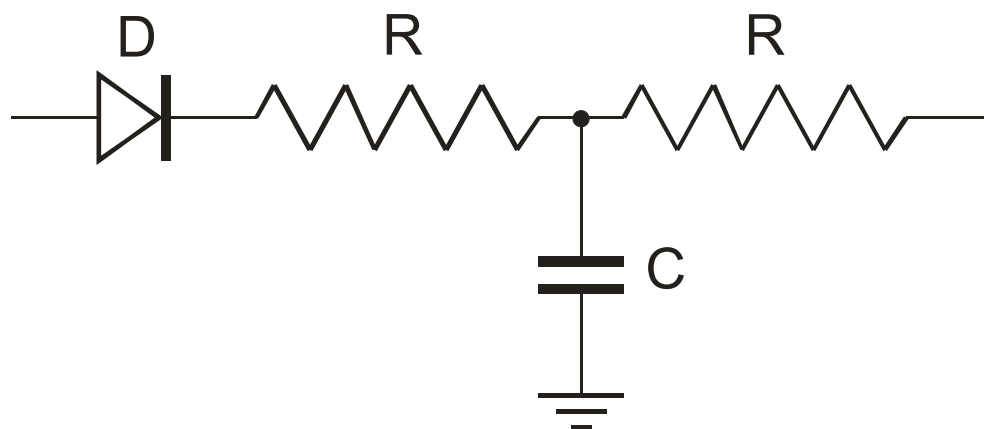
Figure 59. Diode D as an amplitude detector with low-pass RC filter for carrier frequency removal.

5.3.2   Phase sensitive detector

An electronic device called the double-balanced mixer (DBM) offers another means for the nuclear signal detection. It has the ability to multiply two sine wave signals that enter radio frequency (RF) and local oscillator (LO) inputs.

Suppose the RF and LO inputs of the DBM are supplied by two sine wave signals: $S_{RF}=A_{RF}(sin\omega_{RF}t-\varphi_{RF})$ and $S_{LO}=A_{LO}(sin\omega_{LO}t-\varphi_{LO})$ of frequencies ω_{RF} and ω_{LO}, respectively, φ_{RF} and φ_{LO} are arbitrary phase shifts. The double balance mixer performs multiplication of both signals:

$$S(t) = S_{RF} \cdot S_{LO} = A_{RF} \sin(\omega_{RF}t - \varphi_{RF}) \cdot A_{LO} \sin(\omega_{LO}t - \varphi_{LO}) \qquad \text{Eq. } 19$$

Using the trigonometric relation: $\cos(\alpha \pm \beta) = \cos\alpha \cdot \cos\beta \mp \sin\alpha\sin\beta$ one can easily rewrite the previous equation to:

$$S(t) = \frac{1}{2} A_{RF} A_{LO} \cdot \{\cos[(\omega_{RF} - \omega_{LO})t - (\varphi_{RF} - \varphi_{LO})] - \cos[\omega_{RF} + \omega_{LO})t - (\varphi_{RF} - \varphi_{LO})]\} \qquad \text{Eq. } 20$$

In an NMR experiment S_{RF} signal corresponds to a nuclear signal that precessing nuclei induce in the probehead coil and S_{LO} signal is the reference signal that comes from the same source as the carrier frequency that produces the RF pulses. A_{RF} is a time dependent exponential function $A(t)$ that describes nuclear relaxation processes, whereas A_{LO} is the amplitude of the reference signal and can be neglected for simplicity in further analysis as shown in Eq. 21. This is justified by properties of DBMs that at certain levels of the LO signal produce an intermediate frequency signal IF, independent of the LO amplitude.

$$S(t) = A(t) \cdot \{\cos[(\omega_0 - \omega_R)t - (\varphi_0 - \varphi_R)] - \cos[\omega_0 + \omega_R)t - (\varphi_0 - \varphi_R)]\} \qquad \text{Eq. } 21$$

Figure 60 illustrates the double balanced mixer operation. Similarity of the DBM symbol to mathematical symbol $\otimes$ emphasizes its multiplication property.
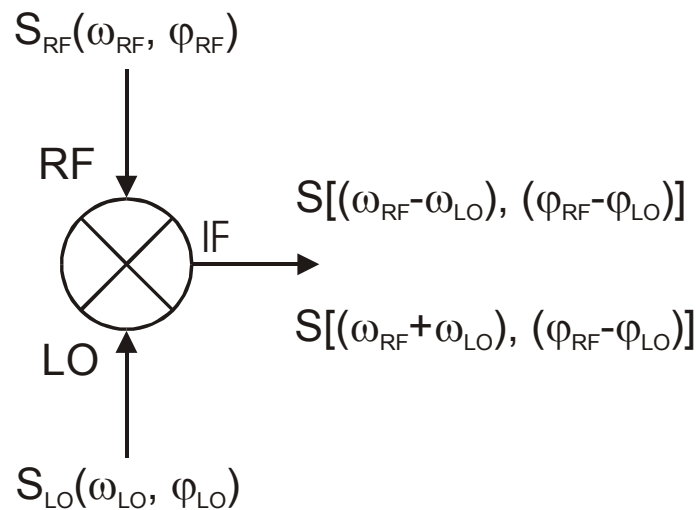
Figure 60. Double balanced mixer operation.

With proper filtering the high frequency term: $\cos[\omega_0 + \omega_R)t - (\varphi_0 - \varphi_R)]$ can be removed and Eq. 21 reduces to a less complex form:

$$S(t) = A(t) \cdot \{\cos[(\omega_0 - \omega_R)t - (\varphi_0 - \varphi_R)] \qquad \text{Eq. 22}$$

or assuming $(\varphi_0 - \varphi_R) = \Delta\varphi$

$$S(t) = A(t) \cdot \{\cos[(\omega_0 - \omega_R)t - \Delta\varphi]\} \qquad \text{Eq. 23}$$

Eq. 22 describes general off-resonance conditions when the frequency of precessing nuclei differs from reference signal.

In resonance when $\omega_0 = \omega_R$ DBM produces a signal:

$$S(t) = A(t) \cdot \{\cos[\Delta\varphi]\} \qquad \text{Eq. 24}$$

which describes the FID envelope and depends on the phase difference between the NMR signal and the reference signal, thus in this application DBM is called a **phase sensitive** detector.

The great advantage of the phase detector is:

- high linearity,
- suppression of unwanted interferences,
- sensitivity to differences between the NMR signal and reference signal frequency and phase that is of utmost importance in further FFT process.

Two parallel combined phase sensitive detectors with a 90° phase shift in reference channels constitute a quadrature detector, which is the basic device used in FT NMR spectroscopy.
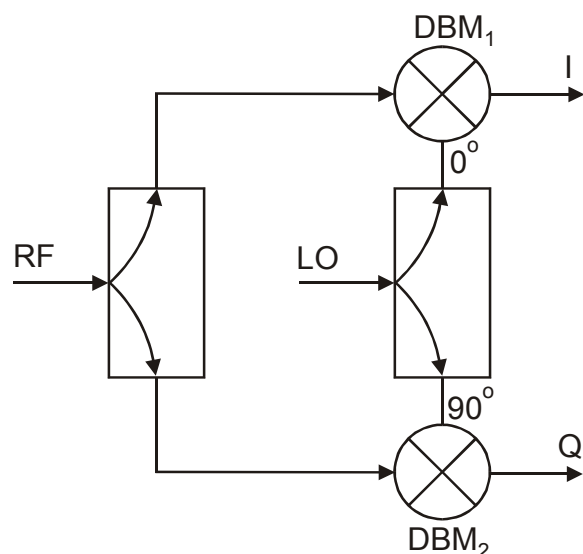
Figure 61. Quadrature detector created from two double balanced mixers, and 0°-0° and 0°-90° power splitters.

Object

Comparison of the performance of phase sensitive detector and amplitude detector.

Instructions

- Needed:
  - Pick-up coil,
  - Variable attenuator about 0-50dB, 1dB step,
  - RF generator of sine wave signal of 15MHz and about 100mV amplitude,
  - Coaxial cable with BNC connectors.

- Preparation
  - Connect experimental setup as shown in Figure 62.
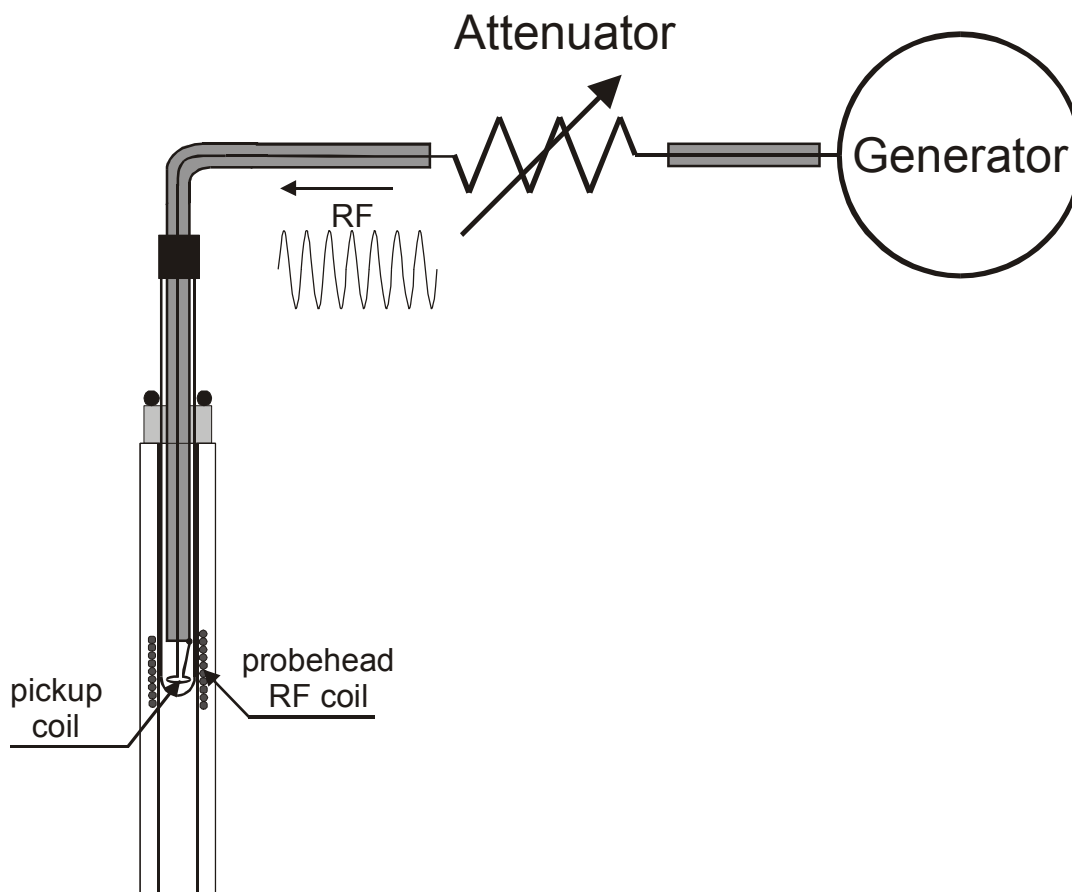
Figure 62. Experimental setup to test spectrometer phase and amplitude detectors.

  - Place pickup coil carefully inside probehead close to the top edge.
  - Set external attenuator for 20dB.
  - Set generator frequency as close as possible of 15 MHz. If there is a means of amplitude control, set the amplitude at very low level.
  - Disconnect transmit cable (**TX**) from the probehead, turn on the

spectrometer and start the control program in **Spectrometer lock-off**, **Spectroscopy mode**.
- ❑ Execute any of one-pulse sequences (**1P_X** recommended).

- • Testing the phase detector

Phase Detection ⊙
- ❑ Switch **Receiver** detector to **Phase detector**.
- ❑ Set **Receiver>Gain** to typical value used in one-pulse experiments with glycerin or water (usually around 20).
- ❑ Adjust the position of the pick-up coil and generator amplitude to have signal covering the whole range of the ADC converter (full data window). If necessary increase or decrease attenuation of the external attenuator. Have room for an extra 25dB to conduct measurements.
- ❑ Adjust generator frequency, and dwell time to see several periods of detected signal.
- ❑ Using horizontal marker conduct measurements of signal amplitude - see Figure 63.

Figure 63. Measurement of the detected signal produced from phase detector. To increase the measurement dynamic (and accuracy) measure peak-to-peak value rather than peak.

- ❑ Repeat measurements increasing attenuation to obtain 20-25 data points.

- • Testing amplitude detector.

Amplitude Detection ⊙
- ❑ Switch **Receiver** detector to **Amplitude detector**.
- ❑ Change the attenuation of an external generator to see the detected signal as a straight line reaching maximum on the data display. Unlike the phase detector the amplitude detector does not sense the frequency difference between generator frequency and spectrometer operating frequency, but responds only to the amplitude change.
- ❑ Using horizontal marker perform measurements of signal amplitude for different attenuation.

Figure 64. Signal amplitude measurements with the amplitude detector.

Results

To display acquired amplitudes as a function of the signal intensity at the detectors input first we have to transform a logarithmic scale of dBms to a linear scale of amplitudes. From the definition **K[dBm]=20log(A)**, where attenuation K is in **[dBm]** and **A** is the ratio of signal amplitudes we have an equation that expresses the signal input in signal attenuation units **A=10$^{K/20}$**. For each attenuation value **K** calculate the corresponding **A** and display the signal output amplitude against **A**.
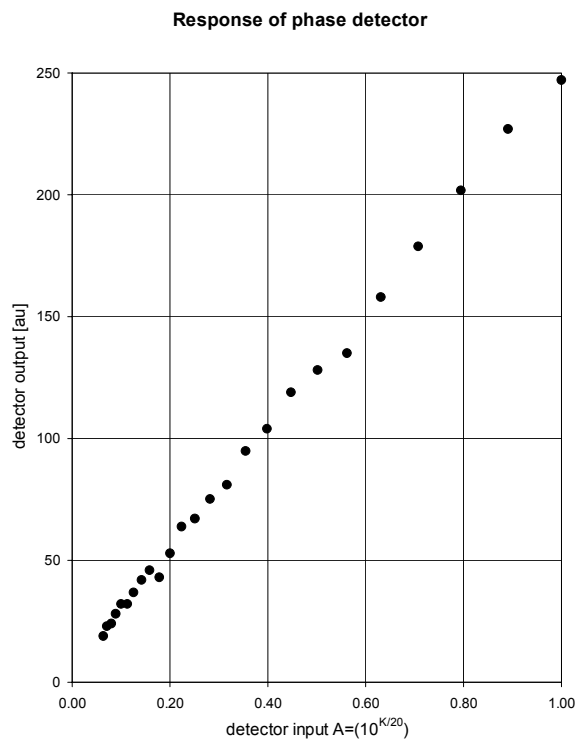
Figure 65. Response of spectrometer phase detector to the linear signal.

Response of amplitude detector
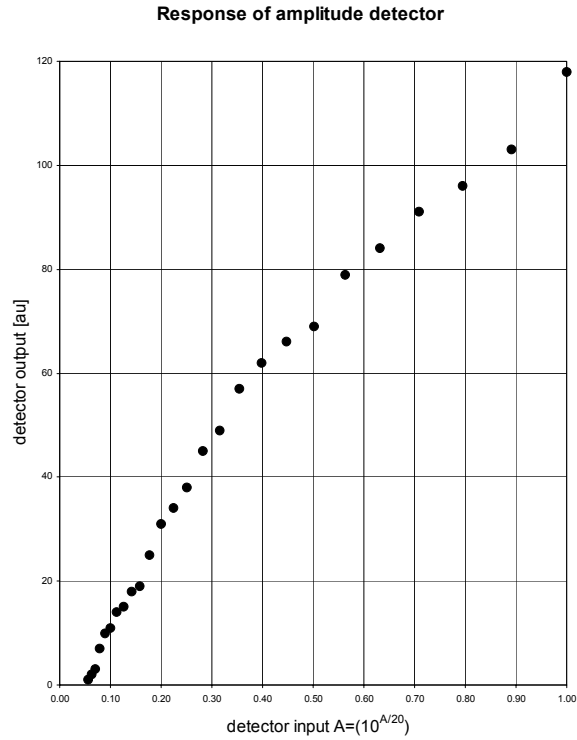
Figure 66. Response of spectrometer amplitude detector to linear signal.

Figure 65 and Figure 66 present responses of phase and amplitude detectors to linear signal. Response of phase detector is very linear from zero, whereas amplitude detector displays non-linearity for signals above 400mV. Amplitude detector is almost non-responding to signals below 50mV.

5.4 "Magic cable" or properties of lambda-quarter cable

5.4.1 Introduction

The PS 15, as with many other contemporary pulsed NMR spectrometers, uses a single resonance circuit for generating an oscillating B_1 field and for the reception of the precessing nuclear signal.

Transmit (TX)

The oscillating B_1 field is produced by a high frequency electric current that runs through the resonance circuit solenoid during the transmit period (Figure **67**). The source of the current is a power amplifier (sometimes called the transmitter to show the analogy to broadcasting) which is capable of amplifying microsecond pulses to several thousands watts of power. The small volume, highly efficient resonance circuit of the PS15 spectrometer requires much less power. Only 2-3μs pulses of 20 watts peak power is enough to generate a $\Pi/2$ pulse that translates to $60V_{peak-to-peak}$ at 50Ω load.

Receive (RX)

During the receive or detection period that follows the RF pulse, precessing spins induce a very weak nuclear signal in the solenoid (about 10μV). This signal is first amplified by a low noise preamplifier before reaching the receiver and detector.

Transmit/Receive switch

There is a conflict of applying power pulses from the transmitter to the resonance circuit and the simultaneous protection of the sensitive preamplifier connected to the same resonator. An electronic device called a multiplexer or transmit/receive switch (T/R) switches the resonance circuit between the transmitter and the preamplifier. The multiplexer must operate at a high frequency, switch very fast, last high power of RF pulses and not introduce any losses or distortion to the nuclear signal.

λ/4 cable and crossed diodes properties

The PS15 multiplexer design based on the impedance transforming properties of the coaxial cable of a length corresponding to 1/4 of the electromagnetic wave length λ (1/4λ) at the frequency of interest and of the nonlinear

Figure 67. T/R switch during the transmit period TX.

Figure 68. T/R switch during the receiving period RX.

properties of crossed semiconductor diodes connected antiparallel.

Generally for a coaxial cable length of any odd number of quarters of wavelength, $\frac{2n-1}{4} \cdot \lambda$, the input impedance of the cable is described by the formula:

$$Z_{IN} = \sqrt{\frac{Z_0^2}{Z_L}}$$

Eq. 25

When **grounded** on one end ($Z_{out}=0$) the cable shows **infinite** input impedance.

The input impedance of the **unloaded** cable drops to **zero**.

After loading the cable with an impedance of $Z_{IN}=Z_0$ the input impedance becomes the cable's characteristic impedance Z_0.

$Z_{in}=0$ $Z_L=\infty$

$\lambda/4$

The wavelength of an electromagnetic wave in vacuum is given by $\lambda = \frac{c}{f}$; where **c** is speed of light in a vacuum, and **f** is the electromagnetic wave frequency. Assuming $c=3 \times 10^9$ m/s and $f=15 \times 10^6$ Hz (15MHz) we can estimate the lambda quarter length as 5 m. In a coaxial cable, however, there is no vacuum but there is the dielectric isolator so the speed of the electromagnetic wave is much slower than 3×10^9 m/s, thus $\lambda/4$ is considerably shorter. With an RG-174/U coaxial cable a quarter lambda line is about **3.3 meters**.
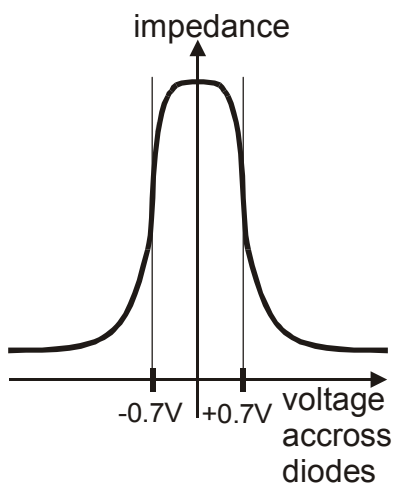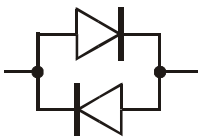
impedance

Due to their strong nonlinear voltage-current dependence, a semiconductor diode shows high impedance properties for low voltages, and low impedance properties for high voltages. Therefore diodes operate like a **switch** which is open for large signals and closed for small signals. Two antiparallel connected crossed diodes combine these properties for positive as well for negative voltages and can operate also as the aforementioned switch for an alternating signal. For silicon diodes this switching point is around 0.7 V.

-0.7V +0.7V voltage accross diodes

T/R switch operation
If combined together a $\lambda/4$ cable and two sets of crossed semiconductor diodes (**Figure 69**) will work as a tricky transmit/receive switch described below.
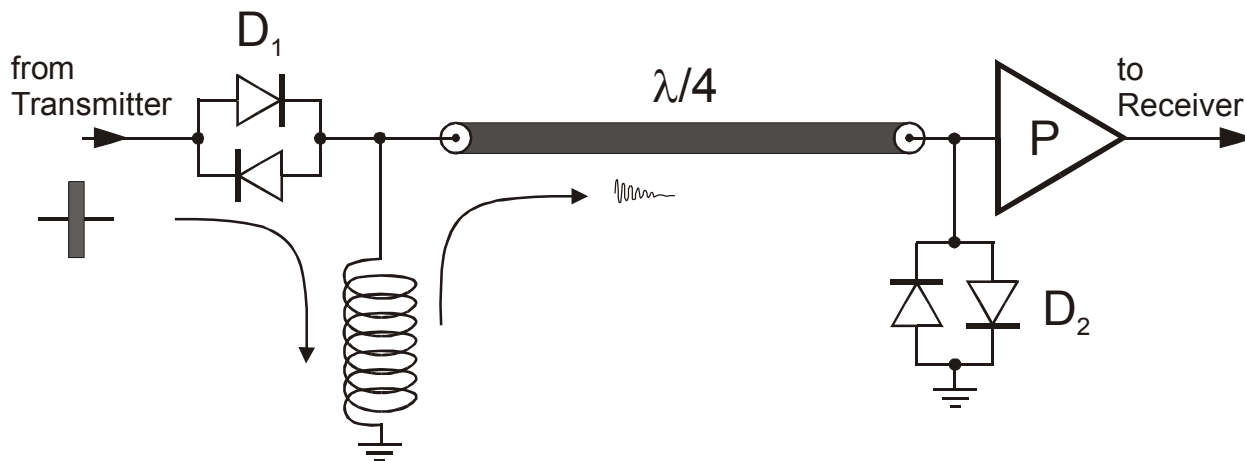
Figure 69. Passive T/R switch.

Transmit period:
- Both crossed diodes D_1 and D_2 conduct during RF power pulses (high voltage opens diodes). As a consequence the transmitter is connected to the resonance circuit while the preamplifier is disconnected from the dangerously overloaded resonance circuit.

Receive period:
- Immediately after the RF pulse is turned off, the impedance of diodes D_1 and D_2 increase (the low voltage case where diodes do not conduct). This closes the path through the D_1 diodes from the transmitter to the resonance circuit isolating it from the noise coming from the transmitter's direction. Meanwhile the high impedance of diodes D_2 opens the $\lambda/4$ coax cable and connects the resonator to the preamplifier.

5.4.2 Experimental

Object

To show "magic" properties of the $\lambda/4$ cable we will conduct a simple experiment by connecting the cable to the output of

the preamplifier and shorten and un-shorten the cable with a piece of wire while observing the FID signal on the data display.

Needed:

- $\lambda/4$ cable,
- BNC jack to shorten cable to the ground,
- BNC T adapter.

Instructions

- Plug a BNC T-type adapter between the probehead **RX** output (this is a preamplifier output) and the unit **RX** input (this is receiver input).
- On the **Setup** page prepare a one-pulse experiment with the glycerin sample.
- Connect opened $\lambda/4$ to the T adapter. Note the drop of signal on the **Setup** data window
- Now shorten the coax cable output with the BNC jack or a piece of wire and pair of crocodile clips to ground. Note signal recovery on the **Setup** data window.

Conclusion

As you see one can not apply common sense to results obtained with a $\lambda/4$ cable operating at 15MHz. Under certain conditions the coaxial cable works as an unique impedance transformer that transforms a low load impedance to a high input impedance (or high load to low input impedance).

5.4.3 More experiments with λ/4.

If you have a signal generator (G) and an oscilloscope (Osc) available in your laboratory you can make a more systematic study of λ/4 cable properties. Connect an experimental setup as shown and change the frequency of the generator with the λ/4 shorted to ground. Look for the maximum of the signal at 15 MHz. Now open the cable, change the frequency and observe the minimum of the signal at 15 MHz. Compare your observations to Eq. 25.
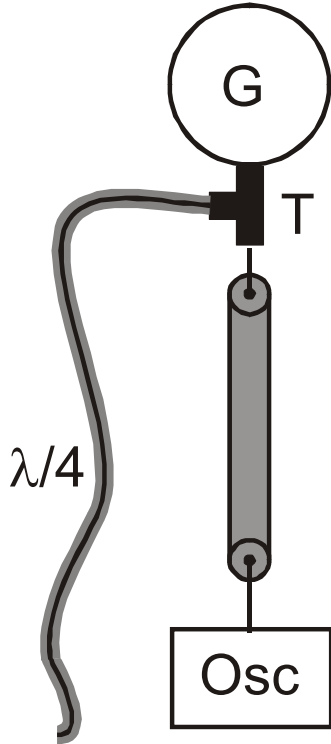
Connect an additional piece of coax cable through the BNC barrel adapter and look at the shift of frequency of the maximum/minimum signal toward lower frequencies.

You can replace the oscilloscope and generator with more advanced device like a network analyzer and have the cable frequency characteristics in a matter of seconds. Figure 71 and Figure 72 show reflected power from **shorted to ground** and **open** λ/4 15 MHz cable, respectively, obtained with Agilent (formerly Hewlett Packard) network analyzer. Note that positions of minimums and maximums fit to these predicted by Eq. 25

Figure 70.
Experimental setup to study λ/4 cable frequency properties.
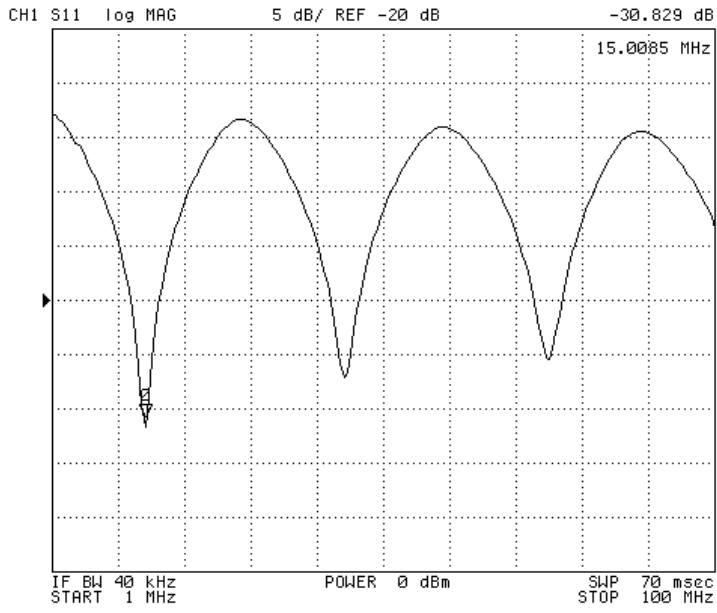
Figure 71. Reflected power from λ/4 15 MHz cable shorted to ground.
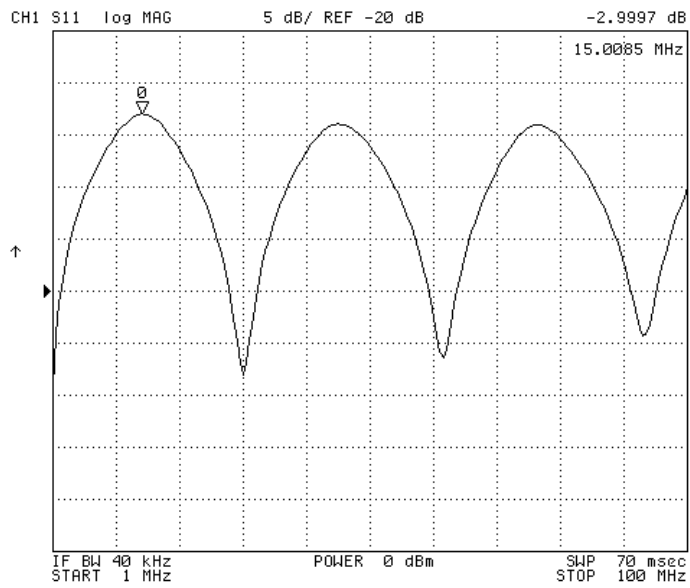
Figure 72. Reflected power from l/4 15 MHz open cable.

5.5 Measurements of a static magnetic field with a tesla meter (Smart Magnetic Sensor)

5.5.1 Introduction

An electric current flowing through a conductor located in a magnetic field experiences a transverse force called the Lorentz F_L magnetic force. This force is defined as a vector product:

$$\vec{F}_L = q\vec{v} \times \vec{B} = qvB \sin \Theta$$

Eq. 26

q - carrier charge
v - velocity of the carrier
B - magnetic induction
Θ - angle between vectors v and B
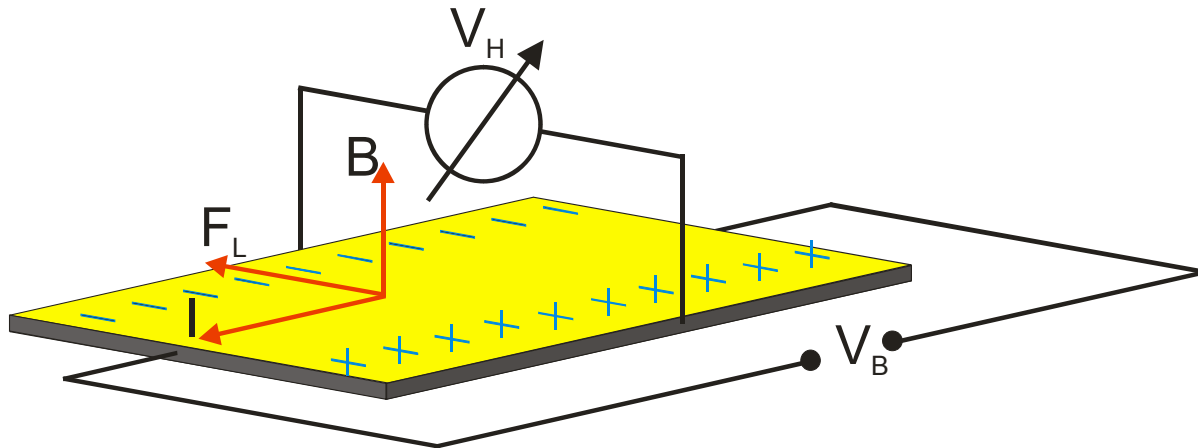
Figure 73. Lorentz force and separation of flowing electric charge (**+/-**) by an external magnetic field **B**.

Eq. 26 implies the following:
  a) The magnetic force is perpendicular to both the current **I** and the magnetic field **B**
  b) The magnitude of the magnetic force **F$_L$** is zero when charges move parallel to the magnetic field (or when the charges are stationary) and reaches a maximum $\pm(qvB)$ when the charges move perpendicular to the magnetic field
  c) Direction of the force can be determined by the "right hand" rule

The Lorentz magnetic force separates moving charge carriers (Figure 73). The separation effect was named *Hall effect* after E.H. Hall who discovered it in 1879. The charge separation produces transverse voltage between two sides of the conductor that is linearly proportional to the magnetic field *B* and is used to measure magnetic field.

TEL-Atomic Inc., introduces a new pocket-sized Tesla Meter Model 2000 equipped with Hall probes that cover the measurements of a magnetic field in the range of 0.01 to 1999 mT. This tesla meter can be used in a series of experiments with a PS15 electromagnet to measure the magnetic field inside and outside the magnet and to illustrate properties of the Hall effect magnetic sensors.

5.5.2 Experiment preparation

Before starting experiments prepare the spectrometer electromagnet and tesla meter probe.

1. For all measurements use the tesla meter axial probe type SMS102. Since the axial probe is too big to fit in a NMR probehead, the probehead should be removed to give free access to the space between electromagnet poles.

To do this, turn off the unit and unscrew the two locking screws from magnet (but do not disconnect any cable) and lay the probehead flat on a table (see Figure 74). Now turn on the NMR spectrometer, but do not start the control program. With the NMR probehead removed and the control program not running, the electromagnet coils are driven only by the current from a regular power supply and neither flux nor NMR-lock field stabilizer is active. Nevertheless precision of the spectrometer current stabilizer is sufficient for stable indications of the tesla meter's last digit.
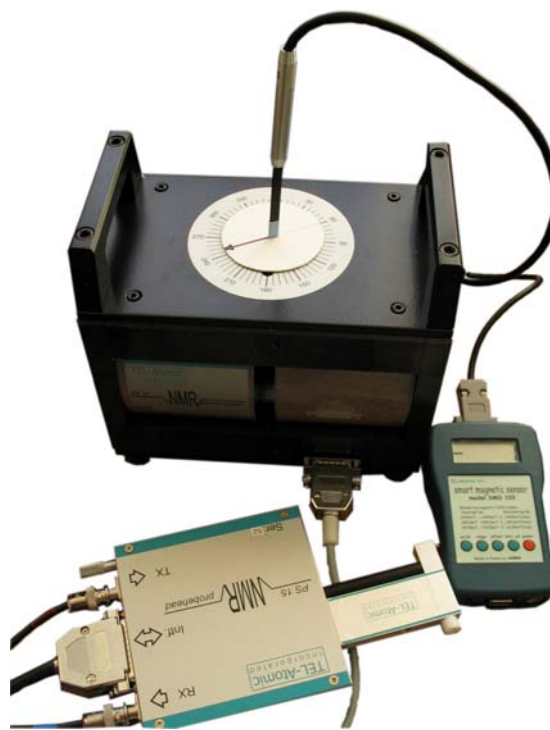
Figure 74. Electromagnet, detached NMR probehead and the tesla meter.

2. Wrap the tesla meter sensor in the middle 2-3 times with ¼" paper tape (see Figure 75).

3. Cut a 1" diameter disc from cardboard 1/8" thick.

4. With a sharp blade cut a rectangular shape in the center that will fit the tesla meter probe. Draw an arrow extending from the probe.

5. Slide the tesla meter probe in the slot. *The arrow will be useful in angle measurements while the edge of the paper tape gives a convenient reference in magnetic field mapping.*

Figure 75. Probe and disc assembly.

5.5.3 Angle dependence of the Hall sensor readings

Generally a magnetic field is a three dimensional vector. A one-axial probe detects Hall voltage only in one direction and as a consequence measures **ONLY** one component of the magnetic field. Measuring the magnitude of this component depends on the orientation of the probe with regards to magnetic the field.

TEL-Atomic's 2000 Tesla Meter Probe is essentially the substance that displays a strong Hall effect. As a consequence it shows an angle dependence between the orientation of a magnetic field and the direction of the charge current I. From Eq. 26 one can expect zero charge separation and zero Hall voltage when B is parallel to v (or I), and maximum indications when B is perpendicular to v.

The purpose to this experiment is to the find main axis of the tesla meter probe. Proper measurement of the magnetic field magnitude requires perpendicular orientation of this axis to the magnetic field.

1. Insert the tesla meter sensor in the slot on the top of the magnet (Figure 76)
2. Measure magnetic field in the current sensor position
3. Rotate sensor and repeat measurements every 20-30 rotations
4. Make a plot of the tesla meter readings B versus the angle Θ
5. Try to fit the $B = f(\Theta)$ plot to Eq. 26 . In the Figure 77 black circles show experimental points while the red line is the fit.
6. For further considerations take into account that the PS15 electromagnet field is oriented along poles' axis (90°-270°)

Figure 76. Tesla meter probe and the hand made disc assembly on the magnet's dial.
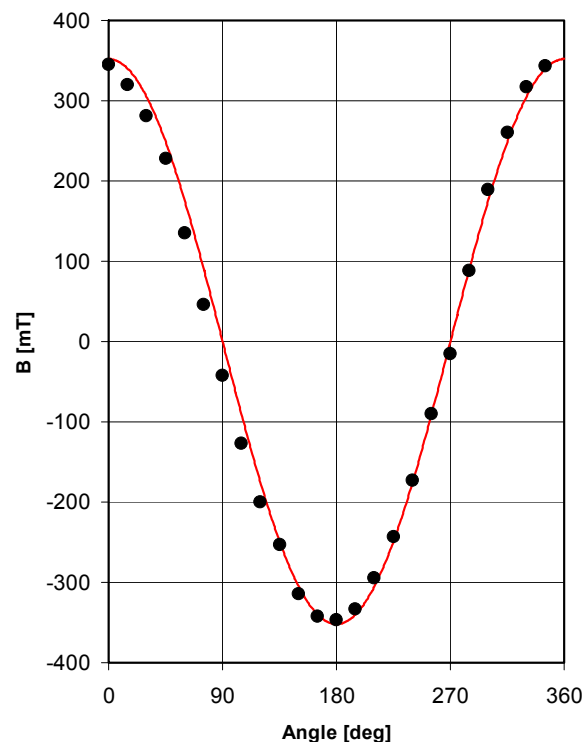
Figure 77. Angle dependence of tesla meter readings (black circles) and data fit to sinΘ function (red line).

5.5.4 Mapping magnetic field

The magnetic field is confined mostly between the electromagnet's poles. The tesla meter provides a convenient way to map the field i.e. to produce 1- or 2-dimensional pictures showing the spatial distribution of the magnetic field.

Mapping requires knowledge of the magnetic sensor position and magnetic field amplitude. In 1-dimensional mapping the distance from a fixed point of reference is needed. In Figure 78 the magnetic sensor is placed in the magnet's center and then moved vertically such that the magnetic field can be recorded every 5 mm of displacement.
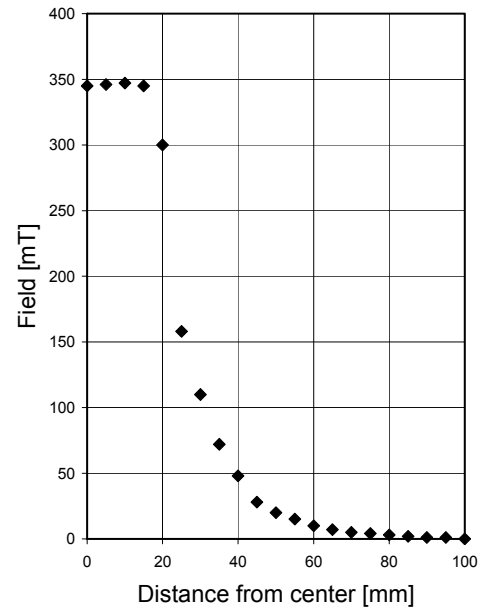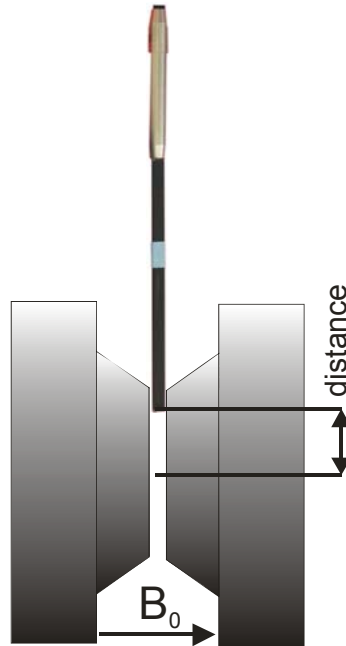
A 2-dimensional mapping presents a certain challenge but can be overcome with some ingenuity of the experimenting person.

Figure 78. Electromagnet's one-dimensional field map.

5.5.5 Measuring magnetic field remanence

A magnetic field in an electromagnet is produced by a direct current that flows through its coils. The amount of magnetization the electromagnet retains at zero driving current (field) is called **remanence**. It must be driven back to zero by a current (field) in the opposite direction.

One can see **remanence** of the PS15 magnet in the following experiment.

With the console off (no current) insert the tesla meter probe between poles. While rotating the probe measure the magnetic field amplitude. Usually remanence varies between 2-5 mT. Note

Figure 79. Remanence field on the hysteresis curve.

that the magnitude of the Earth's magnetic field is an order lower (around 0.05mT) and cannot significantly contribute to the measurement.

6   TOWARDS MORE DIFFICULT EXPERIMENTS

6.1 Angle dependence of spectra shape in the gypsum monocrystal

6.1.1 Introduction

It has been seen from the study of oriented crystals, that ^{1}H NMR spectra of solid samples can give structural information that X-ray crystallography cannot deliver due to poor X-ray scattering on the hydrogen single electron.
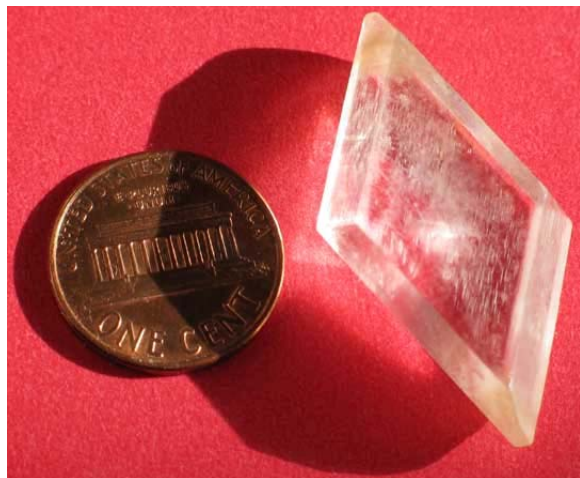
Figure 80. Large gypsum monocrystal. Note high transparency with slightly yellow edges. Long diagonal is about 40 mm.

This observation was first published by G. E. Pake in the early years of NMR[3]. He observed the splitting of the NMR line from water protons in a hydrated gypsum ($CaSO_4 \bullet H_2O$) monocrystal (Figure 80) and powdered samples. The splitting originates from the interacting of magnetic dipoles μ in a static magnetic field B_0. In crystalline solids these interactions produce an additional local magnetic field B_{loc} which contributes to the effective magnetic field acting on each spin. In less rigid substances, (mostly gases and liquids) fast molecular motion averages this local magnetic field to zero.

Since **dipole-dipole** interactions decrease as the **inverse cube** of the dipoles distance, nuclear moments of protons in water molecules of hydrations are predominantly in the local field of its neighbor. Thus protons in water (spin ½) can achieve two positions with regard to the static magnetic field B_0. Some spins will be located in higher fields (when the neighboring spin is parallel to B_0) and some will be in lower fields (when the

---

[3] G.E. Pake, The Journal of Chemical Physics vol.16, p. 327-336, 1948, "Nuclear Resonance Absorption in Hydrated Crystals: Fine Structure of the Proton Line"

neighboring spin is anti-parallel to B_0). In this simplified model, two NMR lines appear symmetrically located along the resonance at B_0.

Of the hydrous sulphates, hydrous calcium sulphate, of the chemical formula $CaSO_4 \bullet H_2O$, known as gypsum, is the most important. (The average American house contains around 5 tons of gypsum construction material!).

The gypsum structure consists of parallel layers of $(SO_4)^{-2}$ groups bonded to Ca^{+2}. Sheets of water molecules separate consecutive layers of strongly bonded ions. The bonds between water molecules in neighboring sheets are rather weak causing the crystal to break when it is a subjected to stress on a plane parallel to the sheets. This property is known as perfect cleavage in the (010) plane.

One can determine proton-proton distance in a water molecule by Pake's method, that is from the angle dependence of NMR line splitting. Assuming a certain angle of H-O-H obtained from crystallographic analysis the value of proton-oxygen distance can be calculated (Figure 81).
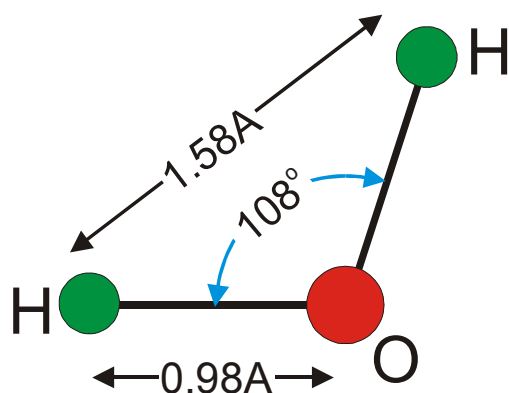
Figure 81. Atoms distances and angle in a water molecule according to Pake. H-H distance of 1.58Å was calculated from spectra splitting. H-O distance was calculated from assumption of $108°$ angle of H-O-H bond.

6.1.2 Experimental

Object

The purpose of this experiment is the **observation of the splitting** of the NMR line originating from water protons located in different local magnetic fields of the gypsum monocrystal. This experiment can illustrate high-resolution NMR spectra in solids.
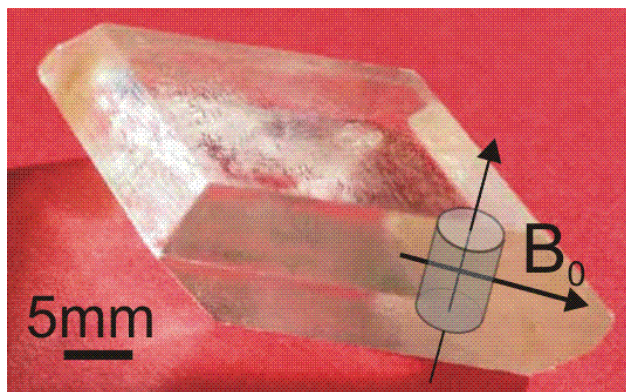
Figure 82. Sample cut from gypsum monocrystal and its orientation with regard to external magnetic field B_0.

The sample has a cylindrical form of approximately 5mm diameter and 6mm long. It was cut from a large gypsum monocrystal as shown in **Figure 82**. The long axis of the sample is perpendicular to a crystal perfect cleavage (plane (010).

Directions

1. Carefully remove the gypsum crystal glued to the 5 mm glass tube from the storage box (Figure 83),
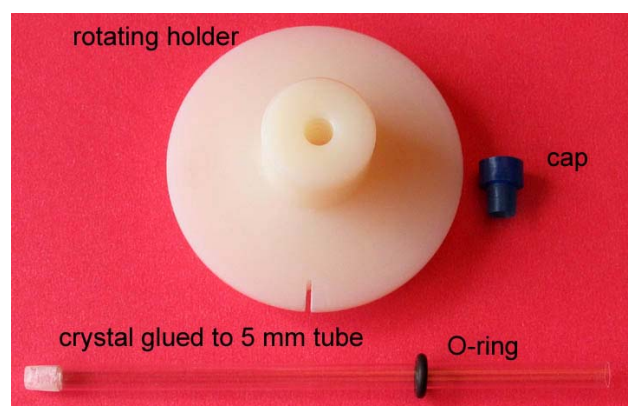
Figure 83. Elements used in the gypsum study.

2. Attach the crystal to the goniometer rotating holder.

   a) Slide the O-ring on the glass tube from the end not occupied by the crystal.
   b) Using this positioner move the O-ring to its right location. To assure proper position of the crystal in the RF coil its center should be L=70 mm from the bottom surface of the holder. If necessary to determine sample position more accurately measure the distance L by mapping the RF field of the probehead coil (see Chapter 5.1)
   c) Slide tube through the center hole in the holder until the O-ring securely nests inside as shown in Figure 84.

3. Insert the sample carefully inside the magnet (see Figure 85).
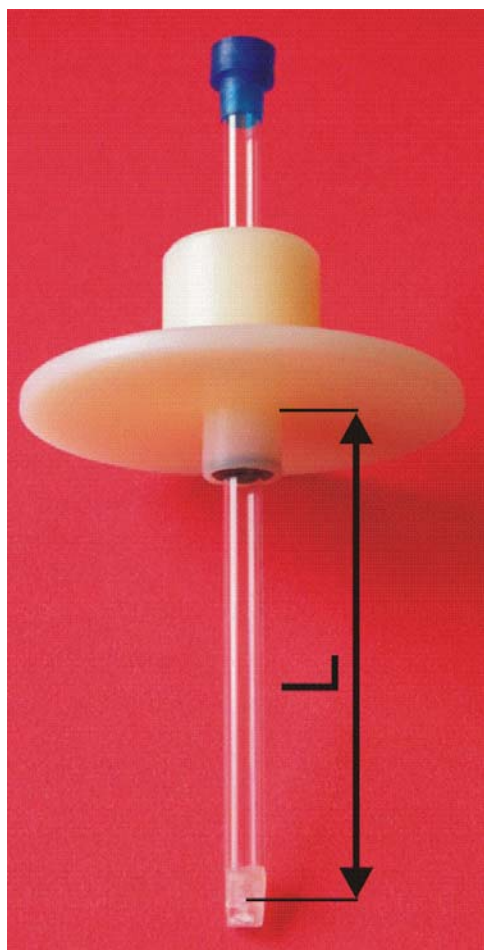
Figure 84. Gypsum crystal attached to the rotating holder. Distance from the crystal center to bottom of the holder (that rests on goniometer dial surface on the magnet) is L=70mm. Check this distance after final assembly with a caliper.
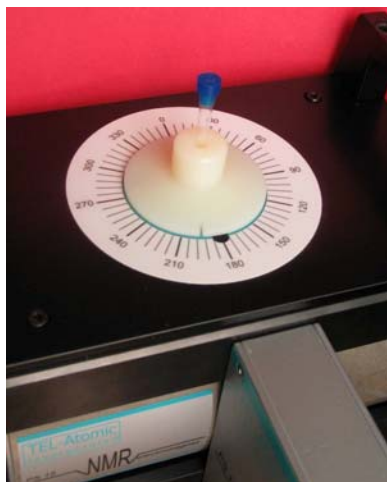
Figure 85. Gypsum crystal assembly in the magnet.

4. On the **Setup** page prepare a simple ONE PULSE experiment using the 1P_X method with the acquisition parameters similar to these in Figure 86.
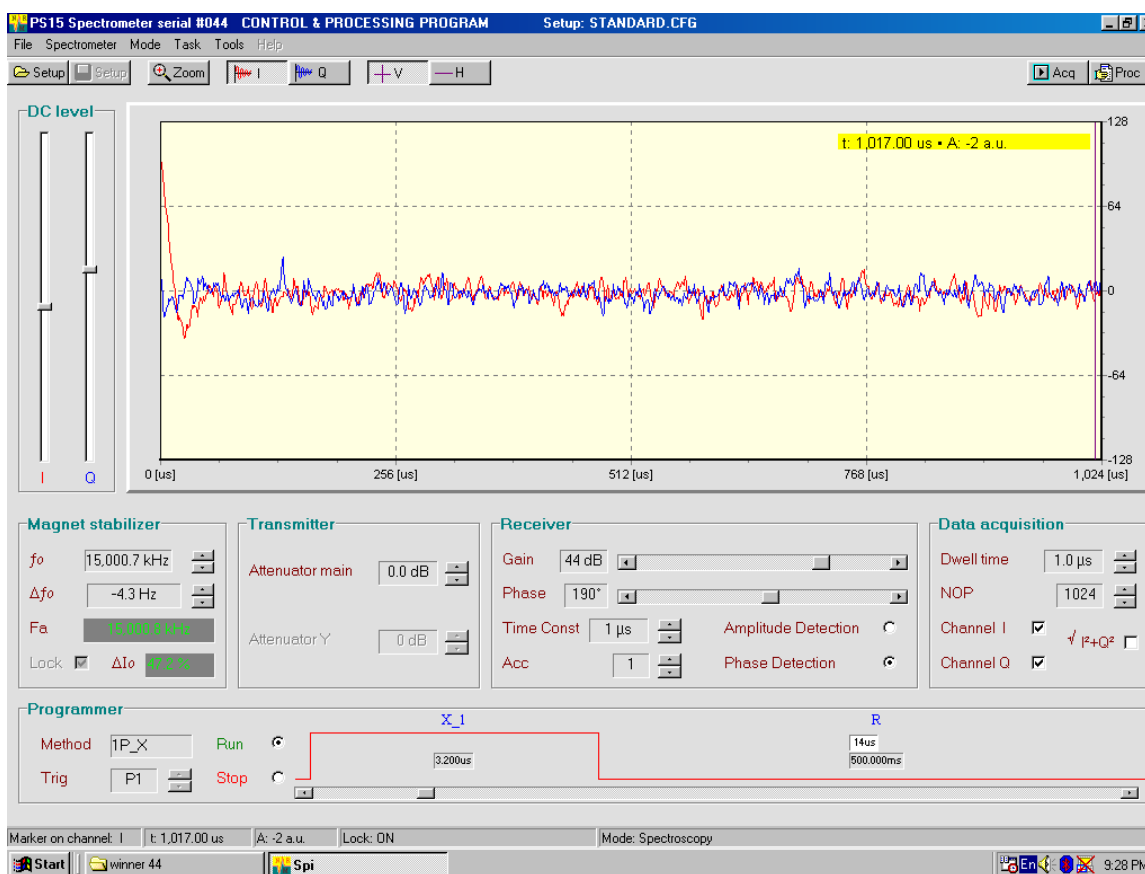
Figure 86. **Setup** page to acquire FIDs from gypsum crystal. Note that signal is very weak and short. Remember to adjust acquisition time and receiver gain accordingly.

5. On the **Data Acquisition** page acquire the signal with at least 128 accumulations to improve Signal-to-Noise ratio.

6. On the **Data Processing** page perform FFT (Figure 87). If there are points affected by "dead time" perform Left Shift (LS) first to remove distorted points. If spectra are to noisy multiply exponentially FIDs by 200-400 Hz.
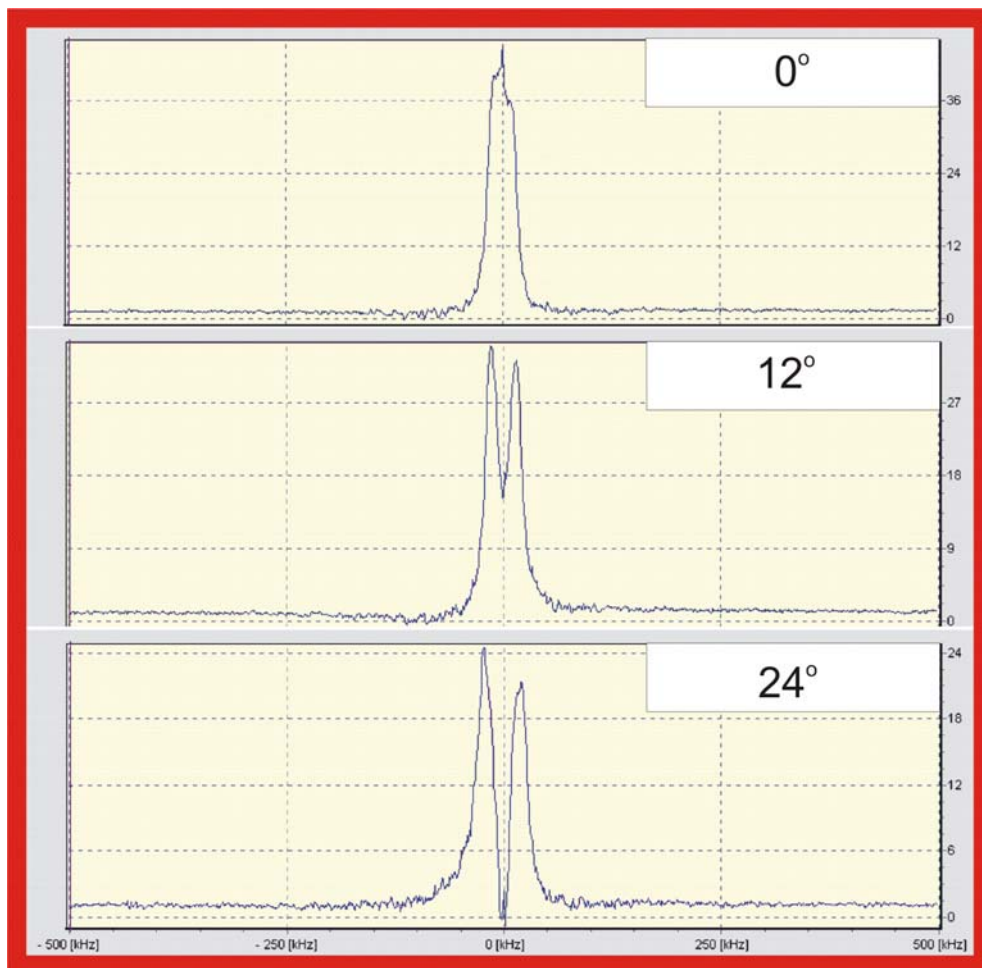
Figure 87. Splitting of the ^{1}H NMR line in gypsum crystal due to the rotation of the crystal. Crystal was rotated clockwise along axis perpendicular to perfect cleavage plane (010). B_0 direction was changing in this plane.

7. Repeat a FID acquisition for different angles to see change of the splitting in the spectra.

Suggested modifications:

- Acquire a large gypsum crystal, make another cut and repeat measurements.

You may purchase gypsum monocrystals from:

Great South Gems & Minerals
38 Bond Drive,
Ellenwood, GA 30294
1-888-933-4367
www.greatsouth.net

- Since cutting gypsum is a difficult task, crush the monocrystal to powder and repeat measurements with a polycrystalline sample.

- Place small amount of dry plaster composition that contains predominately gypsum. Acquire FID of dry powder. Than add drop of water and acquire several FIDs when mixture hardens.

6.2 Rotating frame experiments

6.2.1 Introduction

Effective magnetic field in a rotating frame

The rotating coordinate frame is a convenient reference frame for use in analyzing the interaction of the macroscopic nuclear magnetization M_0 arising from the polarization of individual nuclear spins in the static magnetic field B_0 with rotating magnetic field B_1. In the rotating frame that moves with B_1 field, nuclear spins are stationary or in the presence of static field inhomegeneity they move very slowly. Since the laws of Physics are independent of the reference frame this slow motion of spins in the rotating frame implies that the effective magnetic field in the rotating frame must be much smaller than in a laboratory frame (or zero when spins do not move at all).

The transformation from a laboratory to a rotating coordinate frame gives the following equation for the effective magnetic field B_{eff} in a rotating frame:

$$\vec{B}_{eff} = \vec{B}_0 - \vec{\omega}_R/\gamma + \vec{B}_1 \qquad\qquad \text{Eq. 27}$$

Where ω_R/γ represents a fictitious magnetic field that appears while going from the laboratory to the rotating frame. When a rotating frame moves near the Larmor frequency of precessing spins $\omega_R \approx \omega_0 = \gamma B_0$ the fictitious field cancels B_0 and only B_1 remains to interact with M_0. Figure 88 shows the complete vanishing of B_0 in a rotating frame when $\omega_R = \omega_0$. As a consequence the entire problem of interaction of M_0 with B_0 and B_1 in a laboratory frame is conveniently reduced to rotation of magnetization along the now static field B_1 in the rotating frame in the sense of the nuclear precession.
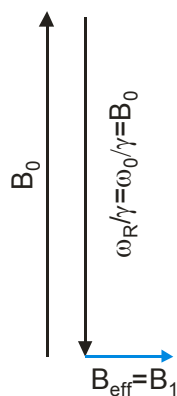
Figure 88. Reducing of effective magnetic field in a rotating coordinate frame when the angular frequency of rotation approaches the Larmor frequency.

In practice the B_1 field amplitude can be easily calculated from the measurements of the

angular frequency of precession of magnetization $\boldsymbol{\omega_1}$ along $\mathbf{B_1}$. Since:

$$\omega_1 = \frac{\Theta}{t_p} = \gamma B_1$$

Eq. 28

Where Θ is rotation angle, t_p is time of rotation that corresponds to the length of the RF pulse t_p.

Since for protons the gyromagnetic ratio $\gamma=2.6752$ [kg^{-1}sA], therefore one can transform Eq. 28 to a simple formula to calculate the approximate value of $\mathbf{B_1}$ in [Gs][4]:

Where t_Π is time of a Π (180°) pulse in microseconds [μs].

$$B_1 = 117.2/t_\Pi$$

Eq. 29

The PS15 20W transmitter, (with the combination of the RF coil which is included with the system and having dimensions of 10mm long and 5mm wide, and quality factor Q$\approx$30), generates t_Π pulse that for protons varies from 5μs to 7μs thus producing a maximum $\mathbf{B_1}$ field in the range of 23Gs to 17Gs. This is of course an amplitude of one rotating component of the $\mathbf{B_1}$ field that follows the direction of rotation of nuclear spins.

"Spin-locking" and relaxation in the rotating frame.

The rotating frame is not only an intellectual vehicle that can be used for a simple vector visualization of NMR effect. A drastic reduction of the magnetic field magnitude when the rotating frame moves close to a precessing nuclei leads to certain physical consequences that can be studied using a series of ingenious experiments.

- When $\omega_R = \gamma B_0$ the radiofrequency field $\mathbf{B_1}$ that is constant in the rotating frame starts to play the role that $\mathbf{B_0}$ plays in laboratory frame. In this lower field, spins precess at a much lower frequency providing information about molecular dynamics in a frequency range of kHz (acoustic waves) rather then in MHz (radio frequency) that is obtained in the laboratory frame of classical NMR.

- If a strong enough $\mathbf{B_1}$ field is applied it can eliminate the effect of line broadening due to magnetic field inhomogeneity $\mathbf{\Delta B_0}$ (Figure 89), as well as dipolar broadening. This can eventually permit high resolution NMR spectroscopy in solids where line broadening has a strong contribution from static magnetic dipolar fields.

---

[4] Use:1T=10^{4}Gs, and [T]=[NA^{-1}m^{-1}] to convert Tesla to Gauss.
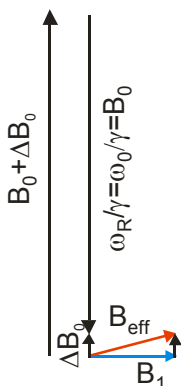
Figure 89. Effect of constant magnetic field inhomogeneity ΔB_0 on effective field.

"Spin-locking" experiment illustrates the benefits of multiple power sequences with independently adjusted time, phase and power of the individual pulses. This feature is available in the PS15 spectrometer. The sequence (Figure 1) consists of two RF pulses.
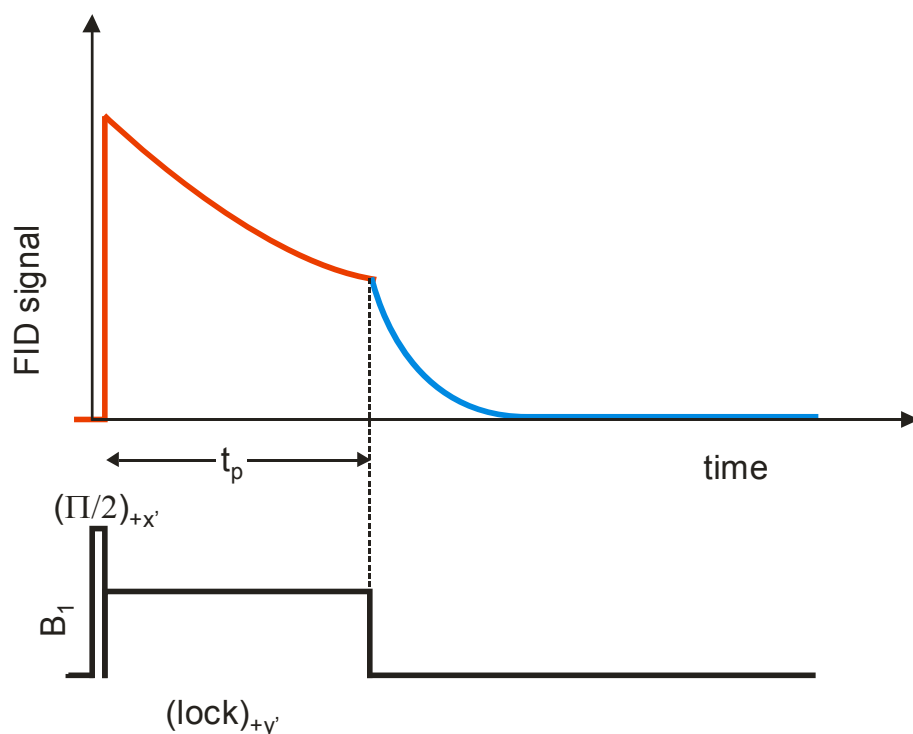
 Figure 90. "Spin-locking" sequence and measuerement of $T_{1\rho}$. During locking, magnetization decreases in the presence of the B_1 field (red line). Nuclear signal is not visible during this period due to receiver blocking by RF pulse. When locking pulse is off, the FID amplitude can be measured. A plot of the FID amplitude as a function of lock time t_p will decay with $T_{1\rho}$ constant.

First is a short $\Pi/2$ pulse along +x axis that moves the magnetization $\mathbf{M_0}$ on the x'y'

plane as seen in Figure **91**a (on the x'y' plane **M₀** becomes **M_y**). Soon after the Π/2 pulse is completed a second much longer RF pulse along +y axis is applied (Figure **91**b). If **B₁** >> **ΔB₀** magnetization **M_y** and field **B₁** are parallel so there is no torque exerted on **M_y** and magnetization is "spin-locked" to **B₁**. As mentioned before **B₁** in the rotating frame starts to play the role of **B₀** in laboratory frame as **B₀** is entirely compensated by the fictitious field ω_R/γ (Figure **91**c).
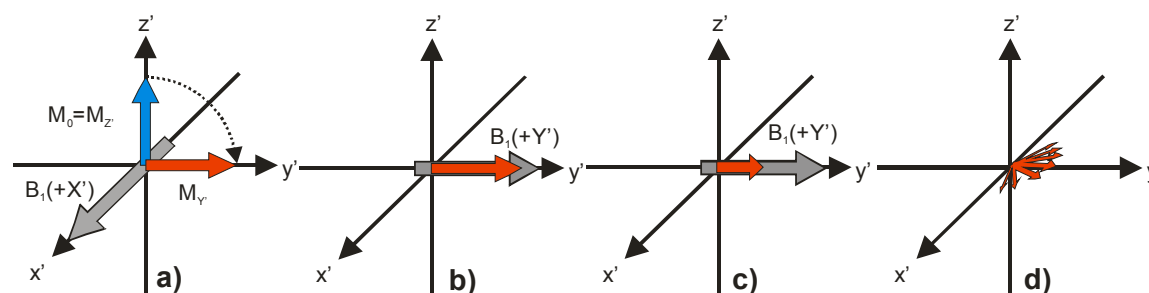
Figure 91. Effect of Π/2 and **lock-pulses** on **nuclear** magnetization **in a rotating frame.**

The longitudinal relaxation process that follows along **B₁** is somewhat similar to spin-lattice relaxation along **B₀** and is called *T₁ in the rotating frame* characterized by a $T_{1\rho}$. Since in a rotating frame the magnetization is polarized in a much smaller field (**B₁**<<**B₀**) therefore magnetization needs to relax from **M_y**=**M₀** to the much smaller equilibrium value (Figure **91**c). When the locking pulse ends the magnetization in x'y' plane inevitably decays very quickly due spin-spin relaxation (Figure **91**d).

Spin-lattice relaxation in the rotating frame is closely related to spin-spin relaxation in the laboratory frame and with the absence of a locking **B₁** field, the relaxation along y' is of course characterized by **T₂**. In liquid samples this is essentially the same time. For instance, when problems with a cumulative error in the train of Π pulses in the standard multi-echo method occur, then spin-locking is more accurate for determining spin-spin relaxation times.

6.2.2 Experimental. $T_{1\rho}$ in rubber and in acrylic.

Object

Measurement of spin-lattice relaxation time in rotating frame $T_{1\rho}$ by "spin-locking method".

Note:
Regardless of the sample used in performing a $T_{1\rho}$ experiment in a rotating frame there are three elementary steps.
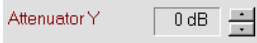
- Estimation of the local magnetic field **ΔB₀**. Measurement of line width at half height in [Hz] and recalculating it to [Gs] is a good measure of the local magnetic field distribution.

- Lock pulse calibration to determine if the **B₁** magnetic field is strong enough to cause spin locking. Assure the correct conditions for spin locking are met when: **B₁ >> ΔB₀**.

- Measurement of free induction decay amplitude as a function of the locking pulse length and final calculating of $T_{1\rho}$.

Instructions:

Estimation of the local magnetic field ΔB₀
1. Insert sample (we recommend starting with a rubber sample) in a sample holder,
2. Switch spectrometer to **Spectroscopy Mode**,
3. Load one-pulse method **1P_X**,
4. Set parameters to acquire FID signal in orthogonal channels (I&Q),
5. On the **Acquisition** page acquire FID signal and store it in a file on disk.
6. On **Acquisition** page perform FFT of the signal.
7. Calculate line width at the half peak,

8. Using formula $\Delta f = \dfrac{\gamma}{2\Pi}\Delta B$ (γ=2.6752 [kg⁻¹sA], 1T=10⁴Gs) convert line width units from frequency domain in [Hz] to magnetic field domain in [Gs].

Lock pulse calibration
1. Switch spectrometer to **Relaxometry Mode**
2. Load method **SL_cal** to calibrate the spin locking pulse,
3. In the **Transmitter** window set the attenuator in the Y channel to zero
   Attenuator Y [0 dB] and determine the length of t_Π pulse[5],
4. Repeat measurement of t_Π for all available attenuations of the pulse (0 through 7),

---

[5] Simply start with the shortest available pulse, increment it by 0.2µs and watch for when the FID signal goes through maximum and becomes zero. For details refer to text on page 17.

Due to the power supply limit, the PS15 transmitter can not operate with full power of 20 W with a duty cycle[6] above 1%. To avoid a decrease of power of the pulse or safety blanking of the transmitter by the software, adjust repetition time t_R according to locking pulse length. For example, using a locking pulse of the maximum available power and a time of (100ms) set T_R no less than 10s.

$T_{1\rho}$ measurement

1. Load method **spin_lock** to measure $T_{1\rho}$,
2. Adjust parameters on **Setup Page** to get a strong on-resonance FID signal after the locking pulse (similar to these on Figure 92). For better usage of the dynamics of the ADC converter move signal noise line below zero level.
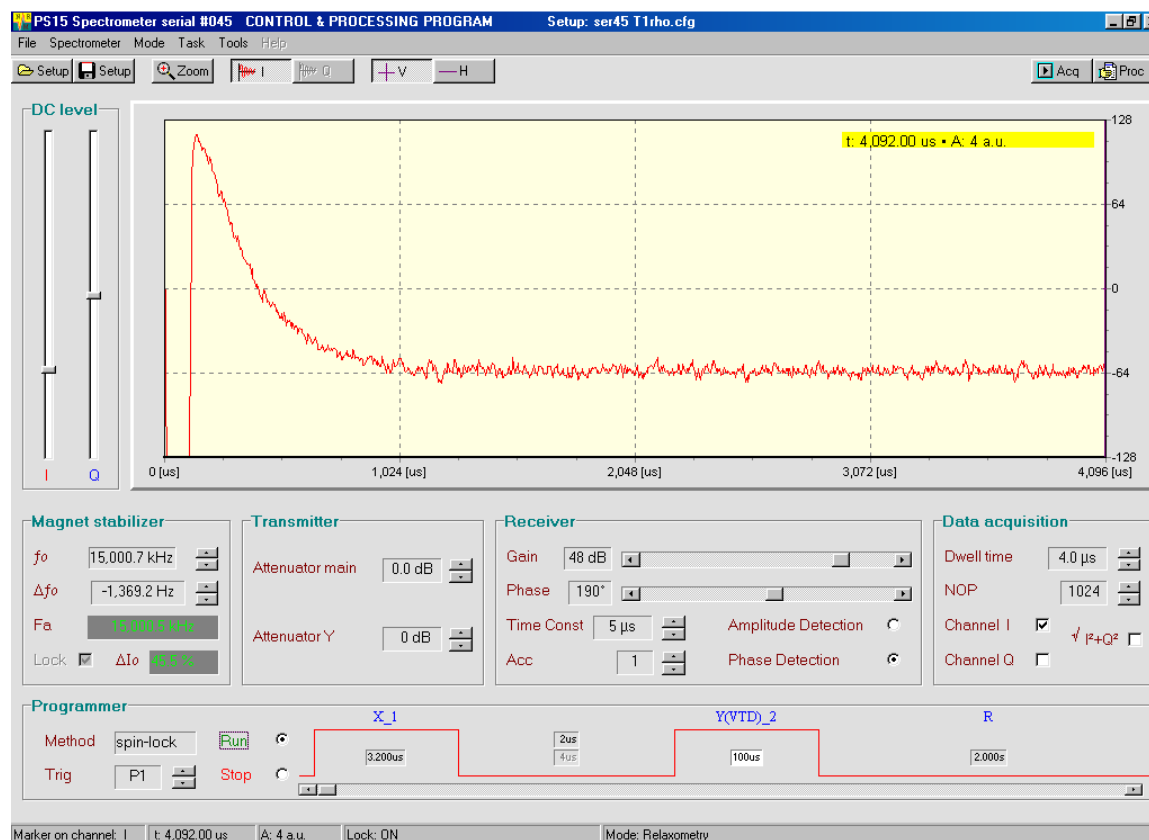
Figure 92. **Setup** page for $T_{1\rho}$ measurements in rubber.

3. Measure FID amplitude as a function of locking pulse width.
   a. **Manually**:

---

[6] Duty cycle is defined as $f_d = \dfrac{t_p}{t_R} \cdot 100\%$, where t_p is pulse time, t_r is repetition time.

- by changing the pulse width of spin locking pulse **Y(VTD)_2** and recording the amplitude of the FID using the horizontal or vertical cursor. To see FID in the same position on the screen select acquisition triggering after the locking pulse (in **Programmer** window set **Trig** box to **P2**) Trig | P2 .

b. **Automatically** by:

- creating on the **Acquisition Page** a file with different times for **Y(VTD)_2**,
- performing an automatic change of the **Y(VTD)_2** pulse and simultaneous acquisition of corresponding FID,
- storage of the complete experiment in a file.

Please remember that automation of the algorithm of data processing requires the setting of acquisition triggering after the locking pulse (**Trig P2**).

4. If data are acquired manually use any program capable of performing regression analysis of the natural logarithm of FID amplitude as a function of **Y(VTD)_2** pulse width (Excel, Origin),

5. If data are acquired automatically go on **Processing Page**, load data file, extract data points and calculate $T_{1\rho}$ by clicking on **SL** button. SL .
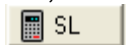
$T_{1\rho}$ in rubber

This part of the *Manual* presents a summary of experimental data used to determine $T_{1\rho}$ in rubber.

■ **Estimation of local magnetic field from spectrum line width**

An NMR spectrum obtained from rubber is shown in Figure 93. The acquired FID was multiplied by an exponential function to improve S/N. This multiplication broadened the spectrum by 50 Hz. After a 50Hz subtraction, the effective line width of the spectrum is **Δf_0=800 Hz** and corresponding **ΔB_0=0.2Gs**.
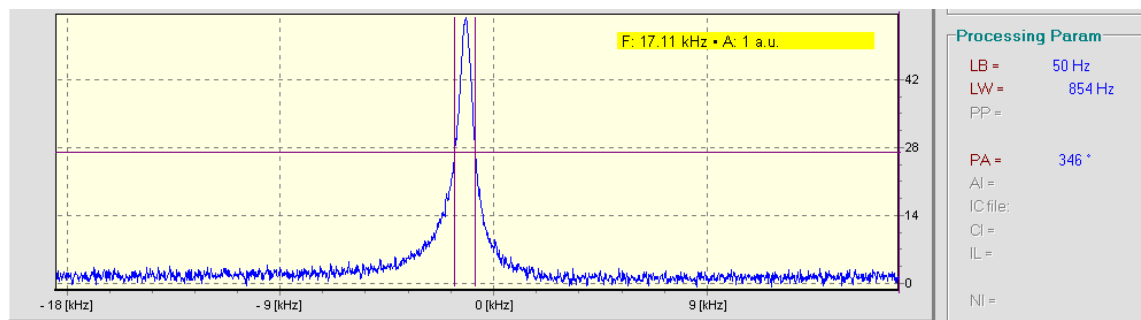
Figure 93. Rubber sample. NMR spectrum after FTT with 50Hz line broadening**.**

■ **Lock pulse calibration**

Figure 94 and Figure 95 and present calibration data of a PS15 unit. Notice that the attenuator on the Y-channel permits the change of **B_1** field from **5Gs** to **17Gs**. Even with the highest attenuation of 7dB the B_1 field (5Gs) is still much higher than the magnetic field inhomogeneity (0.2Gs).
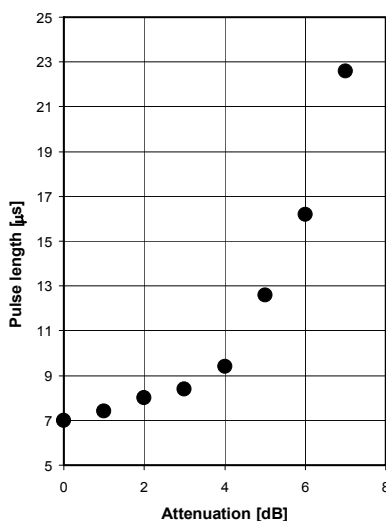
Figure 94. Pulse length of Π pulse for its different attenuations.
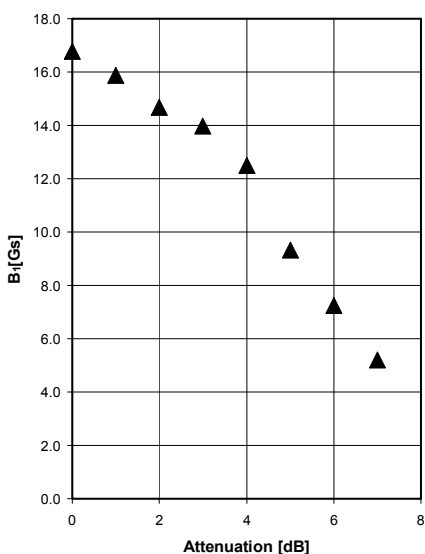
Figure 95. B$_1$ field calibration chart.

- **Measurement of FID amplitude as a function of the length of the locking pulse**

Manual measurements

The experiment with rubber was performed with maximum locking pulse power producing **B$_1$=17Gs** which highly exceeds the static field inhomogeneity estimated from line width **ΔB$_0$=0.2Gs** Time of the locking pulse was varied from 0.2ms to 10ms. Figure 96 shows stack plot with several FIDs.
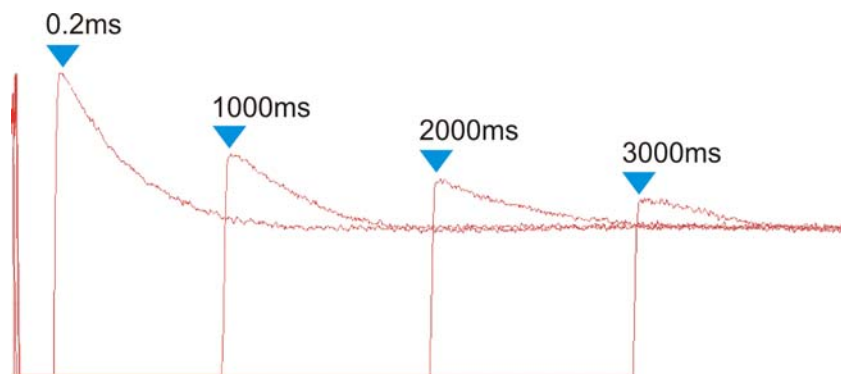
Figure 96. Exponential decay of the amplitude of FID signals in rubber for different locking times.

The dependence of FID amplitude on the locking pulse width with corresponding linear regression is shown in Figure 97. Regression is shown in red: Y=4.71 – 0.35t$_p$. The final value of spin-lattice relaxation time in the rotating frame in rubber is T$_{1\rho}$=2.8 ms.
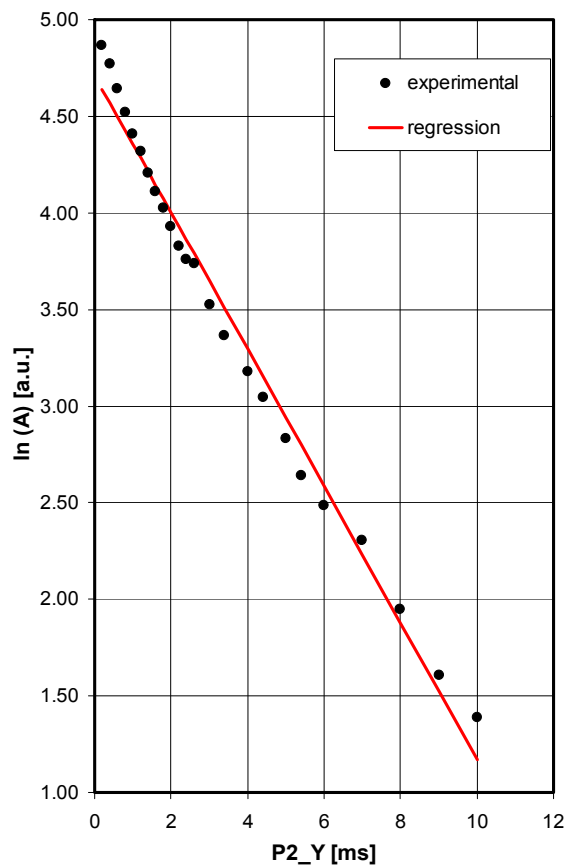
Figure 97. Linear regression analysis of the logarithm of FID amplitude vs. locking pulse length with an Excel program; $T_{1\rho}$=2.8 ms.

Automatic measurements

Data acquired automatically on **Acquisition Page** can be processed on **Processing Page**:

- -load data,
- -extract data points (FIDs amplitudes with corresponding locking pulse width),
- -perform regression analysis clicking on $T_{1\rho}$ by spin lock **SL** button.
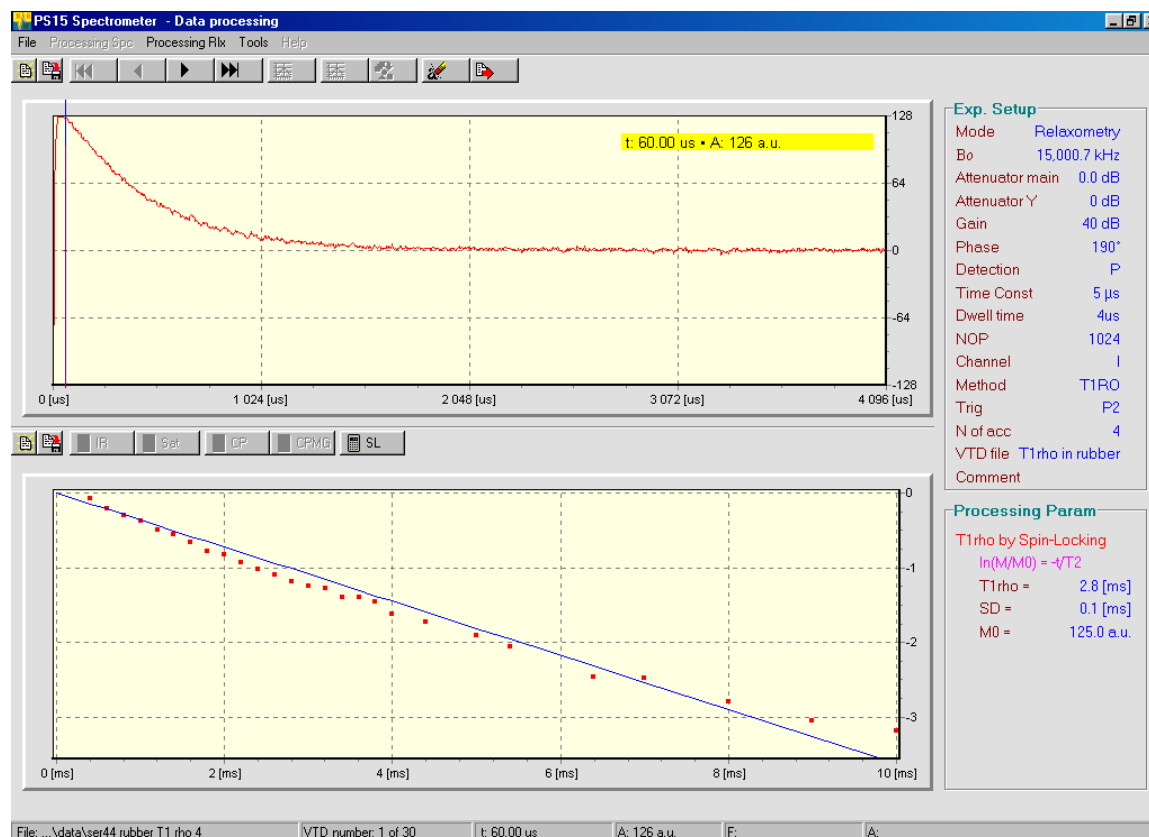
Figure 98. Processing data from $T_{1\rho}$ experiments in rubber. $T_{1\rho}$ =2.8 ms is the exact value obtained with manual measurements and linear regression using Excel.

$T_{1\rho}$ can be measured for different locking pulse power. As mentioned before this corresponds to measurements of relaxation in a rotating frame in different magnetic field ($T_{1\rho}$ dispersion).
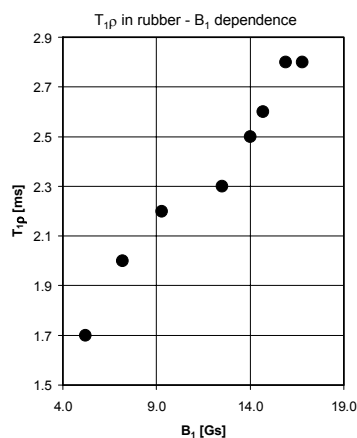
Figure 99. $T_{1\rho}$ in rubber measured for different magnitude of B_1 magnetic field.

T1ρ in acrylic

Since an acrylic sample is a typical solid-state sample it is definitely more challenging in measurements of $T_{1\rho}$ than is rubber.

Acrylic's short FID time requires very careful adjustments of:

- receiver filter (set time constant to 1μs),

- preamplifier gating (set it below spectrometer's "dead time"),

- acquisition time (Dwell Time 0.4μs and Number of Points NOP=1024)

Relatively weak signal needs:
- more Receiver Gain,
- at least 100 accumulations to improve S/N ratio

Since $T_{1\rho}$ is longer than in rubber the expected longest locking pulse will be relatively long (about 40ms). Despite short relaxation in acrylic the experiment can not be pulsed too fast due to spectrometer's transmitter limit. If repetition time **T_R** is too short the locking pulse will simply lose the power before it reaches its end. Use a longer repetition time to let the transmitter's power supply recharge capacitors. Figure 100 through Figure 103 illustrate the importance of proper **T_R** time selection.
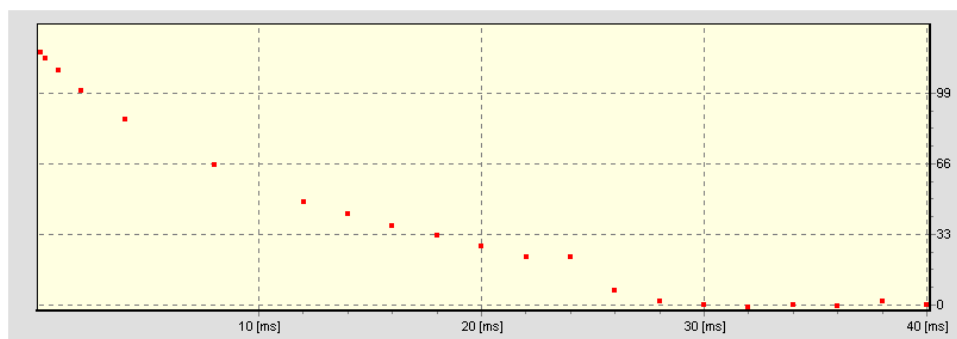
Figure 100. Sudden drop of FID amplitude from acrylic due to locking pulse power decrease at 26ms (T_R=1s)
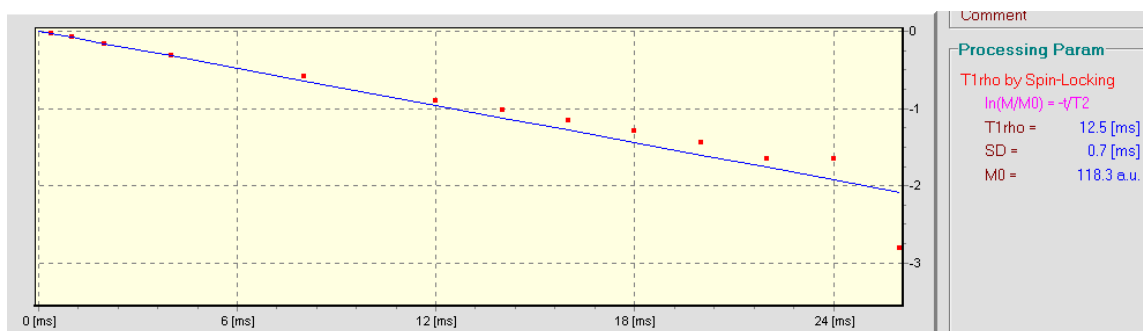
Figure 101. Decrease of transmitter power significantly affects accuracy of $T_{1\rho}$ measurements.
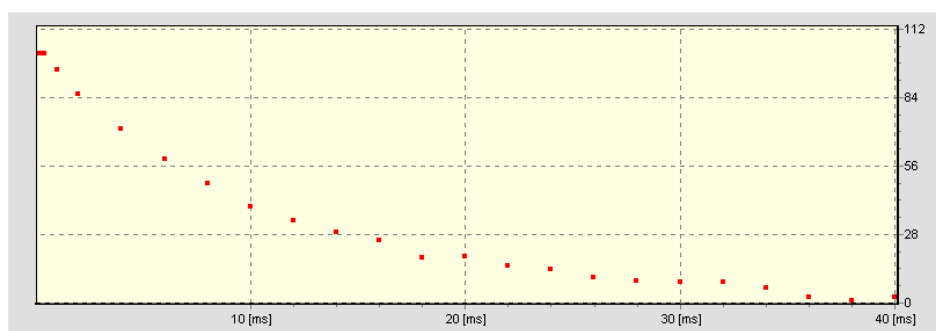
Figure 102. Unaffected, smooth exponential decay of FID amplitude from acrylic (T_R=5s).
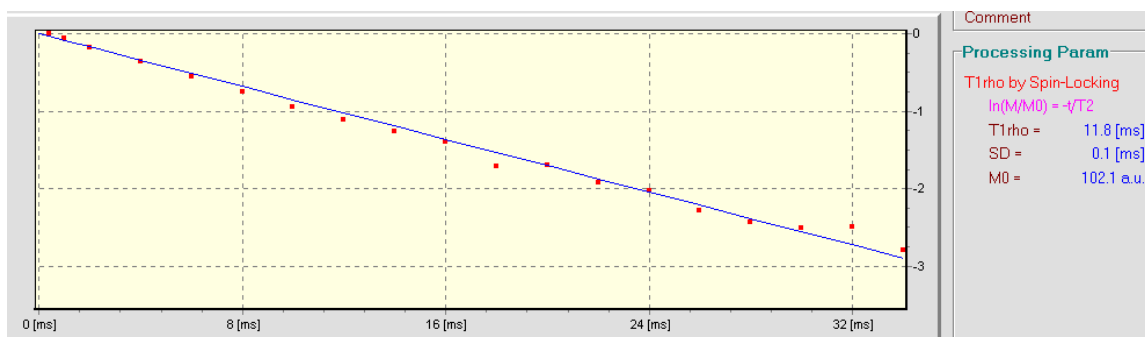
Figure 103. Highly accurate measurements of $T_{1\rho}$ in acrylic when experimental repetition time is long enough to prevent locking pulse drop.

6.3 Multiple spin echoes in three pulse sequence

6.3.1 Introduction

In his classic paper "Spin Echoes"[7], E. Hahn introduces the concept of pulsed NMR and an idea of $\Pi/2$ pulses. He was so attached to the rotation of nuclear magnetization by 90 degrees that even the first nuclear spin-echo, which he called a product of "constructive interference", is generated by $\Pi/2$-τ- $\Pi/2$ sequence (Figure 104) not by the $\Pi/2$-τ- Π as we do now. To explain the formation of the echo after two $\Pi/2$ Hahn uses a somewhat cumbersome three-dimensional "eight-ball" echo pattern.

A much simpler two-dimensional vector model can be used when the echo is created by the $\Pi/2$-τ- Π sequence where the movement of spins is reduced to the x'y' plane (Figure 105).
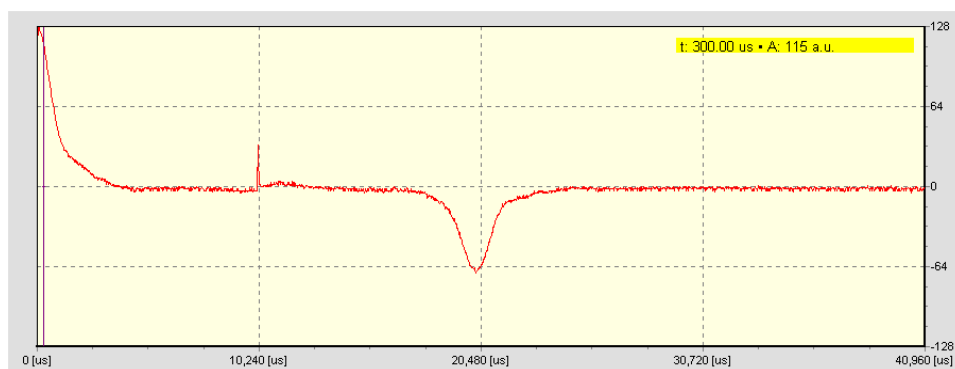
Figure 104. Classic Hahn's spin-echo from water doped with cupric sulphate obtained with two identical pulses (3.6μs-10ms-3.6μs).
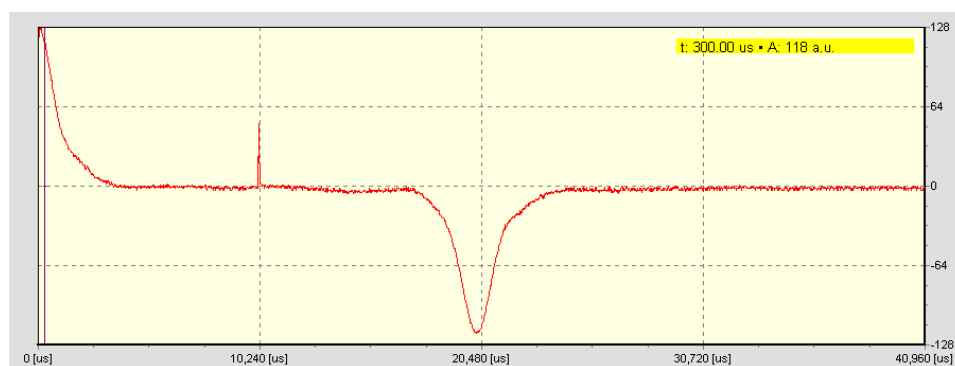
Figure 105. Spin-echo signal after $\Pi/2$-τ- Π sequence (3.6μs-10ms-3.6μs).

---

[7] E. L. Hahn, "Spin Echoes', Phys. Rev. **80**, 589-594 (1950)

When after a time **T** with respect to **t=0** the third identical radio-frequency pulse is applied to the ($\Pi/2$-τ- $\Pi/2$) sequence, four additional echoes appear at times: T+τ, 2T-2τ, 2T-τ, 2T. Figure 106 shows the formation of "primary echo" and four "secondary echoes" in a distilled water sample. This experiment is a reproduction of Hahn's original experiment using the PS15 spectrometer. One difference is that the PS15 phase-sensitive detector can see the actual polarity of echoes (positive when echo is formed along +y' and negative when is formed along –y' axis).
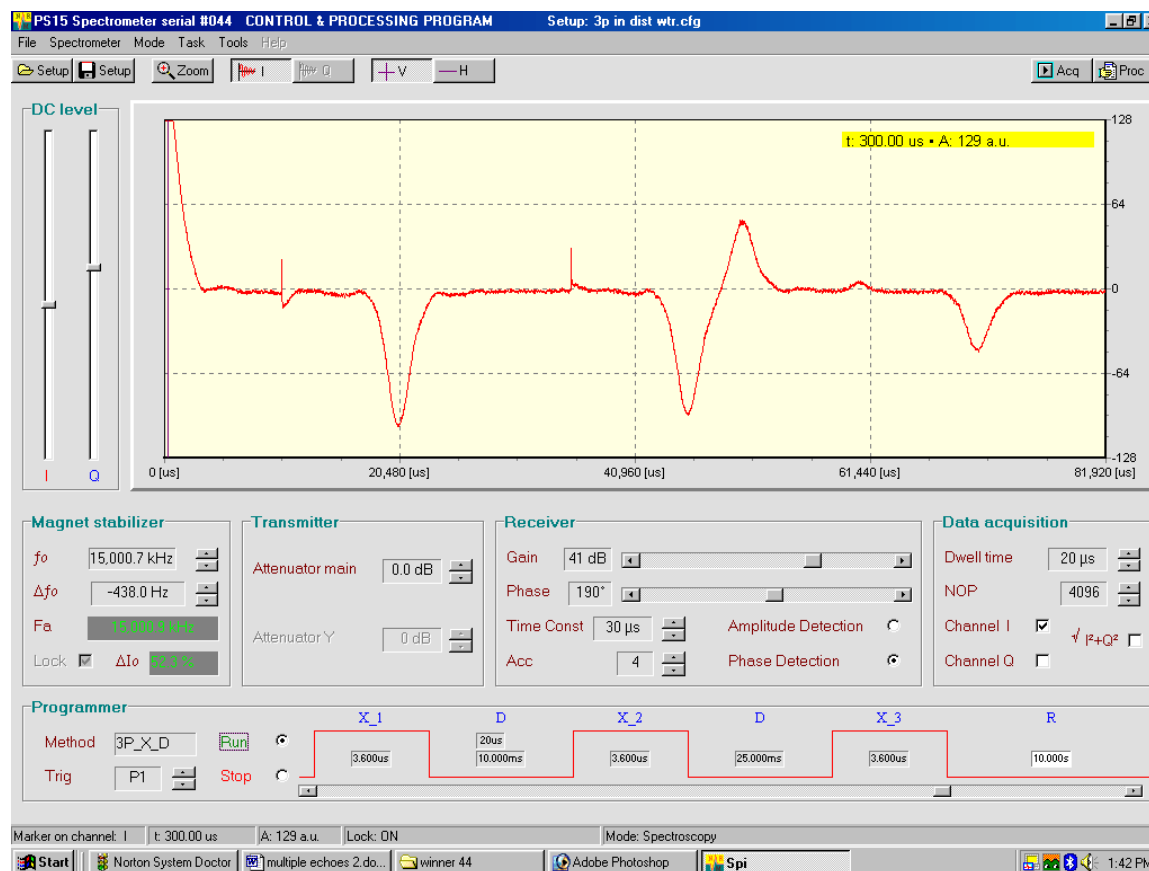
Figure 106. Formation of multiple echoes in distilled water by ($\Pi/2$-τ- $\Pi/2$-T$_D$-$\Pi/2$) sequence: $\Pi/2$=3.6μs, τ=10ms, T$_D$=25ms, repetition time T$_R$=10s

Diagram on Figure 107 shows timing of the appearance of consecutive echoes. Note that secondary echoes have different polarities with the sign depending on whether the spins focus is in x'y' plane along –y' or along +y' axis.
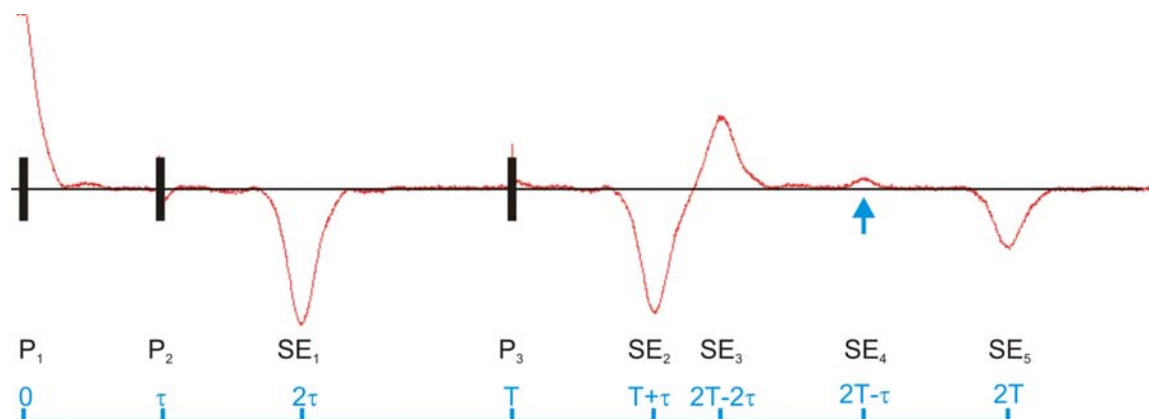
Figure 107. Three-pulse sequence and multiple echoes: P_1, P_2, P_3- radio-frequency $\Pi/2$ pulses. SE_1-primary echo, SE_2, SE_3, SE_4, SE_5 -secondary echoes (SE_2-Stimulated Echo, SE_3-"image echo").

Among secondary echoes the so called "**stimulated echo**" is particularly useful due to its exponential decay ruled by the $1/T_1$ term. If τ is small enough a plot of stimulated echo amplitude versus **T** gives a straight line whose slope is the measure of T_1.

Stimulated echo importance goes far beyond NMR applications. Newly developed pulsed Electron Paramagnetic Resonance techniques utilize the modulation of stimulated electron spin-echo by nuclear spins to measure distances between the paramagnetic center and surrounding nuclei in amorphous materials.

6.3.2 Experimental

Object

Observation of multiple echoes and spin-lattice relaxation times measurements by Inversion Recovery and Stimulated Echo decay in water-cupric sulphate solution. Cupric sulphate was added to reduce T_1 relaxation time in water and make measurements shorter.

Directions

T_1 measurements by Inversion Recovery
- Automatically generate experimental data following instruction on page 48.
- Calculate T_1 either on Winner **Processing** page or using any other program (Excel, Origin, etc)

T_1 measurements by Stimulated Echo. Follow guiding points on the **Setup** page on Figure 108.

- Switch Spectrometer **Mode** to **Spectroscopy** and **Method** to **3P_X_D** (**1**).
- Change data acquisition triggering moment **Trig** from **P1** to **P3** (**2**). This will start data acquisition after the end of third pulse.

- Place cursor on the center of stimulated echo (**3**).
- Set Delay Time **T$_D$** between second and third pulses (**5**).
- Measure echo amplitude **A** (**4**).
- Repeat measurements for longer delays until stimulated echo disappears in the noise.
- Using any statistical program do regression analysis of **ln (|A|)** versus delay time **T$_D$**.

Figure 108. For T$_1$ measurements select and use the 3P_X_D method (**1**), set triggering after P3 pulse (**2**), place measuring cursor on the center of stimulated echo (**3**). Due to short relaxation the third secondary echo is not visible.

- Author used Excel program to create spreadsheet with **A** vs. **T$_D$** data points, perform **Tools>Data Analysis>Regression**, and to display experimental data points and regression on the chart (see Figure 109).
- Following table summarizes measured T$_1$ relaxation times by both methods with additional T$_2$ obtained by Carr Purcell Meiboom Gill method.

Method	Relaxation time [ms]	Error [ms]
T_1 by Inversion Recovery	117	2
T_1 by Stimulated Echo decay	128	5
T_2 by CPMG	97	2

Table 6 . T_1 relaxation times in cupric sulphate doped water by Inversion Recovery and Stimulated Echo. T_2 time measured byCPMG method is of the same order.

T_1 in H_2O+ $CuSO_4$ from Stimulated Echo

$A=5.1 - 0.0078*T$
$T_1=(128 +/-5)$ ms
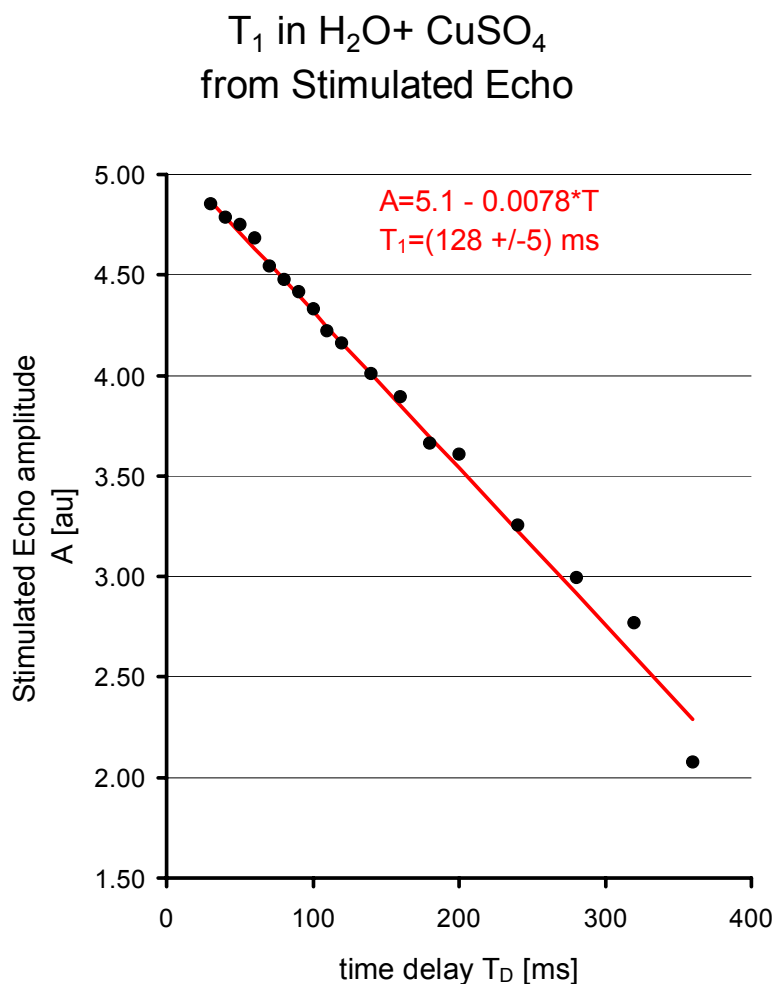
Figure 109. Experimental data points (black) and regression analysis (red line) using Excel program.

7   APPENDIX

7.1 How to load and display relaxation data in ASCII format using EXCEL

1. Prepare the relaxation data ASCII file in the **PROCESSING** page of the PS15 program,

2. Start EXCEL,

3. Load a data file by: File/ Open/All files [*data file name and path*]. In our example we will use later ***gl_t1.prl*** file.

4. EXCEL recognizes immediately that the data format is not EXCEL format and it launches the Text Import Wizard. Follow three steps:

    Step 1 of 3

Original data type-	Fixed width
Start import row at-	4^{8}
File origin-	Windows (ANSI)
Next>	

    Step 2 of 3

    This is Data preview. Check if columns are set properly. If not use CREATE, DELETE, MOVE a break line.

    Step 3 of 3

Column data format-	general
Finish	

5. Data without data header are loaded. Now remove data footer:

    - Mark footer text
    - Select Edit
    - Select Clear
    - Select All

6. Save data in EXCEL format

    Save As

File name	[type a file name]

---

[8] Data header contains always 3 lines

Save as type   [MS Excel Workbook]
Save

7. To display data as an X-Y diagram choose Chart Wizard from Insert>Chart.
    Follow these four steps:

Step 1 of 4
Chart type: X-Y (Scatter)
Chart sub-type: Scatter. Compares pairs of
                            values
Next>

Step 2 of 4:

On data sheet click the range of points to be displayed. A
preview of the data immediately appears.

Step 3 of 4
Titles:

Chart title   Magnetization recovery in
                        glycerin
Value (X) axis: Delay time [ms]
Value [Y] axis: Mz [a.u.]
Axes:

Value (X) axis   check
Value (Y) axis   check
Grid lines

Value (X) axis: Major grid lines
Value (Y) axis: Major grid lines
Legend

Right
Data label   None
Next>

Step 4 of 4

Place Chart   As an Object in **[gl_t1]**
Finish

1	-81
2	-82
4	-72
8	-60
16	-37
32	-1
50	30
75	62
100	81
150	102
200	111
250	115
300	116
350	118
400	119
500	118

Magnetization recovery in glycerin

(chart with axes "Mz [au]" vertical, "Delay time [ms]" horizontal)
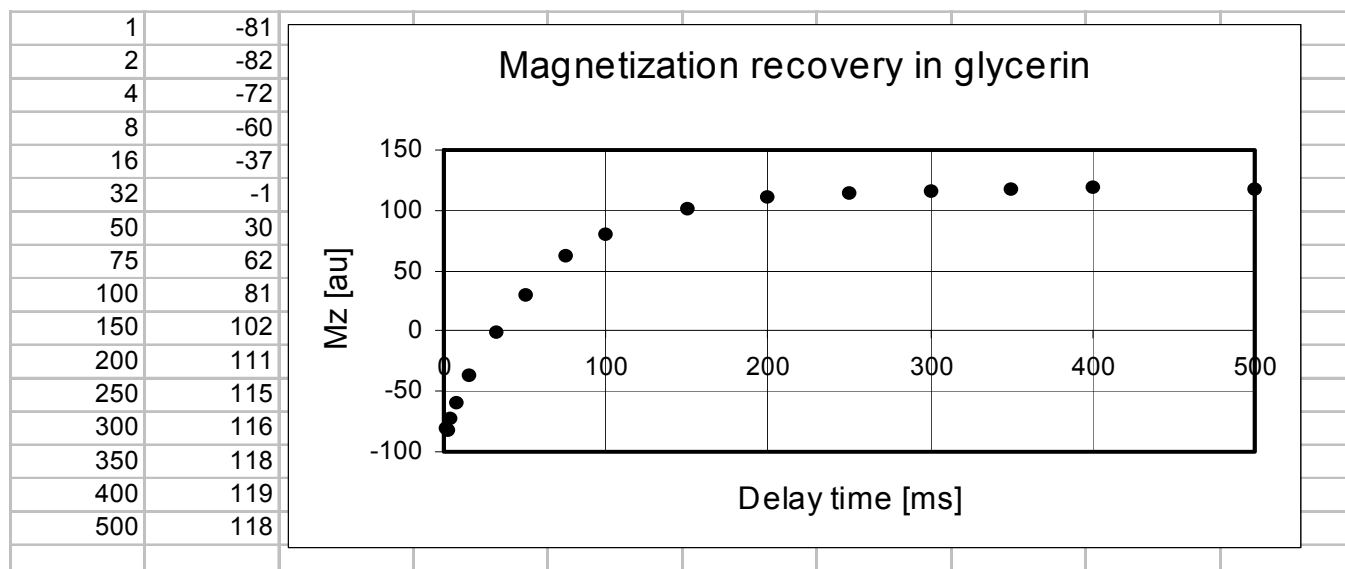
Figure 110. Magnetization recovery in glycerin. Excel presentation**.**

8. Now you can change specific items on the chart by double clicking and modifying it according to your requirements.

9. Save the whole project under the new name [*gl_t1_diagram*].

7.2 How to process relaxation data with Excel program

Excel's SOLVER package provides tools powerful enough to fit relaxation data into specific equations. If the SOLVER command is not on the TOOLS menu, you need to install it. Select Tools>Add-Ins. On list of available Add-ins check Solver and follow instructions.
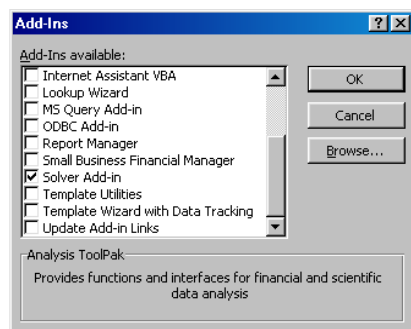
Figure 111. Installing Solver from **Tools>Add-Ins**.

Using data for glycerin and assuming a simple one parameter data fit to equation: M=M1*(1-2*exp(-t/T1)) we will obtain the spin-lattice relaxation time **T$_1$=46.3 ms**.

We can get a better fit with a two- or three-parameter equation but you will encounter some difficulties in interpreting the physical meaning of the parameters.

- Load experimental data to columns **A** and **B**.
- Estimate the maximum value of magnetization in cell **E3:** M1=118
- Estimate T$_1$ in cell **G3:** T1=100
- Select range **C3:C18:** and perform calculations of theoretical magnetization values: {=F3(1-2*exp(-(B3:B18)/G3)}.
- Select range **D3:D18** and perform calculations of squared errors: {=(C3:C18-D3D18)^2}
- Do sum of squared errors by E19**=SUM (E3:E18)**
- In **Tools** select **Solver** and complete items in a **Solver Parameters** box (Figure 112):
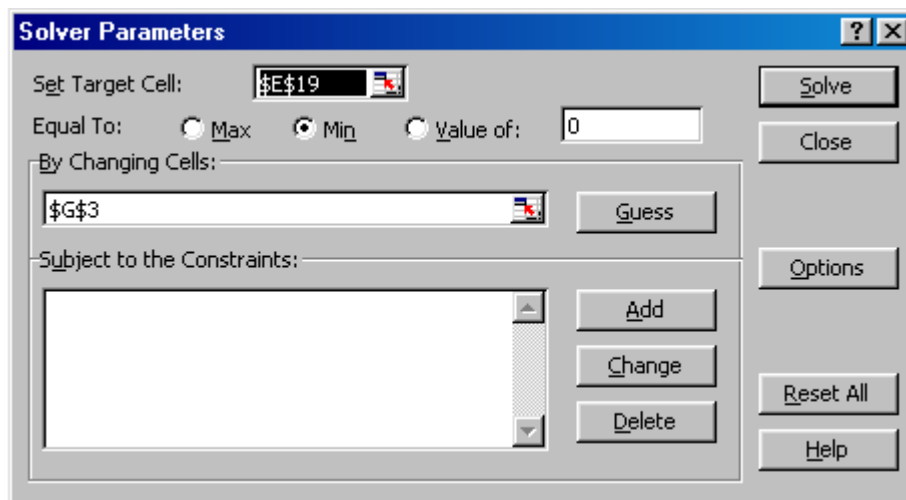
Figure 112. Options in Solver Parameters box.

- **Set Target Cell**, which is sum of squared errors in cell **E19**
- Select **Min** to minimize sum of squared errors in cell **E19** during fitting procedure
- Select T1 in **G3** cell as adjustable cell (in **By Changing Cells** box)
- Click **Solve** to perform calculations.

Figure 113 shows all elements of calculation of T$_1$ with Excel Solver tool.

1/A	B	C	D	E	F	G
2	delay [ms]	Mz [au]	M	Error^2	M1	T1
3	1	-81	-112.95	1021.03	118	46.3
4	2	-82	-108.02	676.78		
5	4	-72	-98.45	699.74		
6	8	-60	-80.52	421.24		
7	16	-37	-49.00	143.99		
8	32	-1	-0.17	0.68		
9	50	30	37.92	62.66		
10	75	62	71.35	87.40		
11	100	81	90.82	96.52		
12	150	102	108.78	45.94		
13	200	111	114.87	14.98		
14	250	115	116.94	3.76		
15	300	116	117.64	2.69		
16	350	118	117.88	0.01		
17	400	119	117.96	1.08		
18	500	118	118.00	0.00		
19				3278.51	**Sum of Error^2**	

SUMMARY
equation used: $M=M1*(1-2*exp(-t/T1))$
result from the Solver: M1=118 [au], T1=46.3 [ms]

T1 by IR in glycerin

Figure 113. Excel worksheet with data and chart.

7.3 How to load and display relaxation data in ASCII format using ORIGIN program

Procedure

1. Prepare the relaxation data ASCII file in the **PROCESSING** page of PS15 main program,

2. Start **Origin**,

3. Begin session with **File>New>Project**

4. Import data file by: **File>Import>ASCII Options**

5. Complete **ASCII Import Options** following hints in Figure 114.
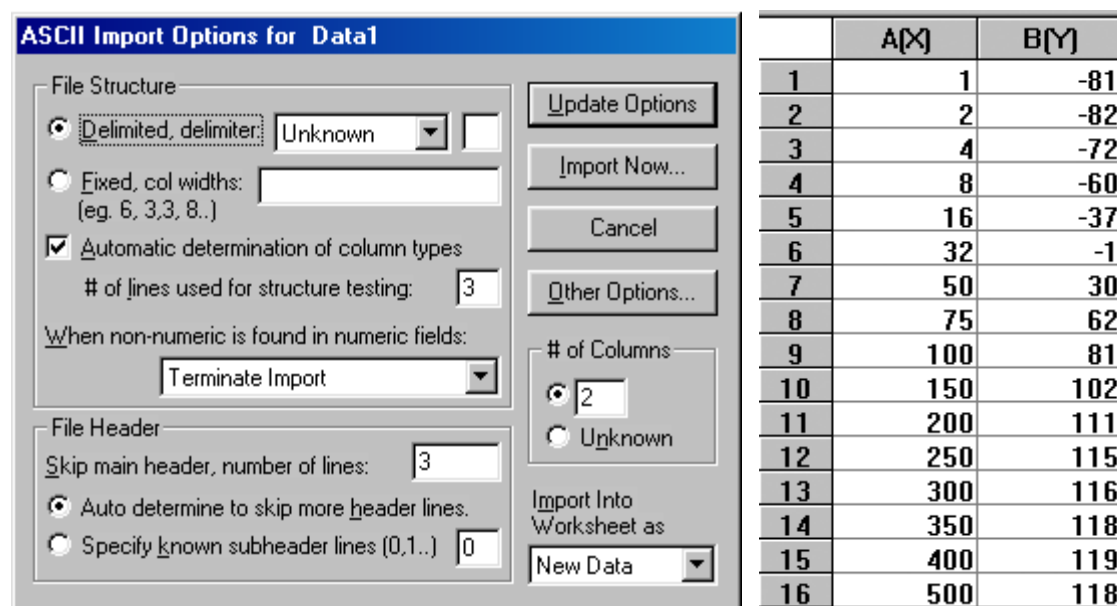
Figure 114. Origin program import ASCII options and data after importing from *prl file..

6. Start Import ASCII by **Import Now**.

7. Browse through *All Files (*.*)* types.

8. Select right file name ***.prl** and **Open** it.

You should now have data loaded without the header and footer. Double check to confirm that the number of columns and rows are correct. Assure that the header and footer are completely removed. Figure 114 shows ASCII Import Options dialog window and set of correctly imported data.

9. Proceed to save project by: **File>Save Project As** in **.opj** file.

10. To display experimental points select **Plot>Scatter** and complete procedure by assignments of columns for plot in Select **Columns for Plotting**.
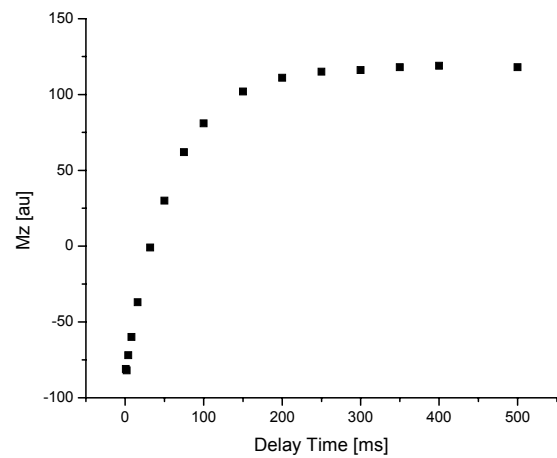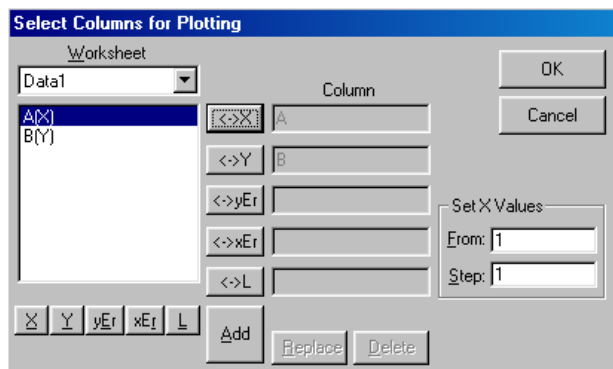
Figure 115. To plot experimental data select right columns and click OK.

7.4 How to process relaxation data with Origin program

There are many ways to calculate T_1 from an experimental data set. A non-linear curve fit is one of most reliable and elegant methods. This option in the Origin program provides a flexible and easy to use tool to find the parameters of the exponential function that describes the magnetization recovery after the Π pulse in the *inversion recovery* method. Theoretically a one- exponential fit (see Eq. 30) requires at least a two parameters. One of the parameters is an equilibrium magnetization M_0, another spin-lattice relaxation T_1.

$$M_z(t) = M_0(1 - 2\exp(-t/T_1)) \qquad\qquad \text{Eq. 30}$$

Translated into Origin language this equation looks like:

$$Y = P1*(1 - 2*\exp(-x/P2)). \qquad\qquad \text{Eq. 31}$$

1. Start **Analysis>Non-linear curve fit**.
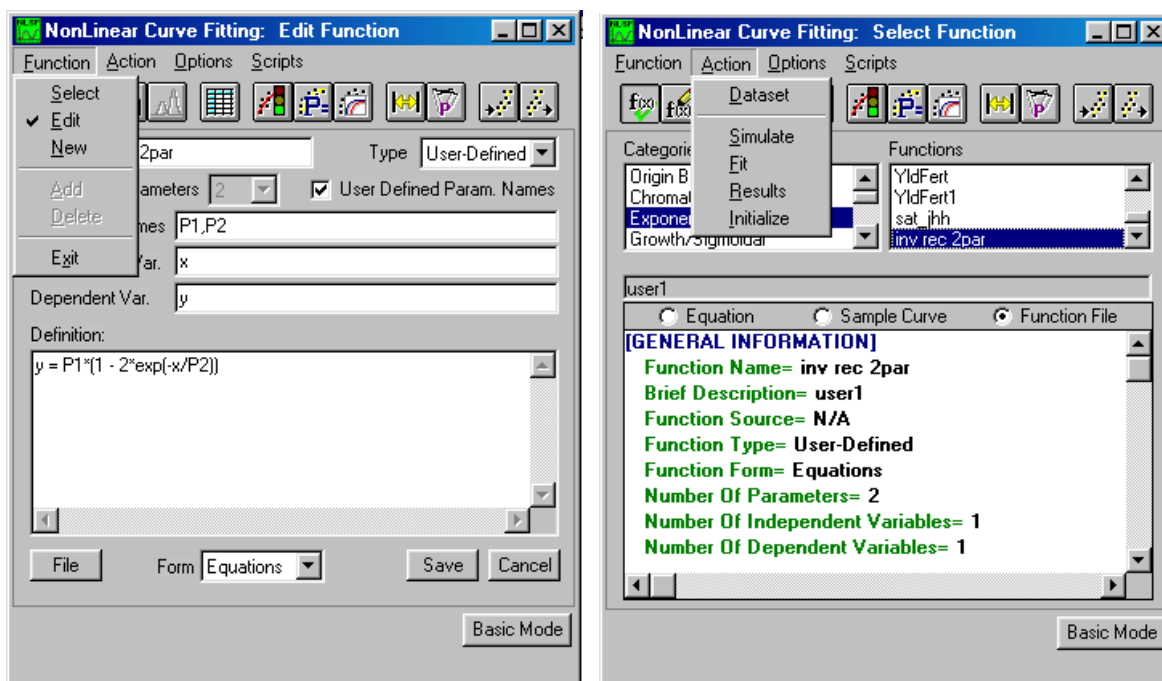
Figure 116. Function and Action options in a **Non Linear Curve Fitting**.

2. From **Functions>Select** load fitting function by highlighting the proper function in **Categories** (Figure 116).

3.   If there is no appropriate fitting function create a function by **Function>New** or **Function>Edit**.
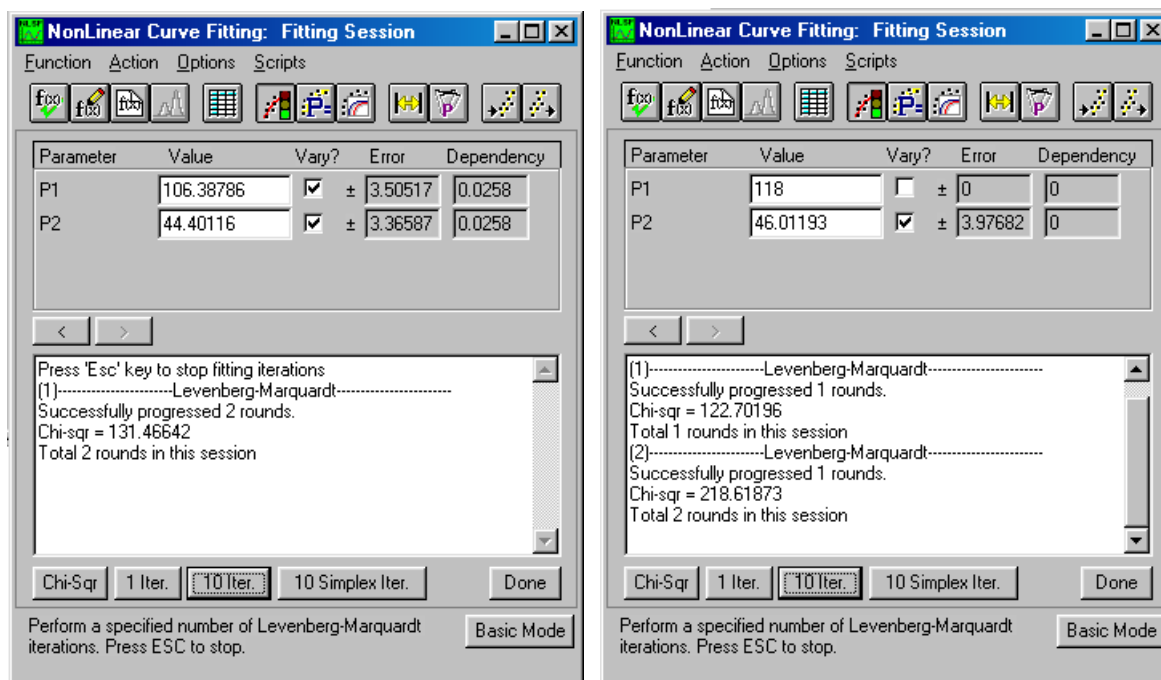
Figure 117. Fitting experimental data with two and with one parameter.

4. In **Action>Data Set** assign

5. Perform fit in **Action>Fit**.

   ❑ Type approximate values for P1 (M_0) and for P2 (T_1).

   ❑ Check **Vary?** box if parameter should vary during iteration.

   ❑ Do iterations.

   ❑ Finish by **Done** when results satisfy you or when there is no further improvement with more iterations.

6. After fitting you can modify fonts, colors, appearance of labels, etc using options in **Format>Plot**.
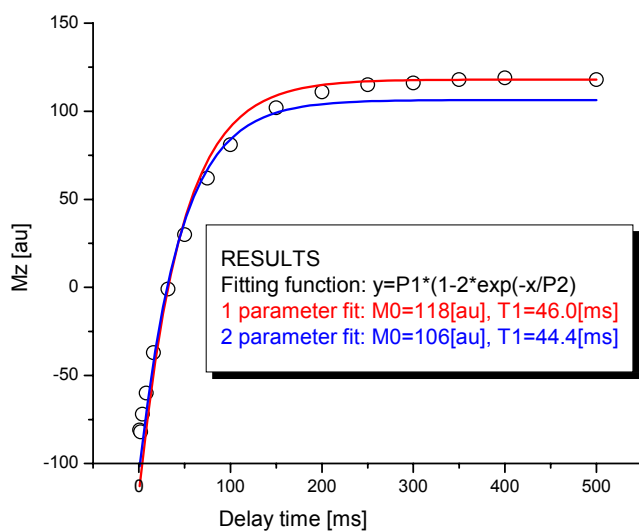
Figure 118. Fitting experimental data for T_1 calculation in glycerin using Origin program. Red line is one-parameter and blue line is two-parameter fit.

Final results of calculations of T_1 in glycerin sample by fitting to the same experimental data set using different programs are presented in Table 7.

	M_0 [au]	T_1 [ms]	Error [ms]	This manual page
PS15	110	**47.0**	±3.3	54
Excel	118	**46.3**		123
Origin	118	**46.0**	±4.0	128

Table 7. Summary of T_1 calculations in glycerin by different programs.

8   LIST OF TABLES

9   LIST OF FIGURES

FIGURE 118. FITTING EXPERIMENTAL DATA FOR T_1 CALCULATION IN GLYCERIN USING ORIGIN

PROGRAM. RED LINE IS ONE-PARAMETER AND BLUE LINE IS TWO-PARAMETER FIT.   128

10   REFERENCES

10.1 Papers:

1. Edward Mills Purcell, H. C. Torrey and R. V. Pound
    Resonance Absorption by Nuclear Magnetic Moments in Solids
    Physical Review, **69**, 37-38 (1946)

2. F. Bloch, W. W. Hansen and M. E. Packard
    Nuclear Induction
    Physical Review **69**, 127- (1946)

3. E. L. Hahn
    Spin-Echoes
    Physical Review, **80**, 580-594 (1950)

4. H. Y. Carr and E. M. Purcell
    Effects of Diffusion on Free Precession in Nuclear Magnetic Resonance
    Experiments
    Physical Review, **94**, 630- 638(1954)

5. S. Meiboom and D. Gill
    Modified Spin-Echo Method for Measuring Nuclear Relaxation Times
    Review of Scientific Instruments, **29**, 688- 691(1958)

6. Richard R. Ernst and W. A. Anderson
    Application of Fourier Transform Spectroscopy to Magnetic Resonance
    Review of Scientific Instruments, **37**, 93-102 (1966)

10.2 Books:

1. Thomas C. Farrar, Edwin D. Becker
    Pulse and Fourier Transform NMR. Introduction to Theory and Methods.
    Academic Press, New York, 1971

2. Ray Freeman
    A Handbook of Nuclear Magnetic Resonance
    Longman Scientific & Technical, UK, 1988

3. Eichii Fukushima and S. B. W. Roeder
    Experimental Pulse NMR. Nuts and Bolts Approach.
    Addison-Wesley, Reading, Massachusetts, 1981

4. Richard R. Ernst, Geoffrey Bodenhausen and Alexander Wokaun
    Principles of Nuclear magnetic Resonance in One and Two dimensions
    Clarendon Press, Oxford, UK 1987

5. Maryvonne L. Martin, Gerard J. Martin and Jean-Jacques Delpuech
   Practical NMR Spectroscopy
   Heyden & Son Ltd, London 1980

6. Eichii Fukushima, Editor
   Key Papers in Physics. NMR in Biomedicine: The Physical Basis
   American Institute of Physics, New York, 1989

10.3 Web references

1. Joseph P. Hornak
   The Basics of NMR
   http://www.cis.rit.edu/htbooks/nmr

2. W. Faulkner
   Basic MR Principles
   http://www.t2star.com/basic_mr/Basic.html

3. Henry Rzepa
   NMR Spectroscopy. Principles and Application.
   Six second year lectures given at Imperial College
   http://www.ch.ic.ac.uk/local/organic/nmr.html

4. Marc Bria, Pierre Watkin, Yves Plancke
   2D NMR Spectroscopy. Or an Help for the Structural Determination of Chemical Molecules
   http://www.univ-lille1.fr/lcom/RMN2D/resum2D_us/us_menu.htm

5. There is a German web page with gigantic list of different links related to NMR we strongly recommend to visit: http://franz.org/www/i120123d.html

11 INDEX